THE EFFECT OF CONTROLLED
INTERMITTENT INTERFACIAL
BONDING...

T. Marston, 1973

DTIC
ELECTE
NOV 28 1995
B

19951121 023

PLASTEC

This is an authorized facsimile and was produced
by microfilm-xerography in 1974 by Xerox University
Microfilms, Ann Arbor, Michigan, U.S.A.

73-24,632

MARSTON, Theodore Utley, 1946-
    THE EFFECT OF CONTROLLED INTERMITTENT INTERFACIAL
    BONDING ON THE TENSILE PROPERTIES AND FRACTURE
    TOUGHNESS OF A BORON-EPOXY COMPOSITE.

The University of Michigan, Ph.D., 1973
Engineering, mechanical

University Microfilms, A XEROX Company, Ann Arbor, Michigan

ii

THE EFFECT OF CONTROLLED INTERMITTENT INTERFACIAL

BONDING ON THE TENSILE PROPERTIES AND FRACTURE

TOUGHNESS OF A BORON-EPOXY COMPOSITE

by

Theodore Utley Marston

A dissertation submitted in partial fulfillment
of the requirements for the degree of
Doctor of Philosophy
(Mechanical Engineering)
in the University of Michigan
1973

Doctoral Committee:

Professor David K. Felbeck, Co-Chairman
Associate Professor Anthony G. Atkins, Co-Chairman
Professor Robert M. Caddell
Professor Kenneth C. Ludema
Professor Gregory S. Yeh

ACKNOWLEDGMENTS

I the author would like to express my appreciation to the thesis committee. Special acknowledgments are due to Drs. Atkins and Felbeck as co-chairmen. Drs. Caddell, Ludema and Yeh have provided valuable counsel and discussion.

I would also like to acknowledge Messrs. Clyde Schoenhals and Clarence Johnson for their advice in the building of the research apparatus and Mr. Lynn Buege for building the timing device.

I appreciate the assistance afforded me by Mr. Larry Allord and Ms. Peggy Hollingworth with regard to the Scanning Electron Microscope.

I wish to express my gratitude to the Department of Health, Education and Welfare for its financial support over the last three years.

Ms. Joan Schaible is appreciated for her excellent job in typing the manuscript.

I extend my greatest appreciation to my wife Jeannine for her support, understanding and love.

iii

TABLE OF CONTENTS

LIST OF TABLES

LIST OF FIGURES

x

LIST OF APPENDICES

A	area, crack area
A_{f_c}	area of the coated filaments
$A_{f_{uc}}$	area of the uncoated filaments
a_{if}	area of the interface
a_m	area of the matrix
a_{ij}	elements of the compliance matrix
b	base
c	crack length
c	velocity of sound
D	debond length
d	filament diameter
δ	deflection
E	elastic modulus
E_f	elastic modulus of the filament
$\bar{E}$	average elastic modulus
ε_f	fracture strain of the filament
ε_m	fracture strain of the matrix
F_{f_c}	fraction coated filament
$F_{f_{uc}}$	fraction uncoated filament
G	strain energy release rate
G'	total work per unit area
G_c	fracture toughness
G_m	shear modulus of the matrix material
	work of fracture $(G_c/2)$

γ'	surface energy
γ_1	incremental work of fracture
γ_{1f}	interfacial fracture toughness
γ_m	matrix fracture toughness
H_z	Hertz, cycles per second
h	height
h_m	mold height
h_t	specimen thickness
K_c	critical stress intensity factor
K_{1c}	plane strain fracture toughness
k_m	machine stiffness
k_t	total stiffness
L_c	coated length
L_{uc}	uncoated length
l_c or l_c	critical transfer length
$\bar{l}$	average pullout length
p	plastic work function
R_o	original resistance
R_i	instantaneous resistance
ρ	density
σ	stress or strength (tensile)
σ_f	fracture or filament strength (depending upon context)
σ_f^*	filament fracture strength
σ_m	matrix stress or strength
σ_m'	matrix stress at filament fracture strain
σ_m^*	matrix fracture strength

σ_x	stress parallel to the loading axis
σ_y	stress perpendicular to the loading axis
τ	shear strength
τ^*	ideal interfacial shear strength
τ_{xy}	interlaminar shear strength
τ_c	interfacial shear strength (coated)
τ_{uc}	interfacial shear strength (uncoated)
τ_m	matrix shear strength
U	total energy
v_{crit}	critical volume
v_f	volume fraction filament
v_{f_c}	volume fraction coated filament
$v_{f_{uc}}$	volume fraction uncoated filament
v_m	volume fraction matrix
X	load

INTRODUCTION

Composite Materials

High strength composite materials have generated a tremendous interest in materials science and its application. A composite material has been arbitrarily defined by Broutman (1967) as a material that must: 1) be man-made, unlike wood, 2) be a combination of at least two chemically distinct materials with a defined interface between them, 3) be combined three-dimensionally, which precludes laminate structures, 4) have properties not exhibited by its constituents (e.g. exhibits synergism).

The three types of heterogeneous materials which comply with the four criteria are: 1) dispersion hardened alloys (reinforcement size 0.01-0.1 microns, up to fifteen volume percent reinforcement), 2) particle reinforced composites (reinforcement size greater than one micron and up to twenty-five volume percent reinforcement), 3) filamentary reinforced composites (filament reinforcement size 0.1 to 500 μm in diameter, from 10 μm to 10 Km in length and up to seventy-five volume percent reinforcement).

The filament reinforced composite material is the focus of this research. It is a two-constituent system (matrix and one type of reinforcement) with the filaments uniaxially aligned. High strength, high modulus materials, which can only be produced in filamentary form, are incorporated into the composite to provide stiffness and to function as the load carrying members of the composite. The matrix serves a multi-fold purpose, to provide a medium for transferal

of the external load to the filaments, to protect the filaments from
contacting one another and provide alignment to the filaments.

The system chosen for this study is the boron-epoxy system.
This composite is chosen for four reasons: 1) both materials
(epoxy and boron) are available from commercial sources, 2) boron
is one of the most promising of the high strength reinforcements
available (ignoring the cost barrier), 3) the system is a commer-
cially viable combination (it is the strongest composite currently
available), 4) extensive laboratory experience has been gained in
this system (Heimbuch, 1970).

The purpose of this research is to explore a concept for the
improvement of tensile and fracture toughness properties through
the use of a controlled, intermittent, interfacial bond strength of
a composite material.

CHAPTER I

Literature Review

I.A Constituent Properties

I.A.1 - Reinforcements

As stated in the introduction, there are three types of composite materials. Only the filamentary composite will be of interest in this research. It is necessary to differentiate the three systems of filamentary composites: 1) whisker reinforced, 2) filament (continuous or discontinuous) reinforced, and 3) in situ (off-eutectic) composite. The first two categories, of interest here, are produced with preformed reinforcements. The third type is grown from the melt using directional solidification.

Whiskers are traditionally single crystals, containing few, if any, dislocations, that have one principal growth direction, and some are the strongest materials known to man (Herzog, 1967). The diameter and length ranges from 0.1 by $10 \mu m$ to 10 by $1000 \mu m$, thus giving an aspect ratio $(\frac{length}{diameter})$ of 100. Although metallic whiskers were the first grown and possess good strength characteristics, they suffer from having high densities and low moduli. Ceramic whiskers, $\alpha-Al_2O_3$, SiC, B_4C, BeO, $C_1Si_3N_4$ are preferred for reinforcement because of their outstanding specific strength $(\frac{\sigma}{\rho})$ and specific moduli $(\frac{E}{\rho})$. Filaments, in contrast to whiskers, are either polycrystalline, amorphous, or a combination of both, and have dimensions from 10-500 μm with aspect ratios varying from 100 to infinity. Table I includes the mechanical properties of the more important filaments. Table I also compares the various whiskers with the weaker continuous filaments.

TABLE I-1

REINFORCEMENT PROPERTIES

(from Sutton, 1966)

Filament Continuous	Melting Point C°	Density Mg/m³	Tensile Strength GN/m²	Specific Strength $10^{10}(N/S)^2$	Young's Modulus GN/m²	Specific Modulus $10^{10}(N/S)^2$	Cross-sectional Area 10^{-6} m²
E-Glass	700	2.55	3.45	1.35	72.4	28.39	10
S-Glass	840	2.50	4.49	1.80	86.9	34.76	10
4H-1	900	2.66	5.03	1.89	100.0	37.59	n.d.
SiO2	1660	2.19	5.86	2.67	72.4	33.05	35
Polycrystals							
Al2O3	2040	3.15	2.07	0.65	172.4	54.60	n.d.
ZrO2	2650	4.84	2.07	0.42	344.8	71.06	n.d.
Graphite	3650	1.50	2.41	1.61	206.8	137.86	5
BN	2900	1.90	1.38	0.72	89.6	47.15	7
Carbon	3550	2.00	2.07	1.03	413.7	206.80	8-10
Multi-phase							
B	2300	2.36	2.76	1.17	446.2	189.10	115
B4C	2450	2.35	2.27	0.95	568.2	240.30	n.d.
SiC	2690	4.09	3.45	0.84	326.2	79.80	76
Metal							
W	3400	19.4	4.00	0.21	406.9	20.97	13
Mo	2620	10.2	2.21	0.21	358.6	35.16	25
Rene 41	1350	8.25	2.00	0.24	165.5	20.03	25
Steel	1430	7.74	4.14	0.53	200.0	25.84	13
Be	1280	1.83	1.28	0.70	241.4	131.91	127
Whisker Ceramic							
Al2O3	2040	3.96	20.69	5.22	427.5	107.95	3-10
BeO	2570	2.85	13.10	4.59	344.8	120.70	10-30
B4C	2450	2.53	13.79	5.47	482.7	191.26	n.d.
SiC	2690	3.21	20.69	6.44	492.7	150.15	1-3
Si3N4	1900	3.18	13.79	4.33	379.3	119.28	n.d.
Graphite	3650	1.66	19.62	12.00	703.4	423.55	n.d.
Metal							
Cr	1890	7.20	8.89	1.23	241.4	33.47	n.d.
Cu	1033	8.92	2.94	0.33	124.1	13.90	n.d.
Fe	1540	7.83	13.10	1.67	200.0	25.54	n.d.
Ni	1455	8.93	3.86	0.43	213.8	23.71	n.d.

n.d. = no data

As stated before, boron filaments were chosen for this research. The filaments were first produced in 1962 by Texaco Experiment, Inc., and are currently being produced by Avco (Massachuetts) and Hamilton Standard (Connecticut). The boron filaments are produced in a vapor deposition process. Continuous 12 μm diameter tungsten filaments are drawn through a reactor containing boron tri-chloride and hydrogen gas. Resistance heating of the filament causes the following reduction reaction to occur:

$$2BCl_3 + 3H_2 \xrightarrow{\text{Heat}} 2B + 6HCl \qquad (I-1)$$
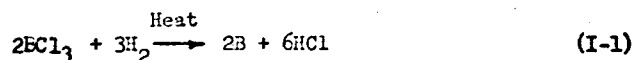
The structure of the boron filament is very complex. The hot tungsten fiber reacts with the boron and forms a brittle tungsten-boride compound. This transformation of the tungsten causes the core of the filament to expand and place the outer sheath of boron in residual tension. This is one of the reasons for the longitudinal cracking found in this size filament. (See Fig. IV-28). The boron deposited was originally thought to be amorphous (Tally, 1959), yet more recent electron diffraction analysis has shown the structure to be very small β-rhombohedral boron crystallites dispersed in a matrix of amorphous boron (Harmond et al., 1966).

The mechanical properties of boron are: Young's modulus - 386 $\frac{GN}{m^2}$, tensile strength 2.98 $\frac{GN}{m^2}$, density 2.56 $\frac{Mg}{m^3}$ (for 100 μm diameter filament), melting point 2300° C, shear strength 3.47 $\frac{GN}{m^2}$, shear modulus 181 $\frac{GN}{m^2}$ hardness is greater than 9 Moh, and Poisson's ratio is 0.21. The filament can be obtained in either 100 or 140 micron diameter continuous filament.

The three spools of boron used in this thesis were obtained from Avco Space Systems and guaranteed to have the following properties:

TABLE I-2

MECHANICAL PROPERTIES OF AVCO BORON FILAMENTS

Property	Spool Number		
	D11061	D11062	YMC672
Tensile Strength GN/m^2	3.00	2.98	3.70
Elastic Modulus GN/m^2	393	402	379
Diameter μm	102	104	141
Density $\frac{Mg}{m^3}$	2.56	2.56	2.48

I.A.2 - Matrix Properties

The second constituent of any composite system is the matrix. The three major types of matrices are polymeric, metallic, and ceramic.

Table III is included to show the different matrix-reinforcement combinations for comparison (Sutton, 1966). Epoxy matrices will be discussed in detail, since they alone are relevant to the present study.

Epoxies are among the most widely used matrix materials in com-

TABLE I-3

COMPOSITE MATERIAL PROPERTIES

Composition		Density $\frac{kg}{m^3}$		Performance	
Matrix	Fiber	Matrix	Fiber	Tensile Strength (GN/m^2)	Specific Strength $(H/S)^2 \times 10^{10}$ *
Al	Boron	2.69	2.52	1.92	0.730
	Borsic	2.69	2.57	1.55	0.552
	Steel	2.69	7.82	1.19	0.230
	EE	2.69	1.85	0.55	0.242
	SiO_2	2.69	2.19	0.61	0.305
	Al_2O_3	2.69	3.97	1.11	0.333
	B_4C	2.69	2.52	0.20	0.077
Ni	B	8.89	2.52	2.64	0.463
	W	8.89	19.3	0.42	0.030
	Al_2O_3	8.88	3.97	1.18	0.104
	C	8.88	1.50	0.34	0.055
Ni-20Cr	Al_2O_3	8.54	3.97	1.76	0.280
Fe	Al_2O_3	7.82	3.97	1.63	0.276
Ag	Al_2O_3	10.48	3.97	1.50	0.221
Epoxy	B	1.28	2.52	2.21	1.163
	C	1.28	1.50	0.55	0.355
	Be	1.23	1.85	0.67	0.428
Ti-6Al-4V	Borsic	4.54	2.67	1.33	0.33

* Assuming 50μ filament.

posite technology. They are strong, rigid, easy to fabricate, produce no by-products and are relatively inexpensive, but they do have limited high-temperature use (< 400° F). (Modern Plastic Encyclopedia, 1971). The epoxies are a family of thermosetting polymers characterized by the epoxide rings (-CH $\overset{O}{\diagup\diagdown}$ CH$_2$) and a two stage polymerization process (Lenz, 1969). The first stage of polymerization produces a linear, low molecular weight polyether. (This condition is known commercially as "B-stage" epoxy and is the "as received" condition for pre-impregnated (Prepreg) boron-epoxy or carbon-epoxy composite tape.) The second stage cross-links the short polyether together into three dimensional polymers as explained by Broutman (1968).

The particular epoxy used in this research is Shell Epon 828, which is a low molecular weight epichlorohydrin/bisphenol A type (DGEBA) epoxy resin. The chemical structure of this epoxy is:

$$CH_2 \overset{O}{\diagup\diagdown} CH-O- \bigcirc -\overset{\overset{CH_3}{|}}{\underset{\underset{CH_3}{|}}{C}}- \bigcirc -O-CH_2-\overset{\overset{OH}{|}}{CH}-CH_2-O- \bigcirc -\overset{\overset{CH_3}{|}}{\underset{\underset{CH_3}{|}}{C}}- \bigcirc -O-CH_2-CH \overset{O}{\diagup\diagdown} CH_2 \qquad (I-2)$$
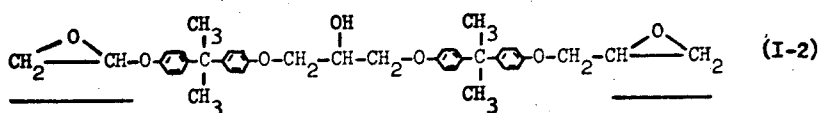
The epoxide rings are the underlined endgroups and are the active sites for the molecule. The resin has a room temperature dynamic viscosity of 10-16 NS/m^2 and an epoxide equivalent of 185-192 (grams of resin containing one gram equivalent of epoxy, see Lee and Neville (1962)).

The epoxy curing agent used was Shell Epoxy Curing Agent Z, which is a mixture of aromatic diamines (no chemical structure

given) and phenyl glycidyl ether ($\bigcirc - O-CH_2 \cdot CH \overset{O}{\diagdown} CH_2$). This combination gives excellent mechanical properties according to Shell (1968), but very little specific information is given.

The effect of the concentration of curing agent and cure cycle of this epoxy system has been extensively studied at the University of Michigan by Helmbuch (1970). The combination of cure agent concentration and curing cycle necessary to provide the best mechanical properties for this system was found to be twenty-five parts of cure agent Z per one hundred parts of 828 resin by weight, with a cure of one hour at 66° C followed by a post cure of 118° C for eleven hours. The following table gives the mechanical properties of the Epon 828 with Z hardener along with the range of values given in the literature for the epoxy family. (Encyclopedia of Modern Plastics, 1971).

TABLE I-4

EPOXY PROPERTIES

Property	Range for General Class of Epoxy	Epon 828 with Z hardener
Tensile Strength	$27.58 - 89.65$ MN/m^2	89.65 MN/m^2
Compressive Strength	$103.44 - 144.82$ MN/m^2	131.0 MN/m^2
Young's Modulus	$2.41 - 3.51$ GN/m^2	2.48 GN/m^2
Elongation (Ultimate)	$3.0 - 6.0\%$	4.8%
Hardness R_m	$80 - 110$	$105 - 110$
Coefficient of Thermal Expansion	$4.5 - 6.0 \times 10^{-6}/C^\circ$	$5.1 \times 10^{-6}/C^\circ$
Heat Distortion Temp *	$46.1 - 287$ C°	145 C°
Density	$1.11 - 1.40$ Mg/m^3	1.20 Mg/m^3
Cure Shrinkage	2 to 3%	2%
Poisson's Ratio	0.34	0.34

* flexural stress 1.71 MN/m^2.

I.A.3 - Interface Properties

The interface between the filament and the matrix is an important entity. After the constituents and the geometry are chosen, only the interface controls the mechanical properties. As will be described in section I-B, the filaments are loaded by a shear stress across this interface. Many of the composite's mechanical properties are dependent upon the strength of this interface, such as transverse strength (Cooper and Kelly, 1967), longitudinal strength (for discontinuous filaments) (Kelly and Davies, 1965), fatigue strength (Boller, 1969), interlaminar shear strength (Prosen, 1969), size of minimum reinforcement (Kelly and Davies, 1965), and longitudinal and transverse modulus (Greszcuk, 1965).

There are two types of bonding present in a composite--mechanical and chemical:

The mechanical bond is due to mechanical interference between the filament and the matrix, whether interlocking or frictional. The strength of the bond is a function of the surface topography of the reinforcement (Harrod and Begley, 1966). Mechanical bonding is considered to be the predominate form of bonding in polymer matrix systems. Boron, having a rough surface resembling that of a corn cob, bonds more than adequately in an epoxy matrix (see Section I-C). Graphite filaments (HMG) have extremely smooth surfaces and efforts are made to "roughen" the surface using oxidation or whisker growth to enhance its bonding to the epoxy (Goan and Prosen, 1969).

Chemical bonding is dependent upon the degree of reactivity between the filament and the matrix. Chemical bonds can be separated

into two categories; the first being the primary or short distance
bond (i.e., metallic, ionic, covalent), and the second being secon-
dary or long distance bonds (e.g., van Der Waal's forces). The
interface or reaction zone will generally become chemically dis-
tinct from either the matrix or filament material (Harrod and
Begley, 1966). The interfacial reaction can also be detrimental
to filament properties (Herring et al., 1971). Metal matrix com-
posites are generally both chemically and mechanically bonded because
of the increased reactivity of the constituents at the temperatures
and pressures necessary for consolidation (Herring et al., 1971;
Braddick, 1971). The shear strength of a chemically bonded interface
is generally greater than the shear strength of the matrix material
(Kreider, 1972).

I.B. Stress, Strain, Strength of Composite Materials

I.B.1. - Strength

In order to predict the properties of a composite material,
it is necessary to have a mathematical model for its behavior. There
are two basic approaches for this modelling, the first being a macro-
scopic analysis, which is simply a rule-of-mixtures approach, and
second, a microscopic analysis called "micromechanics."

Corten (1968) and Grinius (1966) give detailed reviews of micro-
mechanics, which basically is a study of the internal stress distribu-
tions and how they affect the overall performance of the composite.
The effects of geometry, stress concentrations due to filament fail-
ures, non-uniform filament strength, shear stress distribution are

qualified in the analysis; but like many ultra-sophisticated mathe-
matical approaches, it fails to predict some of the trends seen
experimentally (Helmbuch, 1970).

Macroscopic analysis, though simple in approach, is useful in
evaluating a composite's performance. Being a uniform strain
theory, it predicts upper bound behavior (Hosford, 1972). The best
overall treatment of the rule-of-mixtures (or macroscopic) analysis
is found in Kelly and Davies (1968).

In order for the rule-of-mixture analysis to apply, the follow-
ing criteria must be met:

1) Both matrix and filaments are linear elastic materials.
2) All filaments have the same fracture strength.
3) The strain in the matrix is equal to the strain in the
   filament, which is equal to the strain in the composite.
4) The Poisson ratios of the constituents are equal.
5) The filaments are uniaxially aligned in the loading
   direction.
6) The constituents behave when combined as they do when
   separate (e.g., no synergism). (Kelly and Davies, 1965)

The strength of a composite (with continuous filaments) is:

$$\sigma = v_f(\sigma_f) + v_m(\sigma_m') \qquad (I\text{-}3)$$

where σ is the strength of the composite, σ_f is the strength of
the filament, σ_m' is the stress in the matrix at the filament frac-
ture strain, v_f and v_m are the volume fraction filament and
matrix respectively.

The elastic modulus of a composite material is:

$$E = v_f E_f + v_m E_m \qquad (I\text{-}4)$$

with the same subscripts.

The rule-of-mixture analysis predicts a volume fraction filament below which the composite is degraded by the presence of the filaments. This volume is known as the critical volume and expressed mathematically as:

$$v_{f_{crit}} = \frac{\sigma_m - \sigma_m'}{\sigma_f - \sigma_m'} \qquad (I-5)$$

where $v_{f_{crit}}$ is the critical volume, σ_m and σ_f are strengths of the matrix and filament respectively and σ_m' is the matrix stress at the filament fracture strain. The mathematical derivation of equation I-5 can be found in the Appendix. (It is apparent from equation I-3, 4, 5, that a composite material should have as high a volume fraction filament as possible.)

A relationship implicit in the rule-of-mixtures is the critical filament length. The analysis assumes a linear shear stress distribution along the filament axis and the critical transfer length (l_c) defines the shortest filament length necessary to bring the filament stress up to its fracture strength. The critical transfer length is:

$$l_c = \frac{\sigma_f d}{2\tau} \qquad (I-6)$$

where σ_f is the filament fracture strength, d is the diameter, and τ is the interfacial shear strength.

The filaments, being more rigid than the matrix, are loaded by shear stress across the interface. The stress distribution is very important for a composite containing discontinuous (or broken) filaments. The following diagrams (Figure I-1) show both the shear stress

distribution in the matrix and the tensile stress distribution in
the filament, for an elastic matrix and a plastic matrix.
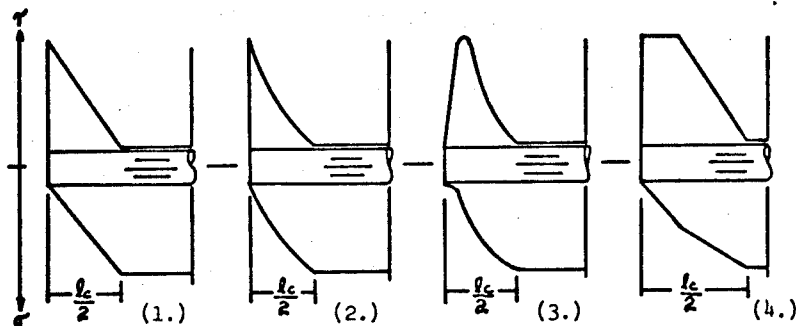
Figure I-1. The shear stress τ and the tensile stress σ distribu-
tions about a filament end. 1, 2, 3 (see text) repre-
sent elastic matrices and 4 plastic.

The stress distribution shown for the elastic matrix are: 1)
the linear stress distribution assumed in the rule-of-mixture analy-
sis, 2) the theoretical stress distribution (Dow, 1963), and 3) the
experimental (photoelastic) stress distribution (Shuster and Scala,
1965).

The theoretical stress-strain curve for a fiber reinforced
material is shown below. (Kelly and Lilholt, 1969)
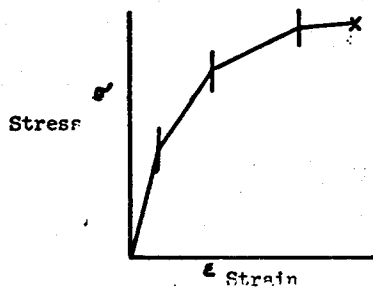
Figure I-2. Theoretical composite stress-strain curve.

The four stages of deformation are: 1) elastic fiber and elastic matrix deformation, 2) elastic fiber and plastic matrix deformation, 3) plastic fiber and plastic matrix, 4) filament fracture and plastic matrix deformation. In the boron-epoxy system only the first two stages will exist. It has been shown by Kelly and Davies (1965) that the matrix must undergo plastic deformation if the fiber is to be stressed to fracture point. (This assumes that the yield strain of the matrix is less than the fracture strain of the filament.)

When the filaments are ductile (e.g., metal wires), the filament fracture strength (σ_f) is uniform and the rule-of-mixture analysis accurately predicts the composite performance. (Although ROM assumptions 1) and 4) are not met, Cooper and Kelly, 1967.) On the other hand, high strength filaments being very brittle, display a wide range of fracture strengths. Figure (I-3) gives the strength distribution of boron filaments (Metcalfe, 1967). This violates assumption 2) and causes the rule-of-mixture's prediction to be more disparate, (Mehan, 1967 and Kreider and Leverant, 1966).
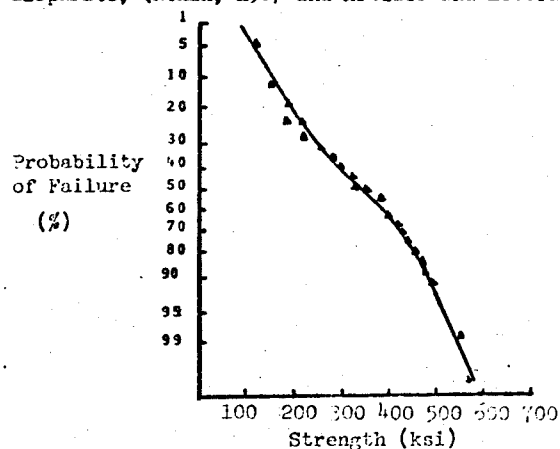
Figure I-3. Boron filament strength distribution.

I.B.2 - Stresses in a cracked body

Cracks present in a stressed body will greatly affect the local stress field about the crack. Cook and Gordon (1964) and others have analyzed the stress distribution for a cracked, but otherwise, homogeneous, infinite isotropic body. Figure I-4 shows (a) - the contours of the stress perpendicular to the loading direction (σ_x), (b) - the contours of the stress in the loading direction (σ_y), and (c) - the shear stress contours (τ_{xy}). It is of interest to note the positions of the maximum σ_x and τ_{xy} contours.

σ_x (a.) σ_y (b.) τ_{xy} (c.)
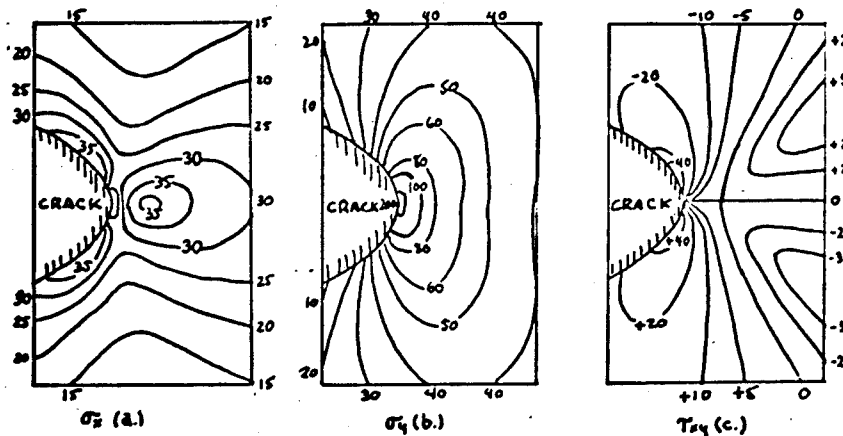
Figure I-4. Stress contours about a crack in an isotropic solid (see text for details).

Cook and Gordon examined the stress state along the crack plane. The only stresses appearing on this plane are σ_x and σ_y , which are shown in Figure I-5 as a function of distance from the crack tip. Note the position of the σ_x maximum, which is about one crack radius ahead of the tip.

A mechanism was proposed for improving the notch-sensitivity of glass by Cook and Gordon. It was argued that if a weaker interface

were placed parallel to the stressed direction (assuming fail-
ure on this plane), it would fail by the σ_x tensile stress.
Figure I-5 indicates that the strength of this interface should be
one-fifth the cohesive strength of the brittle material. Although
there are other proposed failure modes of this interface, (e.g.,
shear failure) a tensile debond is most likely.

Crack Tip Radii
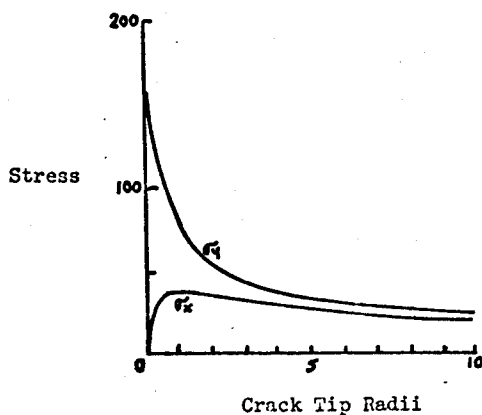
Figure I-5. σ_x and σ_y stress contours in the crack plane
(see text for details).

This mechanism was based on an isotropic material with a plane
of weakness placed before the crack. None-the-less, even current
researchers in the field of composites [Toland, 1972, Hoover and
Allred, 1972, etc.] have ignored these restrictions and applied the
"Cook and Gordon" mechanism to filamentary composites. They assumed
that if the tensile strength of the interface were less than one-
fifth the cohesive strength of the matrix, a matrix crack would
debond the interface and blunt the crack. They met with failure
because of the inherent anisotropy of composite materials.

Gilliland (1967), see Kelly (1971), analyzed the stress distri-
bution of a cracked anisotropic body. The degree of anisotropy was

equivalent to that of a carbon-epoxy composite with fifty percent
filaments. In Table I, a comparison between the isotropic and
anisotropic analyses is given.

TABLE I

STRESS RATIOS IN A CRACKED BODY

	Gilliland (1967) Anisotropic	Cook and Gordon (1964) Isotropic
Maximum σ_y/σ_x	47	5
Maximum σ_y/τ_{xy}	11	4
Maximum τ_{xy}/σ_x	4.4	1.5

It becomes apparent that the interface must be ten times weaker
than was previously estimated. This eliminates the tensile debond
as a failure mechanism for high volume percent filament composites
that have any useful interfacial shear strength.

The degree of anisotropy is directly related to the volume
percent filaments for a given system. The low interface strength
necessary for tensile debonding forces the critical transfer length
to be excessively long.

Some experimental evidence is available to substantiate the
above hypothesis. Cooper and Kelly (1967) experimentally determined
the (σ_y/σ_x) strength ratio for tensile debonding in the Copper-
Tungsten system. Even though this is among the most isotropic of
composite systems, the strength ratio was over two and a half times

that predicted by the isotropic analysis.

I.C. Fracture Studies of Composite Materials

The major portion of the fracture study of composite materials with polymeric matrices has been performed on the fiberglass system, (cf, Corten, 1967; Broutman, 1967; Bouc, 1962). There, the fibers have a fracture strain comparable to that of the matrix, so that debonding of the fiber without breaking is often seen. In contrast, the breaking strain of boron fibers is much less than that of the matrix, so that the glass fiber data are not generally applicable to the system of interest here.

Mullin et al. (1968) performed the early fracture analysis work on the boron epoxy system. They were able to identify four fracture modes. The four modes appear schematically in Figure I-6.
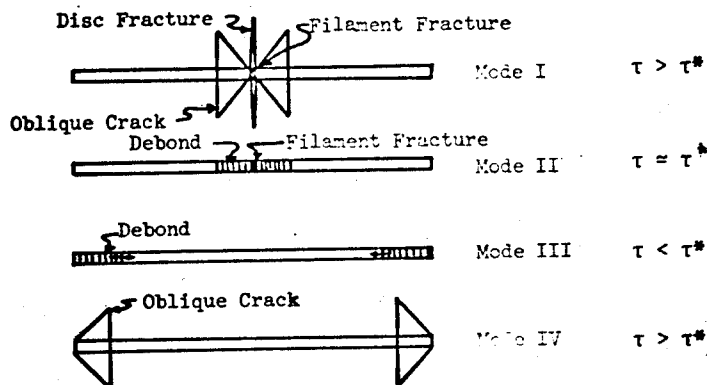
Figure I-6. Fracture modes in boron epoxy composites (Mullin et al., 1968).

Mode I is characterized by a disk shaped matrix and/or oblique
matrix cracks emanating from a filament fracture. For Mode I to
be operative, it is necessary for the composite to have a strong
interfacial shear strength.

A second mode of failure, Mode III, is a result of too low
an interfacial strength, ($\tau < \tau^*$). The filament in this
case completely debonds from the matrix beginning at the highly
stressed filament ends, as seen in Figure I-2. Mode II is the
result of a composite having an interfacial strength intermediate
between those of Mode I and Mode III. The filament fails and its
fracture energy is dissipated in the debonding of the interface.
It should be noted that the debond does not continue along the
length of the filament as in Mode III. Mode IV is a special fracture
mode operable under the conditions of a weak matrix and a strong
interface. The matrix fractures in the highly stressed filament end
region.

It is obvious that Mode II is the most desirable fracture mode;
for future reference, the interfacial shear strength associated with
Mode II will be called τ^*. It follows that the interfacial shear
strength of Mode I is greater than τ^*, and Mode III has an inter-
facial shear strength less than Mode II's.

The type of fracture mode operating in a composite is dependent
upon interface strength, matrix strength, filament strain energy,
strain rate and notch sensitivity of its matrix, and strain history
(Mullin, 1968).

Recent work by Heimbuch (1970) on boron-epoxy composites does
not show all of the fracture characteristics described above. For

example, Mode IV is not observed, oblique cracks in Mode I are not
observed, and the effect of strain rate is not evident in the
transition from one mode to another. The matrix epoxies are dif-
ferent and it can be assumed that DEN 438 used by Mullin et al.,
is more strain rate sensitive than EPON 828 used by Heimbuch.

Further work by Mullin et al. (1970) and Heimbuch (1970) shows
the effect of altering the interfacial strength. Using simple
monofilament specimens, Mullin showed the effect of reducing the
interfacial shear strength. By coating boron filaments with
graphite and teflon they were able to reduce the interfacial shear
strength to a τ* value and less than τ* value respectively
from the high interfacial strength of the 'as received' filament.
The shear strengths were not quantified in any way. Figure I-7
shows the effect of the different interface strengths on the stress-
strain behavior of simple composites.
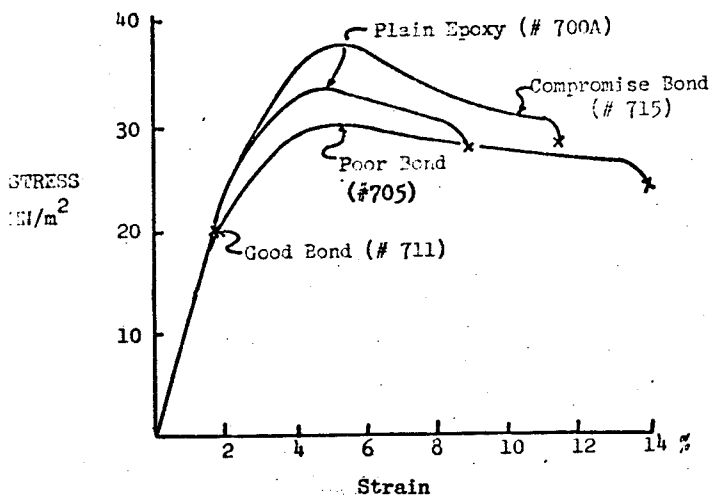
Figure I-7. Stress-strain curves for coated monofilament composites.

It should be noted that these composites are far below the
critical volume. It should also be noted that the strain (elonga-
tion) to failure of the "poor bond" specimen (#705) exceeds that
of the plain epoxy (#700A). The teflon coated sample (#715) ex-
hibits Mode II type of failure and the graphite coated (compromise)
bond (#701) exhibits Mode III failure; the fiber even after frac-
ture partially reinforces the composite. The 'as received' or
good bond (#711) exhibits Mode I failure.

Heimbuch also found an enhancement of tensile properties with
a degradation of interfacial strength. He used a wetting agent
(WD40) as a bond reducer and showed an increase in strain to failure
in composites with a volume fraction filament varying from 1-50%.
The strain to failure of the composite never exceeded the strain to
failure of the matrix material.

Heimbuch has shown a transition fracture mode in simple compos-
ites by altering the matrix ductility. A "brittle" epoxy can with-
stand fewer filament failures than a "ductile" epoxy. He altered
the ductility of the matrix material by altering the amount of curing
agent and the cure cycle.

The fracture mechanisms in metal matrix composites have been
investigated by a number of researchers (Herring et al., 1971;
Braddick, 1972). The fundamental difference between polymer matrix
composite failure and metallic matrix composite failure lies in the
ductility and strength of the matrix. A typical metallic matrix
composite fractures in two steps. First the filaments fracture either
randomly or cummulatively with no matrix separation, and the fila-
ment fracture energy being dissipated in plastically deforming the

matrix. After the filaments have failed locally, the matrix separates. A crack, per se, does not propagate from filament to matrix to filament as in the polymer systems.

Fracture propagation in the ceramic or non-metallic elemental matrix composite system is distinct because the strain to failure of the matrix is less than the strain to failure of the filament. A ceramic matrix composite will fail in two steps; first the matrix fails in a series of closely spaced parallel cracks perpendicular to the filaments. The spacing is a function of the interface strength. The filaments, being the main load carrying members, do not fracture until their strain to failure is reached. (See Cooper and Kelly, 1968; Sambell et al., 1972; and Cooper and Sillwood, 1972.)

I.D. Fracture Toughness Considerations

I.D.1. - Homogeneous Materials

The fracture toughness of a material is the energy required to propagate a crack through unit area, and quantifies a material's resistance to a crack propagation.

The discrepancy between the theoretical fracture strength (E/10) and the measured fracture strength (E/1000) of completely brittle materials was explained by Griffith (1924). He proposed that real materials contain flaws and it is these flaws that reduce the fracture strength. If the material were completely brittle, (e.g., no irreversibilities such as plastic deformation), the flaws would not grow until the strain energy release rate with crack extension exceeded the rate of increase of surface energy, and then they would grow catastrophically. Mathematically, then, the stress necessary for

unstable crack propagation in an infinite solid is:

$$\sigma_f = [\ 2E\gamma' / \pi c]^{1/2} \qquad (I-7)$$

where γ' is the surface energy, E is Young's modulus, and c is the half-length of the flaw.

The Griffith theory was modified and applied to 'quasi-brittle' materials by Orowan (1948). If the plastic deformation were restricted to a very thin layer surrounding the crack, and if there were no gross yielding (i.e., the remainder of the material was elastic), the following equation could be applied:

$$\sigma_f = [\ Ep\ /\ c\ ]^{1/2} \qquad (I-8)$$

(Felbeck and Orowan, 1955)

The important thing to note is the replacement of γ' by P, the plastic work function (actually it is (p + γ'), but p >> γ' and (p+γ' $\simeq$ p).

Irwin (1956) originated the concepts of fracture toughness and fracture mechanics. The original fracture toughness equation is:

$$K_c^2\ /\ E = G_c \qquad (I-9)$$

where G_c is the crack extension force and K_c is the fracture toughness. An alternative definition for G_c is the critical strain energy release rate and K_c is the critical stress intensity factor. Fracture mechanics is the "science" of predicting, mathematically, the fracture strength of a cracked member, assuming that the fracture

toughness is an invariant property of the material. When fracture
mechanics is applied to a brittle, infinite plate, the fracture
strength is:

$$\sigma_f = [\ EG_c/\ \pi c\ ]^{1/2} \qquad\qquad \text{(I-10)}$$

The problem in fracture mechanics is in determining the quantity
G_c , because the specimen design must preclude plastic deformation
(or other irreversibilities). For a more complete treatment of frac-
ture mechanics, see Tettleman and McEvily (1969) and Brown and Srawley
(1968).

An experimental method for determining the crack extension force
(G_c) was advanced by Irwin and Kies (1952), using the following equa-
tion:

$$G_c = (P^2/2)\ \partial(1/k)/\partial A \qquad\qquad \text{(I-11)}$$

The quantity "P" is the load at which the crack propagates, and $(\partial(1/k)/\partial A$
is physically the change in specimen compliance with crack area. The
equation is derived in the Appendix.

The main thrust in recent years has been to derive the fracture
toughness parametrical relationship analytically rather than experi-
mentally. (Brown and Srawley (1968).

The fracture toughness equation for an isotropic, linear elastic
material always takes the form:

$$K_{1C} = \sigma\sqrt{a\pi c} \qquad\qquad \text{(I-12)}$$

where σ is the net cracking stress, and 'a' is a function of the geometry and starting crack length. This factor 'a' is analytically determined from the exact or approximate solutions to the crack stress equations (ASTM STP 381, page 30).

An alternative approach to the fracture toughness question has been advanced by Gurney and Hunt (1967) using a work balance theorem for a quasi-static crack growth. The work theorem for a quasi-static process is:

$$Xdu - d \text{ (strain energy)} - G'dA = 0, \qquad (I-13)$$

where X is the external load, u is the displacement of the test piece, G' is the irreversible and delayed reversible work per unit area of crack surface, and A is the crack area.

The fundamental difference between this last theory and the previous ones is the emphasis on the quasi-static crack propagation (stable cracking) using a strain energy analysis, rather than a crack stress analysis. The Gurney theory takes into account the strain energy of the test piece, stiffness of the testing machine, etc.

With the proper specimen design, the strain energy of the test piece can be minimized to a point where the crack is driven stably by the testing machine, and not unstably by the specimen strain energy.

If non-linear elastic effects and residual stresses are negligible, the Gurney equation may be written:

$$Xdu = GdA + \tfrac{1}{2}d\ (u.x) \qquad (I-14)$$

where G is now the fracture toughness. The (x/u) relationships may be obtained from elasticity theory.

If a quasi-static crack growth condition is met, the complete fracture toughness parameters, G and $\frac{dG}{da}$ may be generated from a single test. (See Appendix for a graphical representation of the Gurney approach.) For a more complete treatment of this theory, see Gurney and Hunt (1967) or Atkins et al. (1972).

All of the previous equations were derived for isotropic and homogeneous materials. Filamentary composites are inherently inhomogeneous and anisotropic. The effect of the anisotropy has been included by Sih et al. (1967). Irwin's isotropic relationships:

$$G_c = K_c{}^2 / E \qquad (I-8)$$

becomes:

$$G_c = K_c{}^2 \{[a_{11}a_{22}/2]^{1/2}[(a_{22}/a_{11})^{1/2} + (2a_{12} + a_{66})/2a_{11}]^{1/2}\} \quad (I-15)$$

The a_{ij} are the elements from the compliance matrix.

It has been hypothesized and "proven" that linear elastic fracture mechanics is applicable to anisotropic cracked bodies if the stresses are applied in the planes of symmetry (Beaumont, 1971).

I.D.2. - Composite Materials

The filamentary composite materials exhibit much greater fracture toughness than their constituents separately (Outwater, Murphy, 1967, and Kelly, 1970). The increase can be attributed to a composite's inhomogeneity and, therefore, to its interface. Fiberglass has a fracture toughness about three orders of magnitude over that of its constituents.

Many mechanisms have been advanced to explain this synergism, including: frictional work of filament pullout (Cottrell, 1964; Kelly, 1965); debonding of the interface before filament fracture (Outwater, Murphy, 1967); redistribution of stresses following filament failure (relaxation of stresses) (Beaumont et al., 1972). This paper will advance a fourth theory in Chapter V.

The filament pullout (or frictional work) theory of energy dissipation was the earliest of the analytical work of fracture theories (Kelly, 1965). The mechanism of pulling the fibers out of the matrix absorbs the energy. These assumptions were made: 1) fibers will break randomly, 2) the original shear strength of the interface, "τ", is maintained during filament pullout, and 3) there is negligible plastic flow of the matrix. Mathematically, the work of fracture due to filament pullout is:

$$\gamma = v_f \sigma_f l_c / 24 \qquad (I-16)$$

where γ is the work of the fracture, v_f is volume fraction filaments, σ_f is the strength of the filaments and l_c is the critical transfer length.

This theory generally predicts higher values for the work of fracture than actually measured. This is due in part to the second assumption (maintained shear strength) Beaumont, (1971). Equation I-16 is derived in the Appendix.

The debonding theory was first advanced by Outwater and Murphy (1967) and is predicated on the assumption that the filament debonds over a length under the influence of the crack's stress field before the filament fractures. Figure I-8 schematically shows the debonding

process (see section I.B.2).
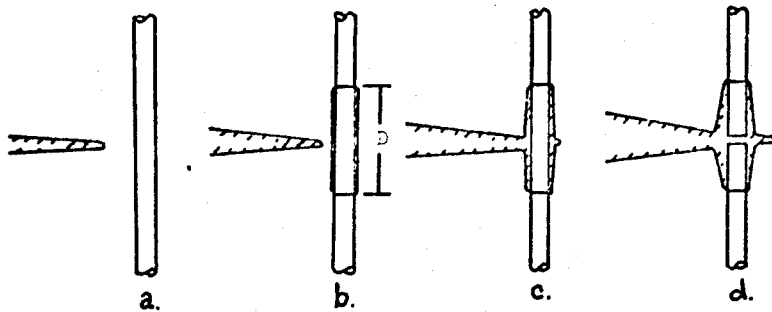
Figure I-8. Schematic representation of the debond mechanism.
a - crack approach, b - debonding of the interface,
c - crack continuation with the filament intact,
d - filament fracture.

Physically, the energy of the debonding process is equated to
the elastic strain energy stored in the filament after debonding.
(See Appendix for the derivation of the work of debonding.) The work
of debonding is:

$$\gamma = v_f \sigma_f^2 D / 4E_f \qquad (I-17)$$

where v_f is volume fraction filaments, σ_f is the filament's strength,
E_f is filament modulus and D is the length of the debond zone (this
must be measured experimentally).

The debond theory works very well for the fiberglass system for
which it was developed, but with less success for other composite
systems (see Beaumont and Phillips, 1972). Implicit in the theory is
the relationship of the failure strain of the matrix being equal to or
less than that of the fiber. In Table II, a comparison between the
strain to failure of glass, boron, and carbon fibers, and that of typi-
cal matrix materials is shown.

TABLE I-5

FRACTURE STRAINS OF SELECTED MATERIALS

Material	Strain to Failure (%)
Boron	0.8
S-Glass	2.4-5.1
Graphite	0.4-1.0
Epoxy	2.0-6.0
Polyester	2.0-5.0

This table shows why the debond mechanism is possible in the fiber-glass and not in the boron or graphite epoxy system.

The relaxation theory of the work of fracture has been recently advanced by Beaumont (1972). The energy dissipating mechanism is the redistribution of strain energy from the fiber to the matrix. When a filament fractures, the relatively unstressed matrix surrounding the filament break must assume the load. Figure I-9 shows the redistribution of stresses.
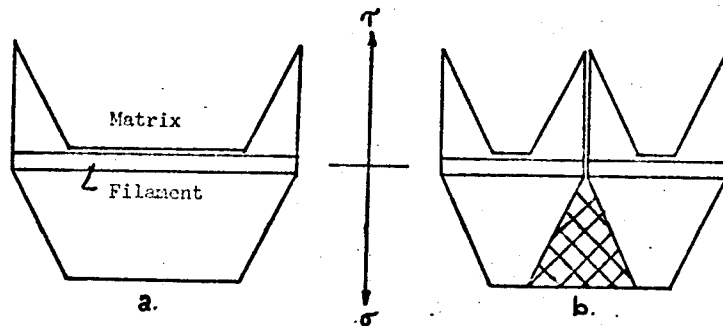
Figure I-9. Schematic representation of the relaxation mechanism.
(a) stress distribution before filament fracture,
(b) stress distribution after fracture, the cross-hatched area represents the amount of strain energy lost.

The cross-hatched portion represents the filament strain energy con-
sumed. A derivation of the relaxation theory may be found in the
Appendix, the end result being:

$$\gamma = v_f \sigma_f^2 l_c / 6E_f \qquad (I\text{-}18)$$

Where γ is the work of the fracture, and l_c is the critical length.

The work of fracture of a composite material is measured by
graphically integrating the load-deflection curve of a fracture tough-
ness test. This will be the work (or energy dissipated) in fracturing
the specimen. This quantity is divided by the net cross-sectional
area of the specimen, giving the work/unit area or work of fracture
denoted by γ . (It should be noted that this is not the surface
energy ' γ' ' found in the Griffith equation.)

CHAPTER II

The Intermittent Bond Concept

The concept of a controlled, intermittent, interfacial bond strength in a composite material is to be applied and evaluated in this thesis. Many mechanical properties of a composite are dependent upon a strong interfacial bond between the fiber and the matrix, as shown in section I.A.3. None-the-less, a viable composite must possess a certain fracture toughness, which is dependent upon a weak interface. A compromise between mechanical properties and fracture toughness must be made if the bond strength is considered invariant along the fiber.

There would be no need for a low bond strength if all the filaments failed at the same stress, since the composite would fail completely when the composite strain reached the fracture strain of the filaments. Boron filaments (see Figure I-3) exhibit a wide range of strengths, from 1.30 to 3.40 $\frac{GN}{m^2}$ (190-490 ksi). If the first filament failure initiates a catastrophic crack as a result of a strong interface, the maximum filament strength (σ_f) that can be used in the rule-of-mixtures analysis is 1.3 $\frac{GN}{m^2}$ (190 ksi) rather than the average strength of 3.00 $\frac{GN}{m^2}$ (435 ksi), delineated in section I.B.2. The potential strength of the composite is reduced to below 1.0 $\frac{GN}{m^2}$ (145 ksi) and it is no longer a competitive material, as the raw material cost of boron-epoxy is $450/kg.

A composite can be made to exhibit the favorable mechanical properties of a strong interfacial bond and the fracture toughness of a

weak interfacial bond, if an alternating bond strength is introduced
along the filament. Figure II-1 shows a filament intermittently
coated with a material that reduces the interfacial bond, giving
regions of high and low interfacial strength.
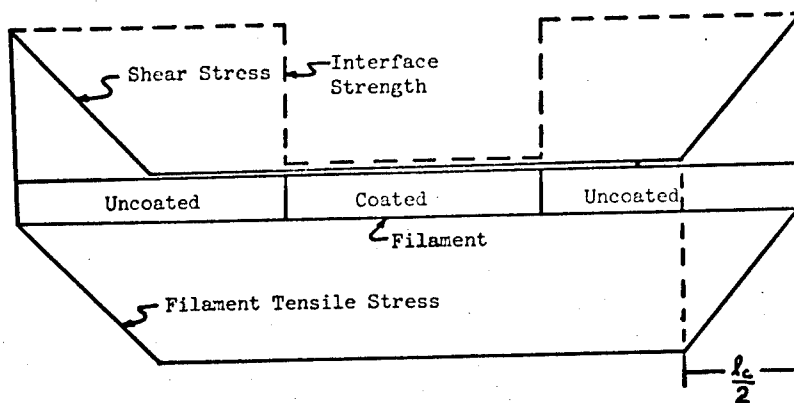
Figure II-1. Schematic representation of the intermittent bond
concept.

The area above the filament shows the shear stress distribution
of the interface, and the area below shows the tensile stress distri-
bution in the filament (see Figure I-1). Superimposed over the shear
stress distribution is the interfacial bond strength distribution,
denoted by a dashed line. A simple criterion for the interface fail-
ure is employed: if the applied stress exceeds the interfacial
strength, the bond fails. Note that the low bond strength affects
neither the shear stress distribution nor the tensile stress distri-
bution. The area of the tensile stress distribution of a filament
gives a measure of reinforcement afforded to the composite.

The intermittent-bond type of composite prevents low strength
filament failure from initiating catastrophic cracks in two ways:
first, by preventing matrix crack formation through debonding of the

interface, and second, stopping matrix cracks by blunting or tensile
debonding.

Figure II-2 shows the sequence of events that prevent a fila-
ment failure from initiating a matrix crack. The coated region
exhibits mode III behavior, the debonding does not continue the
length of the filament but stops at the beginning of the high strength
region. As a result , partial reinforcement is still provided by the
broken filament
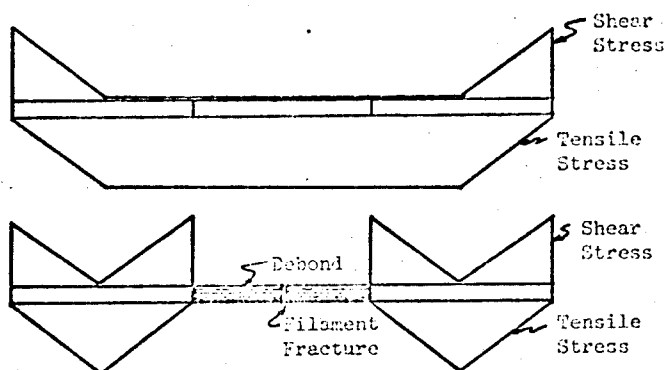
Figure II-2. Filament fracture in a coated (weakly bonded) region
(see text for details).

The debond mechanism is operative only when the fractures occur
in the low strength region. The flaws which cause these filament
failure are randomly distributed along the filament, hence the per-
centage of fractures that occur in a coated region are:

$$F_{fc} = L_c / L_c + L_{uc} \qquad \text{(II-1)}$$

where L_c and L_{uc} are lengths of the coated and uncoated regions.

On a certain number of occasions $(1-F_{fc})$, the filaments will fail
in a high strength region. This region exhibits mode I type of frac-

ture because of the high interface strength, and the matrix cracks are formed from filament failure. The regions of high and low strength bonds will be randomly arranged in the composite, therefore, a crack can only propagate across a finite number of filaments ($\frac{1}{F_{fc}}$) before it encounters a weak interface region. As seen in section I-B-1, the stress field associated with a crack will debond an interface one crack tip radius away if the interface has a tensile strength of one-fiftieth the cohesive strength of the matrix. Assuming the tensile strength of the weakly bonded region is below this figure, the crack will be blunted by this debonded interface. Figure II-3 shows a matrix crack encountering a weakly bonded region.
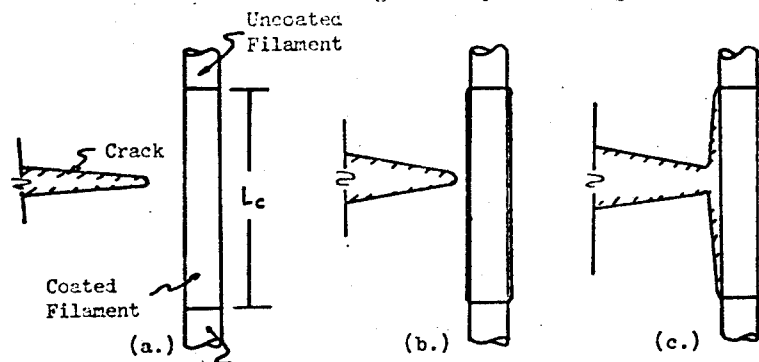
Figure II-3. Tensile debond mechanism (see text for details).

The design strength of the interfacial bond in the coated region is restricted by both mechanisms. The shear strength must be less than T^* and the tensile strength must be one-fiftieth that of the cohesive strength of the interface. The exact relationship between shear strength and tensile strength has not been deduced. Experimentally, the tensile strength of an "as received" boron epoxy inter-

face is from 6.9 - 8.3 $MN/_m2$ (1.0 - 1.2 ksi); and the shear strength, depending on the test method, is from 41.3 - 69.0 $MN/_m2$ (9.0 - 10 ksi). A ratio of one to eight is assumed in this research, for all conditions of boron filaments.

CHAPTER III

Experimental Procedure

III.A   Specimen Design

III.A.1.   Tensile Test Specimen

III.A.1.a.   Composite Specimens

A tensile specimen design for the boron epoxy system was chosen, incorporating a monolayer of boron filaments. The monolayer consists of twenty-five filaments spaced 0.25 mm apart, center to center distance, with the filaments running continuously lengthwise through the specimen. The dimensions of the test section are   6.7 mm (0.263 in) wide by 1.6 mm (0.0625 in) thick, and 57.3 mm (2.25 in) long. This gives a volume fraction filament of two percent. This percent filament is slightly above the critical volume for this system, as discussed in section I-C-1, indicating the composite strength will be slightly greater than the matrix strength. The composite, none-the-less, will be filament fracture controlled, since the ε_f of the composite will be the ε_f of the filament. The composite fracture strain will be used to measure the effectiveness of the intermittent coating. Figure III-1 shows the specimen dimensions.

Low volume fraction filament composites are easier to fabricate, consume less boron filament than high volume fraction filament composites, and are still filament fracture controlled. The simple composites have an additional advantage: the fracture sequence can be easily deduced using fractographic analysis. The fracture sequence will determine the feasibility of the intermittent bond concept (see
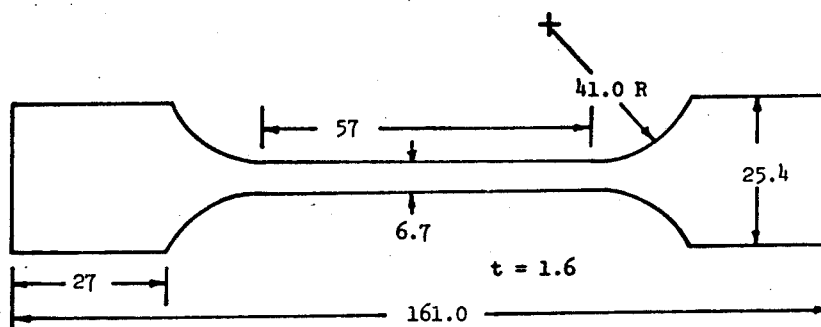
Figure III-1. Composite Tensile Specimen. All dimensions are in mm.

section II-1).

III.A.1. b. Matrix Specimens

The matrix material, though not of primary importance in this research, must not become a source of error by varying in properties too much. To monitor the quality of the matrix properties, tensile specimens of pure epoxy were cast in the same molds as the composite specimens. An accurate stress-strain relationship for the epoxy was obtained using precision strain measuring devices (see section III-B). The specimen would also expose any defects in the mold design or molding procedure. Since the specimens were to be compared only with one another, a non-ASTM type of specimen was deemed adequate.

III.A.1. c. Pullout Specimens

Pullout test specimens were designed to evaluate the coating. This specimen is simply a cylinder of epoxy, cast around a coated or

uncoated filament. The free end of the fiber is glued in a hypo-
dermic needle to facilitate gripping in the tensile machine. To
avoid breaking of the filament, tho height of tho epoxy cylinder
must be less than one-half the critical length, as defined in sec-
tion I-B-1 . Figure III-2 shows the mold and a complete specimen.
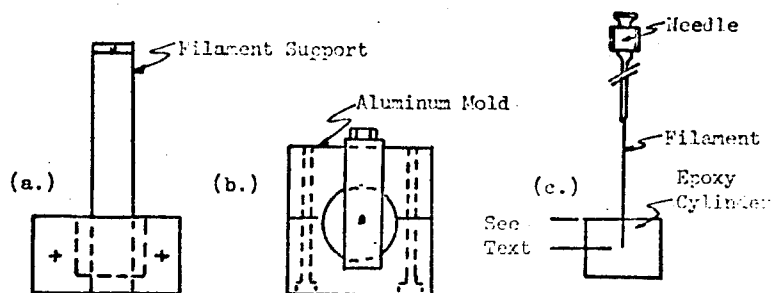
Figure III-2. Drawing of the pullout specimen and its mold.
(a) mold-front, (b) mold-plan and (c) complete
specimen.

III.A.1. d. Filament Tensile Specimens

A small number of filament tensile tests were run to determine
if the mechanical properties of boron filaments degrade with time,
since the spools were purchased in 1968. A section of filament was
glued into two hypodermic needles spaced 25 mm apart. The needles
were then gripped in the tensile machine using standard friction
grips.

III.A. 2.   Fracture Toughness Specimens

Fracture toughness cannot be measured in a simple composite as
can the composite fracture strain. A volume fraction filament
specimen of forty percent was chosen because it gives realistic
toughness values, corroborated in recent literature. The specimen
design chosen was a square bar of composite 5 mm x 5 mm by 40 mm
long. Two notches were cut with a diamond saw at the midsection
of its beams, forming a triangular test section. The test is con-
ducted in three point bending, putting the tip of the isosceles tri-
angle in tension. The tip experiences an infinite stress, according
to elasticity theory, and the fracture consistently begins at the
tip. The design was advanced by Tattersal and Tappin in 1967 for
use in practically all materials. It has been widely accepted by
composite researchers. Figure III-3 illustrates the specimen design.
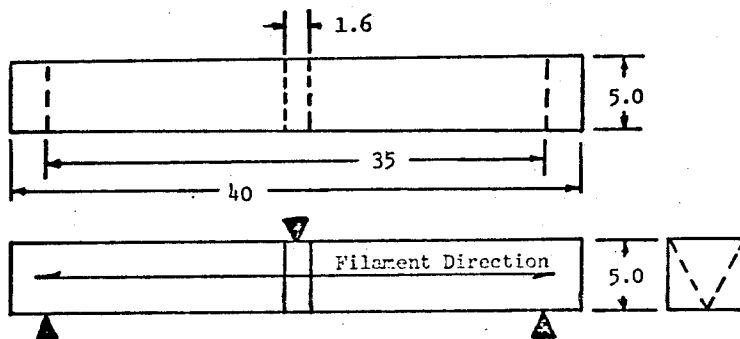
Figure III-3. Notched three point bend fracture toughness specimen.
All dimensions are in mm.

The specimen was designed to measure crack opening (Mode 1)
fracture toughness. To avoid incorrect toughness values, the
fracture must be completely tensile in nature. To preclude any
shear failures, the ratio of transverse shear stress to flexural
stress must be minimal. Using Sattar and Kellogg's theory of
bending failure (1969), a length to span ratio of 7.5 was chosen
for the specimen.

For reasons which will be discussed in Chapter V, namely
gross filament damage, the bend toughness specimen gives question-
able results. A tensile fracture toughness specimen was designed
to minimize filament damage using criteria set forth in ASTM STP 410
(1966). Figure III-4 gives the specimen design. The specimen con-
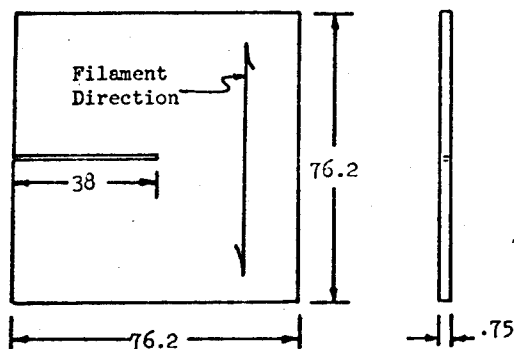
Figure III-4. Compact Tensile Specimen. All dimensions
are in mm.

sists of five layers of boron filaments spaced 0.19 mm center to
center distance, cast in an epoxy with external dimensions of 0.750
mm (0.03 in) thick by 76.2 mm (3.00 in) long by 76.2 mm (3.00 in)
in height; this gives a volume fraction filament of 48 percent.

A starting crack length of 38 mm was employed, the specimen being gripped with pad type friction grips in the tensile machine.

III.B. Mechanical Testing

III.B.1. Tensile Testing

All mechanical testing was conducted on a "table top model" Instron tensile machine with a full load capacity of 500 kg. The load cell, number 500 kg - 025, was calibrated for 1, 5, 10, 20 and 50 kg per division. One division equals one-tenth of the full-scale deflection. The cross-head velocity of this screw-driven machine was normally 0.5 mm/minute except where noted. The tensile machine was calibrated every test series using dead weights as per instruction. All tensile tests were run with an initial grip separation of 95 mm, using the standard Instron friction grips.

All tensile strain measurements were made with an Instron strain gage-type extensometer using clip-on mounting. The extensometer drives the load chart through a strain gage amplidyne. The extensometer model number G-51-11M, serial number 3458, had a 25 mm gauge length and a maximum deflection of 2.5 mm. The extensometer is linear to better than one percent throughout its range. The extensometer was calibrated before and after each test series using a micrometric calibrator. The average of twelve calibration measurements, six taken before the test and six after, was used to convert chart travel to specimen strain. The maximum spread of calibration measurements was less than two percent.

The following Table III-1 gives the strain magnification factors
for the various tensile tests.

TABLE III.1.

TENSILE STRAIN MAGNIFICATION FACTORS

Tensile Specimen	Magnification Chart Distance Specimen Extension	Maximum Strain
Composite	1000	1%
Epoxy (for modulus)	1000	1%
Epoxy (for failure strain)	200	5%

III.B.2. Fracture Toughness Testing

III.B.2.a. Bend Specimen

The fracture toughness bend specimens were tested in a three-
point bend jig in the Instron testing machine. The jig consists of
a base plate and an anvil. The ground steel base plate supports two
parallel, hardened steel cylinders, 6.5 mm in diameter, epoxied
35 mm apart (centerline to centerline distance). The anvil is simply
a ground steel block with a 6.5 mm (diameter) hardened steel cylinder
epoxied to the center of the block. Figure III-5 is a photograph of
three-point bending jig with a toughness specimen in the Instron
testing machine.

The tensile machine is converted for compression testing by
placing the load cell below the specimen. After calibrating with
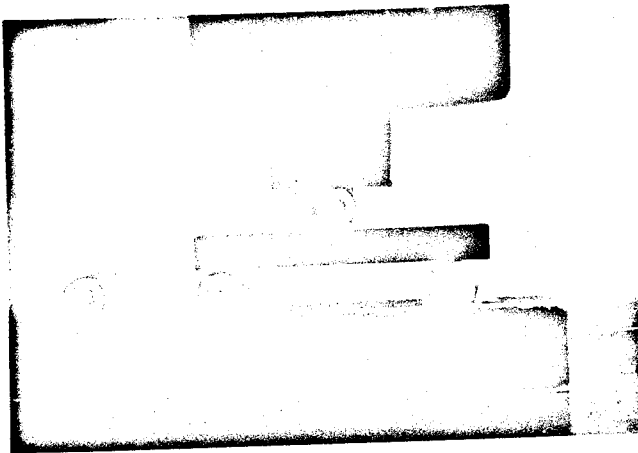
Figure III-5. Three point bend jig with specimen.

dead weights, the base plate is placed on the compression platen and
its weight is balanced out electronically. The specimen is then
centered over the cylinders by matching the test section with the
scribed mid-line of the base. Next, the anvil is centered over the
specimen and the cross head of the machine is lowered manually until
contact is made with the anvil.

All bend tests were conducted with a cross head velocity of
0.5 mm/minute with a chart speed of 50 mm/minute and a full scale
sensitivity of 100 kg. The ratio of specimen deflection to chart
distance was 100:1. Any change in these standard test conditions
was noted with the data.

When testing in compression with a screw driven testing machine,
it is always necessary to account for machine stiffness. This is

particularly true when determining the modulus of a compression or flexural specimen, because the measured stiffness is the sum of the specimen stiffness (the quantity desired) and the machine stiffness. The machine stiffness can be ascertained by compressing the load cell directly with the cross head. The machine stiffness of the Instron used in this research is given in the Appendix.

In fracture toughness testing, the area of the load deflection curve is important and the correction for machine stiffness is unnecessary if the specimen fractures in a controlled manner, that is, if the machine strain energy does not cause instability in the specimen. Figure III-6 illustrates an idealized load-deflection curve of a bend toughness specimen. The solid line represents the load deflection curve of the total system. If the machine deflection is subtracted from the total response, the resulting load-deflection curve represents the response of the specimen, as shown by the dashed line. The areas of the two curves are the same, demonstrating that the strain energy of the machine is reversible. No correction is necessary if the final load is allowed to approach zero.

III.B.3. Interlaminar Shear Strengths

The interlaminar shear strengths of the composite bars used for the fracture toughness bend specimen were measured with a short span, three-point bend test. The transverse shear stresses are greatest for short spans. Shear failure could be insured if the span to depth ratio were from four to one. (ASTM STP 460, 1969) The test conditions were identical to the fracture toughness bend test except that the cylinders were spaced 20 mm apart and the full scale sensi-
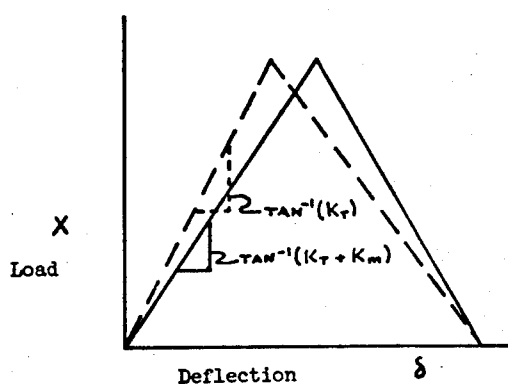
Figure III-6. Idealized load-deflection curve for three point
              bending.

tivity of the load cell was increased to 200 kg.

III.C. Specimen Preparation

III.C.1. **Preparatory Methods**

III.C.1.a. Filament Coating

The coating assembly has three components, the filament drive
system, the filament positioning device, and the actual coating
mechanism including the timer.

The filament drive system is a standard filament spool (sup-
plied by Hubbard Spool Company), supported by bronze bearings in a
bolted steel frame and driven by a variable speed motor. The gear
motor rotates the spool through a chain drive. The overall gear
reduction is 290:1; the diameter of the spool is 226 mm (8.9 in).
The peripheral or filament velocity is continuously variable from
0-22.6 mm/s (0-0.89 in/s). A standard 0-150 VDC power supply is

employed to power the motor. Figure III-7 is a photograph of the complete coating device showing the filament drive system.
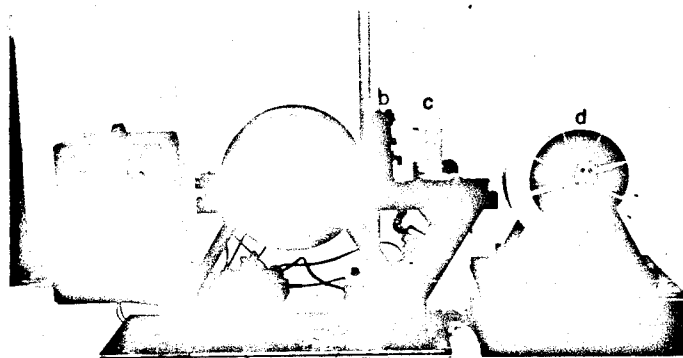
Figure III-7. Filament coating apparatus. (a) driver spool,
             (b) coater, (c) filament positioner and (d)
             as-received boron filament spool.

During the coating or winding of the filaments, a slight tension must be maintained to control the position of the filament. A combination spool holder and tension device was designed for the experiment. Figure III-7 shows the spool holder set up for the coating operation. The spool was mounted on an aluminum hub, which rotated on a 12.7 mm (0.5 in) diameter steel shaft. The shaft was supported in a bolted steel frame. The tension was provided by a spring acting through a teflon friction disc. The tension in the filament was controlled by adjusting the compressive force on the friction disc.

The function of the filament positioning device is to locate the moving filament accurately in the coater in both the vertical

and lateral directions. The filament passes through a hypodermic
needle mounted in a plexiglass block, which is attached to a modi-
fied Jominey bar indexing frame (Wilson Instrument Company). A
dial indicator is mounted on the frame to measure the lateral posi-
tion of the filament. The position of the filament is controlled
by a lead screw drive which was originally designed to be rotated
by hand. A later addition to the positioning device was the
installation of a synchronous motor to drive the lead screw. Figure
III-8 shows the filament positioning device attached to the winding
frame.
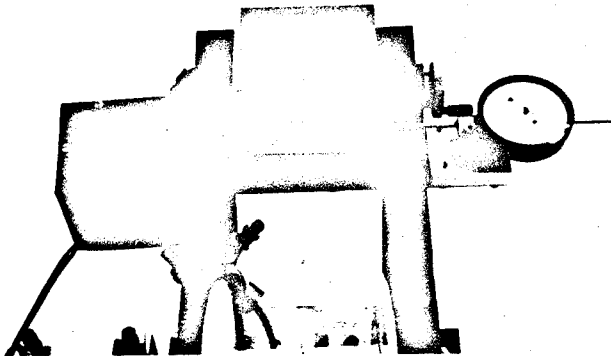
Figure III-8. Filament lateral positioning device.

The filament coater which is, in effect, the heart of the mecha-
nism, is pictured in Figure III-9. The mechanism is essentially two
soft rubber rollers, coated with silicon vacuum grease (SVG), posi-
tioned above and below the moving filament. One of the rollers is

attached to a pneumatic cylinder. When the lower roller is forced into contact with the upper roller, a layer of SVG is deposited on the moving filament. The rollers are coated before each run with SVG and are rotated by a racket and pawl arrangement. Details of the coater are enumerated in the Appendix. The pneumatic cylinder is driven by air, regulated to 20 psig, and controlled by a solenoid air valve (Skinner model V550B).
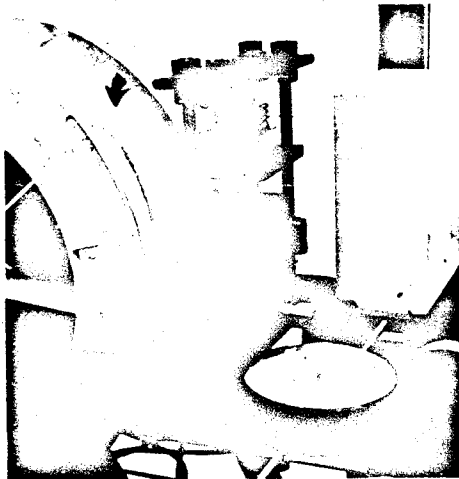
Figure III-9. Filament coater detail. Note intermittently coated filament (see arrow).

The length of the coating deposited on the filament is controlled by both the speed of the moving filament and the time the rollers are in contact. In order to control the coating accurately and reproducibly, an electronic timer was designed. The frequency range of the timing pulse is variable from 625 Hz to 0.026 Hz, while the length of the "on" pulse can vary up to ninety percent of the length of the timing pulse. A circuit diagram of the timer is included in the Appendix.

The timer consists of an astable vibrator (to provide the timing pulse), driving a monostable vibrator (to provide the "on" position of the timer). The range of the timer is extended by channeling the output of the monostable vibrator through a series of decade dividers.

The interface between the integrated circuit voltage of 5.0 VDC and the solenoid voltage of 115 VAC is provided by a transitorized relay, whose circuit diagram can be found in the Appendix.

The response of the coater at various time frequencies was determined using a Bently Distance Detector (Model D-252 #5404). The calibration curves for the coater are included in the Appendix.

III.C.1.b. Epoxy Preparation and Cure

It was essential to minimize the variation of properties from one epoxy batch to another. To control the cure temperature variation, a vacuum oven and pump were obtained. This combination permitted curing the epoxy under a partial vacuum. The National Appliance Oven Model Number 3851 had a temperature range of room temperature to 200° C with a $^+_-2°$ C variation and could maintain a vacuum of 10 μm Hg. The vacuum pump was a Cenco HiVac 2 (#1460) double stage pump with a gas ballast. The pump had a rated pumping capacity of 4.16 x $10^{-3} \frac{m^3}{s}$ at atmospheric pressure and a maximum vacuum of 0.1 μm Hg. A photograph of the curing oven and pump appears as Figure III-10.

The epoxy matrix material was prepared in the following manner to minimize the variation from batch to batch. The ratio of Shell Curing Agent Z to Shell Epoxy 828 resin was standardized to 25 parts of Z to 100 parts of 828 by weight (see section I-A-2). The curing
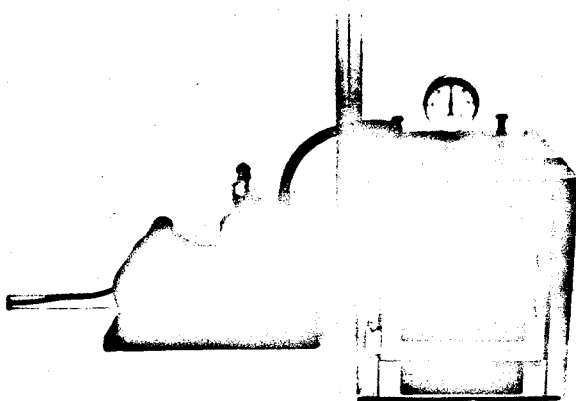
Figure III-10. Vacuum curing oven and pump.

agent was always measured out first using an Ohaus Dial-o-gram scale
with a rated accuracy of 0.1 g. The curing agent was weighed in
disposable polypropylene beakers, 400 ml (4×10^{-4} m^3) capacity
Tri-Pour Beakers), thus reducing contamination of the epoxy. The
correct proportion of Epoxy 828 was measured out and thoroughly
mixed with the curing agent by stirring with a clean· stainless
steel spatula for approximately 45 s. The epoxy misture was then
evacuated to about 100 μm Hg in the vacuum oven. The epoxy remained
at this pressure for about 7 minutes, and was then ready for casting.
After casting, the epoxy was cured for one hour at 66° C followed by
eleven hours at 123° C under a vacuum of 380 mm Hg.

III.C.2. Composite Specimen Fabrication

The composite specimens must have accurate and reproducable filament placement to eliminate this as a potential variable. A specimen winding device was designed to minimize the variation of spacing from specimen to specimen (described in III.C.1.)

The monolayer specimens were produced on the apparatus pictured in Figure III-11. It is the basic winding frame with the filament alignment jig substituted for the coating spool.

a   b
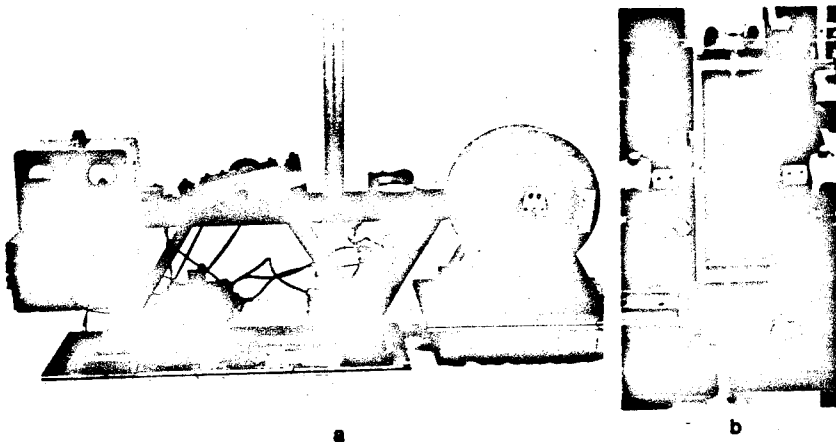
Figure III-11. Tensile specimen winding apparatus. (a) side view,
(b) mold detail showing the intermittent coating
on the wound filament.

The filament alignment jig consists of four endcaps positioned on an aluminum spacer. Between the endcaps are placed two molds for casting epoxy around the filaments. The critical dimensions of the jig are included in the Appendix.

The endcaps, which contain filament locating grooves, have been previously described by Heimbuch (1970). The caps are a block of

steel grooved circumferentially and then split into quarters. The
grooves are accurately positioned with respect to one another and
to the block face. The twenty-five grooves are spaced 0.25 mm
(0.01 in) apart and are 0.10 mm (0.004 in) deep.

The aluminum spacer was machined to accept the four endcaps
and to provide an accurate mounting surface for the two molds. The
12.8 mm (0.5 in) diameter hole was bored on a jig-borer to insure
the perpendicularity of the hole to the side of the spacer. The
three piece mild-steel molds are bolted together and then bolted
to the spacer.

The alignment jig is assembled on a gauge block to insure
proper alignment of the four endcaps and the molds. The end of each
mold is sealed using a cemented cardboard dam. A section of the dam
10 mm wide is removed to provide space for the filaments.

The procedure for wrapping a composite specimen is as follows.
First mount the coated spool of filament on the spool support and
adjust the friction spring. The proper filament tension can only be
ascertained by trial and error. Then take the free end of the fila-
ment and bind it in the split rubber pad at the end of the spacer.
Wind the filament into the twenty-five grooves sequentially. Bind
all the filaments under the other rubber pad and cut the filament
from the spool. Next, cement cardboard pieces over the spaces in
the mold dams and apply fast-setting epoxy to the ends of the molds.
The epoxy should be allowed to set for one-half hour and then the
procedure should be repeated with the second mold. After the second
application of epoxy is set, cut the filaments between the dam and

the endcaps and remove the molds.

The epoxy matrix material is mixed and evacuated as described in Section III.C.1, and then poured into one grip section of each mold. The molds are then tilted to allow the epoxy to "run" through the gauge section of the tensile specimen. The epoxy molds are "topped off" with epoxy and placed in the vacuum oven. The oven is pumped down to 380 mm of Hg and cured for one hour at 66° C followed by eleven hours at 123° C. The curing time is controlled by a standard appliance timer.

After the molds have cooled to room temperature, the specimens can be removed without dismantling the molds. If the molds are coated with a teflon utensil repair spray every five specimens, the composite can be removed by inserting a spatula blade between the mold and the specimen. The spatula should be carefully pushed into the gauge section without bending the specimen. The main advantage of this method is the prevention of casting flash (see Heimbuch, 1970). The grip sections were ground flat using a Dremel hand grinder to facilitate gripping in the tensile machine.

III.C.3. Fabrication of Bend-type Fracture Toughness Specimens

The bend-type fracture toughness specimens were cut from composite bars cast in the mold pictured in Figure III-12. The cavity of the mold was 5 mm (0.197 in) deep by 5 mm wide by 190 mm (7.50 in) long. The cavity length was eventually reduced to 133 mm (5.25 in) by inserting epoxy spacers into the mold as a measure to conserve boron filament.

The composite bars were produced in the following manner. A
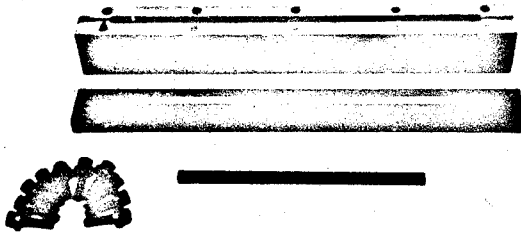
Figure III-12. Fracture toughness specimen mold and bar.

length of boron filament with the desired surface condition was wound
onto the driver spool of the winding device. The length was measured
with a rotation counter affixed to the frame. For a forty percent
filament composite bar 133 mm long, having 1250 filaments, 159 m
(655 ft) of filament were needed. The filaments were then cut from
the spool and laid on a sheet of teflon. The filaments were handled
with gloved hands to reduce contamination. The filaments were cut
to the desired length using a single-edged razor blade. The razor
blade was pressed across the filaments, causing a localized brittle
fracture to occur. The extent of the damage to the filament was
restricted to about 1 mm (0.04 in) on either side of the cut. The
mold bottom halves were cleaned, assembled, and heated. Mixed and
previously evacuated epoxy was poured into the heated mold. The

epoxy was then evacuated again until the bubbling stopped. The mold was removed from the oven and the filaments were laid into the mold by hand. The filaments were collimated by running a scapel up and down the length of the mold cavity. The mold was again evacuated to remove any residual bubbles. After removing the mold from the oven, the filaments which had been expelled from the mold during the evacuation were replaced. The mold cover was then placed over the cavity and its bolts tightened in unison. The excess epoxy was extruded from the mold through the relief cuts at the ends. The bar was then cured for one hour at 66° C followed by eleven hours at 123° C in a vacuum of 320 mm of Hg. After curing, the bar was easily removed by splitting the mold.

The notched test sections of the fracture toughness specimens must be produced in the composite bar, as described in Section III.A.4. The notches were cut with a 1.59 mm (0.0163 in) thick diamond wheel mounted on a Cincinnati cutting-grinding machine. Figure III-13 is a photograph of the grinder set up for notching the specimens. A special jig was built from mild steel to hold the composite bar at an angle of 63.4° with respect to the table of the machine. The details of the jig are included in the Appendix. Two cuts were made to form the isosceles triangle and were spaced as needed. The bar could then be cut up into individual sections or left as one piece. Preliminary tests showed that there was no difference between the performance of individual specimens and the performance of a single bar with multiple test sections.

Figure III-13. Grinding apparatus for notching fracture toughness specimens.

III.D. Fractographic Analysis

III.D.1. Scanning Electron Microscopy

Many of the effects of the intermittent bond on the fracture sequence are manifested on the fracture surface of the composite. Scanning electron microscopy was the primary means of examining and photographing fracture surfaces in this research. Some optical microscopy was used for comparison and low magnification photography.

The scanning electron microscope (SEM) used in this research was a Japan Electron Optics Laboratory, Co., Ltd. (JEOL), U-3 microscope. The reader unfamiliar with the operation or theory of the SEM can find an informative survey discussion in Murr (1970).

Specimen preparation of the composite fracture surfaces for the SEM is as follows. The specimens were cut off about 1.6 mm (0.063 in) below the fracture surface using the diamond saw for the bend type of specimen, or a heavy pair of shears for the composite tensile specimens. The fracture surface pieces were then glued to brass cylinders, 12.7 mm (0.5 in) in diameter and 10 mm (0.4 in) high.

The epoxy in the composite is an insulating material and will "charge" like a capacitor unless a conductive layer is deposited on the surface: the electrons absorbed by the specimen from the electron beam must be conducted away from the sample or will adversely affect the electron beam. The secondary electron emission will be enhanced if the deposited material is of high atomic number. The early specimens were coated with chromium (Cr) in a standard vacuum evaporator. The chromium layer was not continuous, thus permitting localized charging of the sample to occur which resulted in poor quality micrographs. A glow discharge apparatus was later installed for coating the specimens. The glow discharge process involves ionized gas molecules striking a metal target and displacing metal atoms. The target in this apparatus was gold (Au). The Au atoms would even reach reentrant corners of the specimen if placed in the glow region. The Au coating was uniform across the fracture surface, as shown by the enhancement of the image quality and lack of charging.

The coated samples were then examined in the SEM. An accelerated voltage of 15 KV was routinely employed. If the metallic coating were

discontinuous, the voltage was reduced to 5 KV to minimize charge effects. The resolution and signal-to-noise ratio of the image was reduced correspondingly. Higher voltages were seldom employed to minimize specimen damage. The photographs were taken from 35 to 10,000 times magnification. All pertinent data for the micrographs included in Chapter Four are given in the Appendix.

The film used to record the images was Polaroid 55 P/N film. The film produces both a positive and a permanent negative. The image size was 60 mm by 60 mm. The correct intensity and contrast were determined using a wave form monitor calibrated for a fifty second scan rate.

III.D.2. Optical Microscopy

A limited amount of optical micrography was performed on the fracture surfaces. A Leitz Ortholux microscope was used for the magnification range of 50 to 450 times. Internal and oblique incandescent illuminators were used as needed. A standard Nikon F body and microscope adapter were used to photograph the images with Kodak Tri-X film exposed at ASA 300. A Polaroid camera body using Polaroid 107 ASA 3000 speed film was also employed. A Gossen Microsix-L exposure meter indicated the correct exposure. The equivalent "F-stops" for the microscope are as follows: f-11 with the 20X eyepiece; f-4 with the 10-X eyepiece; f-1.4 with the 5X eyepiece. Specimens were photographed in both the "as fractured" condition and the SEM prepared condition.

Low magnification pictures (less than 50X) were taken using a Bausch and Lamb Stereo-zoom 7 microscope. An adapter was made to

attach the Nikon body to the microscope, thus enabling one to focus
the image critically. The film used in the camera was either H & W
control film rated at E.I. 80 or Kodak Tri-X Pan rated at ASA 300.
Negatives were printed as 89 mm x 127 mm (3.5 x 5 in) prints on
glossy paper.

III.D.3. Macroscopic Photographs

Equipment and macrophotographs were taken with a Canon
Pellix 35 mm camera with a Canon 50 mm f 3.5 macro lens. The film
used was H & W control film rated at E.I. 80 and the exposure deter-
mined with the internal meter of the camera.

CHAPTER IV

Experimental Results

IV.A. Test Data

The experimental results of this research are presented in this chapter. The data will be presented in chronological order to demonstrate the evolution of the thesis in lieu of a systematic presentation.

IV.A.1. Epoxy Results

IV.A.1.a. Stress-Strain Data

Preliminary tests were conducted with plain epoxy tensile specimens to evaluate the matrix material and standardize the casting procedure. Subsequent tests were conducted to determine the reproducibility of the matrix properties.

The epoxy, as stated in section I-2, was a combination of twenty-five parts Shell Curing Agent Z per hundred parts of Shell Epon 828 resin by weight. The cure cycle was standardized at one hour at 66° C followed by eleven hours at 123° C under a partial vacuum of 380 mm (15 in) of Hg.

Table IV-1 gives the mean mechanical properties of the epoxy along with the individual high and low values. The strain is determined using an extensometer (see section III-2) to measure the specimen elongation and the formula:

$$\varepsilon = \Delta L/L_o \qquad\qquad (IV-1)$$

where ε is the axial strain, ΔL is the elongation of the test section, and L_o is the original length of the gauge section. The fracture strength, σ , is calculated by dividing the maximum load by the original cross sectional area. The fracture strength is numerically equal to the tensile strength because this particular epoxy never attains a tensile instability (a zero slope in the load elongation curve).

The tensile specimens are cast in open-top molds, and a meniscus forms on the free surface. The curvature of the meniscus is a function of the amount of epoxy cast in the mold. The area of the cross section is approximated by the following formula:

$$A = W(h_t + h_m)/2 \qquad (IV-2)$$

where A is the area, W is the width of the specimen (6.67 mm or 0.263 in), h_t is the maximum thickness of the cross section, and h_m is the mold height (1.57 mm or .0625 in). The elastic modulus, E , is determined from the initial tangent slope of the load elongation using the following relationship:

$$E = \Delta X/\Delta \varepsilon A \qquad (IV-3)$$

where E is the elastic modulus, ΔX is the change in the load of the tangent, $\Delta \varepsilon$ is the change in the strain of the tangent and A is the original cross-sectional area.

TABLE IV.1.

Epoxy Tensile Results

	Fracture Strain	Tensile Strength	Elastic Modulus
	%	MN/m^2 (ksi)	GN/m^2 (x 10^5 psi)
Mean Value	2.79	66.5 (9.64)	3.21 (4.65)
High Value	5.12	92.5 (13.42)	3.73 (5.40)
Low Value	1.54	43.5 (6.31)	2.69 (3.90)

A tabulation of all the individual specimen properties can be found in the Appendix.

The stress-strain behavior of all of the epoxy specimens are consolidated into the stress-strain curve shown in Figure IV-1. The fracture stresses and strain are denotated by x's. It is of interest to note how well the points blend into the curve, remembering how disparate the extreme values are.

IV.A.1.b. Griffith Analysis

The form of the stress-strain curve of the epoxy, Figure IV-1, is that of an elastic material. The epoxy is not linearly elastic because the slope of the stress strain curve is changing. Preliminary tests show that the plastic strain is only a small percentage of the total strain. An epoxy specimen loaded to a total strain of 4.5% and unloaded showed a plastic strain of less than 1/4%, or about 5% of the total strain. Higher strain rate tests showed even less
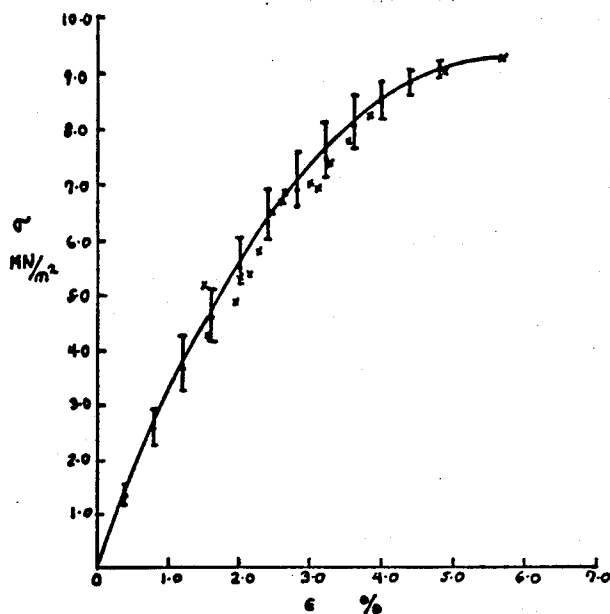
Figure IV-1.   Stress-strain curve for the epoxy matrix
material.

plastic strain. Therefore, the epoxy can be assumed to be non-linear

elastic (i.e., having a changing modulus). The elastic nature of the

epoxy deformation and the wide range of strength values would suggest

that Griffith-type flaws were present in the material (see section

I-D).

The Griffith equation for fracture strength in Irwin's notation

is (equation I-10):

$$\sigma = [\ EG_{c}/\ \pi c\ ]^{1/2} \qquad\qquad (IV-4)$$

where σ is the strength, G_{c} is the critical strain energy release

rate, c is the crack length and E is the elastic modulus. Since the

elastic modulus of a non-linear elastic material is not constant, an integrated average elastic modulus shall be used.

The integrated average elastic modulus, $\bar{E}$, is calculated by equating the non-linear elastic strain energy with a hypothetical linear elastic strain energy. The area under the stress-strain curve (Figure IV-1) represents the strain energy of the epoxy. This area was measured using a Keuffel and Esser polar planimeter (model no. 4236) and averaging three values. The strain energy of the hypothetical linear elastic epoxy is

$$U = 1/2 \ (\bar{E})^2 \ \epsilon \qquad\qquad (IV-5)$$

where U is the strain energy, and ϵ is the elastic strain, which is numerically equal to the anelastic strain. If the measured strain energy is equated to IV-5, an integrated average modulus, $\bar{E}$, is calculated to be 2.46 GN/m^2 (3.57 x 10^5 PSI), which is 25% lower than the initial tangent modulus.

The flaw size, c, was estimated from the fracture surface using either scanning or optical microscopy. The location of the flaw was determined from the fracture surface markings, see Figure IV-2. The size of the flaw was estimated from measurements taken from photographs or microscope stage movement. The flaws were generally ellipsoidal, fan-shaped, or quarter circles; the area of each was calculated using the appropriate formula. The flaw in the analysis was assumed to be circular in cross-section, and the characteristic dimension, c, was simply the radius of a circle whose area (πc^2) was equal to measured flaw area.
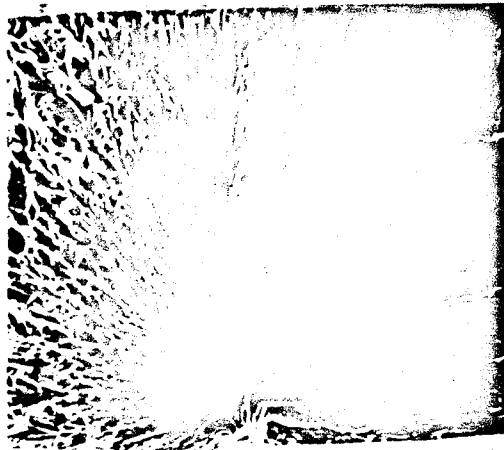
Figure IV-2. SEM fractograph (55x) of a plain epoxy tensile specimen. The initiating flaw appears as a dark circle in the lower central portion of the fracture surface. The flaw radius is approximately 0.22 mm.

Thirteen epoxy specimens were analyzed; the fracture strength, σ_f , and the flaw size, c, were tabulated and are included in the Appendix. Figure IV-3 is a graphical plot of the data with σ_f^2 plotted on the ordinate and 1/c plotted on the abscissa. A straight line was drawn by eye through the data points. A more sophisticated approximation technique was not warranted because of the inexact nature of the data. The slope of the line ($\Delta\sigma_f^2 / \Delta(1/c)$) is equal to the product ($\overline{E} G_c / \pi$) from equation IV-4.

$$G_c = \{\Delta(\sigma_f)^2 \pi/(\Delta(1/c)\overline{E})\} \qquad\qquad (IV-6)$$

Substituting values of $\Delta\sigma_f^2 = 18 \times 10^7$ $(psi)^2$, $\Delta(\frac{1}{c}) = 166$

$\bar{E} = 3.57 \times 10^5$ psi into equation IV-6 awards Gc a value of 9.5 in-

lb/in^2 (1.69 KJ/m^2). Corten (1968) cites a value for Gc of 6.1 in-

lb/in^2 (1.07 KJ/m^2) for an epoxy of a different composition using

a centrally notched tensile bar specimen.
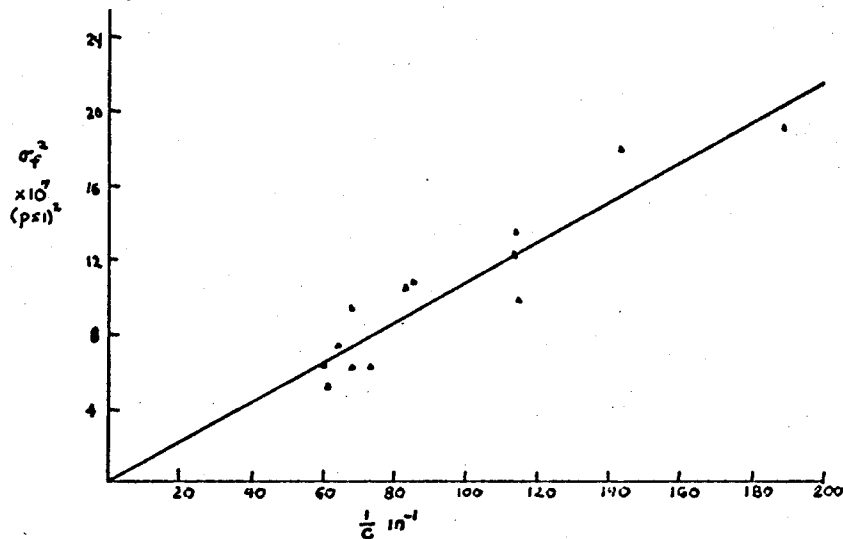
Figure IV-2. (Strength)^2 - reciprocal of the flaw radius curve
for the epoxy matrix material.

IV.A.2. As-received Boron-Epoxy Composites

Test Results

Monolayer composite tensile specimens were produced with

as-received (uncoated) boron filament in the manner described in

Section III-3. This test series established a baseline performance

for the boron-epoxy system. A total of fourteen tests were con-

ducted; a tabulation of the mechanical properties can be found in

Appendix A. Table IV-2 gives the mean, high and low values for

strain to failure, fracture stress, and elastic modulus. The physical properties were determined in the same manner as described in Section IV-1, except for the elastic modulus. The elastic or Young's modulus of the composite specimens is determined by using a finite strain tangent. The initial (or zero strain) tangent method (as described in section IV.A.1) for determining the modulus is not meaningful with this type of specimen. A typical stress-strain curve of a composite tensile specimen is shown in Figure IV-4.
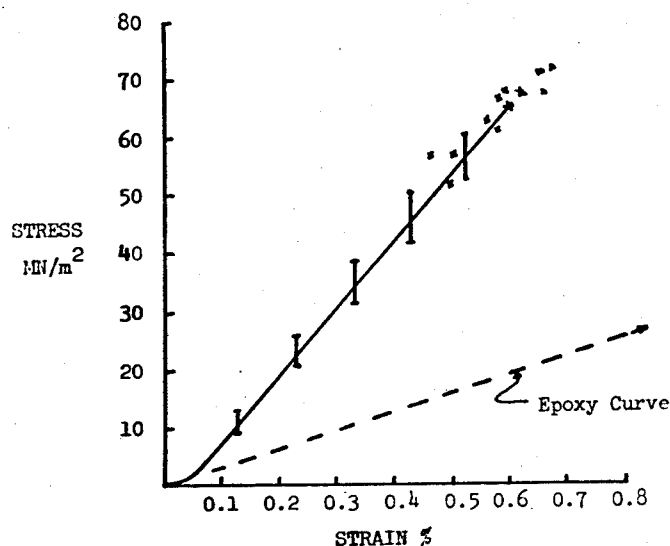
Figure IV-4. Stress-strain curve for uncoated boron filament composite.

Notice how the shape of the stress-strain curve changes for the first few hundredths of a percent strain. The composite modulus is taken from the slope of the curve past this initial non-linear portion, generally at about 0.2%. There are many possible explanations for this initial non-linear behavior, such as slight specimen bending or

a compressive prestrain of the filaments due to the differential thermal contraction of the composite. (The thermal coefficient of the expansion of the matrix is 5.1×10^{-6} in/in $^\circ$ C and that of the filament is 2.7×10^{-6} in/in $^\circ$ C). The important thing to note is that this comprises a very small percentage of the total strain.

All of the stress-strain data were incorporated into one stress-strain curve as shown in Figure IV-4. The stress-strain curve of the epoxy is also included for comparison. The relative strengths of the epoxy and the composite are nearly equal, but the strain to failure of the epoxy is much greater than that of the composite. The strain to failure of the composite is of the same order of the strain to failure of the filament, indicating that the composite is thus "filament controlled".

TABLE IV.2.

Physical Properties of Uncoated Monolayer
Composites

	Fracture Strain $\%$	Tensile Strength MN/m^2 (ksi)	Elastic Modulus GN/m^2 (x 10^6 psi)
Mean Value	0.582	65.6 (9.51)	11.0 (1.60)
High Value	0.670	74.4 (10.79)	11.9 (1.73)
Low Value	0.448	52.8 (7.66)	10.4 (1.51)

The mean strain to failure is 0.58% and, if one assumes a constancy of strain, this corresponds to a filament stress of 2.20 Gn/m^2, indicating mode I type of behavior (see section II-1). No filament fractures (audible emissions) were heard prior to composite failure.

IV.A.3. Filament Pullout Data

The filament pullout test (see section III-1) was originally designed to evaluate the interfacial shear strength of various filament treatments and/or coatings. After the preliminary tests were conducted, it was decided that a full monolayer composite specimen containing treated fibers would give a more meaningful evaluation of the coating than the simple pullout tests method. Two serious problems developed with the pullout test: maintaining filament alignment during the casting and curing of the epoxy. The second problem stemmed from the difficulty of holding the specimen in the tensile machine without placing the filament in torsion. The tests were inconclusive, hence the filament pullout test was rejected for the evaluation of the coatings. The effects of the coatings would be most realistically represented in full-size monolayer specimens.

IV.A.4. Filament Coating Tests

The object of this test series was to determine the proper coating that would meet the following criteria: (1) The coating must lower the interface strength below the limits set forth in section I-C-2., (2) The coating must be relatively easy to apply at room temperature and not "creep" along the filament due to surface tension, (3) The coating must be stable under curing conditions,

e.g. not inclined to volatilize. The measure of effectiveness of
the coating was the strain to failure of the coated composite.
Several coating materials had been tried and rejected before this
research, namely acetone, kerosene, mineral oil, and collodion
(Heimbuch, 1970). The materials chosen for this evaluation pro-
gram were: WD 40, an organic wetting agent manufactured by the
Rocket Chemical Company; Cutmax 568, a hydrocarbon oil manufactured
by Houghton Inc.; teflon sheet and rod manufactured by DuPont
Chemical Co.; and Silicon grease, manufactured by Dow Corning.
Graphite was not chosen because the data from Mullen et al. (1970)
indicated it failed to lower the shear strength sufficiently to
obtain mode III failure (see section I-C).

The method of application for the preliminary tests was as
follows: The liquid materials, WD 40 and Cutmax, were used to
saturate a wad of cotton through which the filament was then drawn.
The silicon vacuum grease (SVG) was applied by drawing the filament
between greased fingers. Both methods produced visually uniform
coatings. The solid teflon was made to adhere to the filament by
simply abrading the teflon with the rough surface of the boron fila-
ment. This process removed a layer of teflon about 0.01 μm thick
(Ludema, 1970). The tensile results of the coated samples are shown
in the following table.

The average stress-strain curves for the coated monolayer spec-
imen are shown in Figure IV-5. It is apparent that SVG coating
material was the most suitable.

TABLE IV-3

Mechanical Properties of Coated
Monolayer Composites

Coating Material	Fracture Strain	Tensile Strength	Elastic Modulus
	%	MN/m^2 (ksi)	GN/m^2 (x 10^6)
Cutmax	0.750	69.0 (10.0)	9.2 (1.33)
WD 40	0.855	81.5 (11.82)	9.8 (1.42)
Teflon	0.605	67.5 (9.79)	11.7 (1.70)
SVG	3.40	96.4 (13.98)	8.85 (1.29)
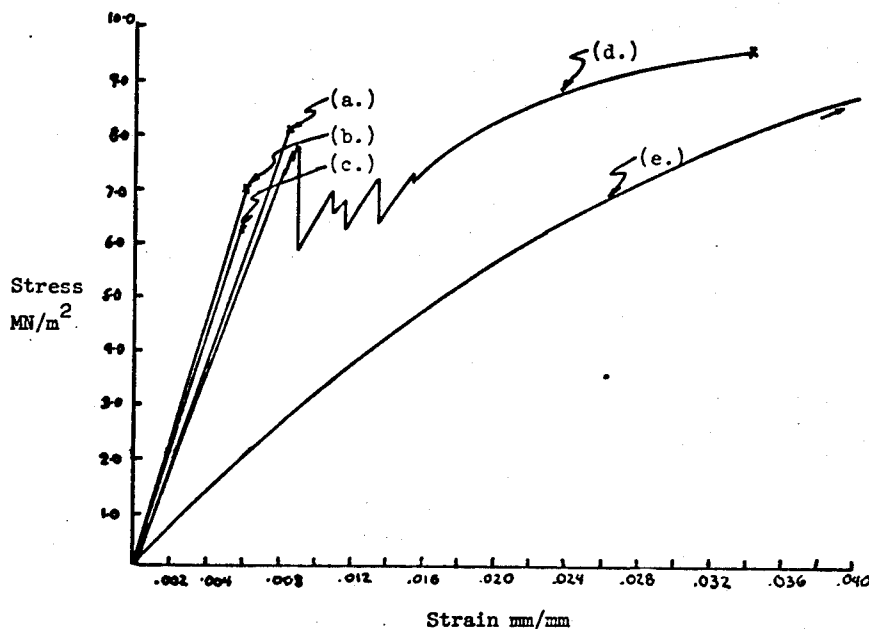
Figure IV-5.   Stress-strain curves for uniformly coated composites,
a - WD-40 coated, b - Cutmax coated, c - Teflon
coated, d - SVG coated, and e - plain epoxy.

IV.A.5. Intermittently Coated Tensile Tests

Silicon vacuum grease (SVG) was chosen from the coating
evaluation tests as the bond reducing agent in this research (see
section IV.A.4). The grease was an ideal material - besides ful-
filling the bond strength degradation requirement, it was viscous,
tenacious, stable in most solvents and unaffected by temperatures
up to 200° C, as well as possessing a vapor pressure of less than
10^{-6} m of Hg. A coating device was designed, as described in
section III-C, to accommodate SVG.

The variables to be investigated in this portion of the research
were: (1) the ratio of coated to uncoated length (L_c/L_{uc}), or equiva-
lently the ratio of the volume of coated filament to the volume of
uncoated filament; and (2) the ratio of the uncoated length to the
filament diameter ratio. This ratio (L_{uc}/d) must be greater than
the critical transfer length (see section I-B-1). It was decided
to set this ratio equal to one hundred, since this would accommodate
interfacial shear strengths as low as 15.9 MN/m^2 (2300 psi), which is
weaker than the lowest bond strength of untreated boron epoxy cited
in the literature.

The only remaining independent variable was the ratio of coated
length (or volume) to the total filament length (or volume). The
ratio tested ranged from a low of 38% to a high of 81%. The ratio
of coated to uncoated length ranged correspondingly from 0.61 to
4.25   . The lower limit of 38% was set by the coater design,
and the upper limit determined by the specimen design.

The reason for the lower limit of 38% was as follows: (1) the
uncoated length was predetermined at one hundred filament diameters

(10 mm); (2) the soft rollers of the coating device distorted when
in contact and produced a contact region 6.3 mm (0.250 in) wide
as shown in Figure IV-6.
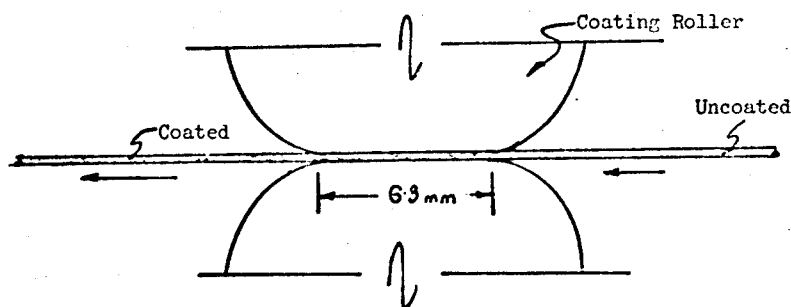
Figure IV-6. Geometry of the coating rollers during contact.

The shortest coated length (L_c) was 6.3 mm, therefore, the
smallest ratio $L_c/(L_c + L_{uc})$ was 0.38 (6.3 mm/16.3 mm). The upper
ratio of $L_c/(L_c + L_{uc})$ was limited to 0.81, because the cycle length
($L_c + L_{uc}$) must be less than or equal to the gage length of the
tensile specimen [57 mm, (2.25 in)] for there to be at least one
coated and one uncoated length in the test section for each filament.
The longest coated length was then equal to 47 mm, (1.85 in) (Gage
length - L_{uc}). Therefore, the highest possible ratio $L_c/(L_c + L_{uc})$
is 0.825 (47 mm/57 mm).

Table IV-4 provides a summary of the test results of the tensile
properties of the intermittently coated, monolayer composites. All
of the properties given in Table IV-4 were determined in the manner
discussed in section IV.A.2. A tabular list of all the tensile tests
appear in the Appendix A.

TABLE IV-4

The Mechanical Properties of Intermittently Coated Composites. (Coating Material - SVG)

V_o/V_f	L_c/L_{co}	L_{co}/d	STRAIN			STRENGTH			MODULUS	Number
			Mean %	High %	Low %	Mean MN/m² (psi)	High MN/m² (psi)	Low MN/m² (psi)	Mean GN/m² (x10⁶ psi)	
0.38	0.612	90	0.772	0.875	0.770	73.8 (10.7)	76.6 (11.1)	67.9 (9.9)	10.75 (1.56)	4
0.45	0.818	110	0.798	0.825	0.775	75.8 (11.0)	73.3 (11.4)	74.8 (10.8)	10.75 (1.55)	4
0.50	1.00	90	0.741	0.820	0.700	78.1 (11.3)	86.9 (12.6)	72.8 (10.6)	10.62 (1.54)	7
0.55	1.22	95	0.783	0.850	0.710	76.5 (11.1)	79.3 (11.5)	73.8 (10.7)	10.75 (1.55)	4
0.65	1.86	110	0.768	0.785	0.740	80.7 (11.7)	81.0 (11.8)	80.0 (11.6)	10.69 (1.55)	4
0.75	3.00	90	0.805	0.945	0.670	74.1 (10.7)	73.6 (11.4)	68.3 (9.9)	10.34 (1.50)	6
0.75	3.00	49	0.770	0.780	0.760	72.9 (10.6)	74.1 (10.7)	72.7 (10.4)	10.75 (1.55)	2
0.82	4.26	90	0.781	0.840	0.735	74.2 (10.8)	77.2 (11.2)	72.7 (10.4)	10.55 (1.53)	4
0.00	0.00	∞	0.582	0.670	0.448	65.6 (9.5)	74.4 (10.8)	52.8 (7.7)	11.00 (1.60)	24

IV.A.6. Fracture Toughness

IV.A.6.a. Average Work of Fracture

This test series was performed to determine the fracture tough-
ness of uncoated boron-epoxy composites and the effect of an inter-
mittent coating on the fracture toughness. The specimens were
notched, three point bend type specimens as described in section
III-1. The physical properties of the composite tested were as
follows: flexural strength--1.20 to 1.28 GN/m^2 (174-186 ksi),
tensile modulus--154 to 174 GN/m^2 (22.3-25.2 x 10^6 psi), volume per-
cent filament--40 to 45%, density--1.66 to 1.73 MG/m^3 (.0599-.0624
lb/in^3). The composite was produced in bar form and notched with
a diamond saw to produce the test sections (see section III-3).

The tests were conducted in an Instron testing machine and the
load plots were plotted on a chart recorder. Dynamic effects can
be neglected because of the low crosshead velocities involved (0.5 mm/
min) (83   m/s); therefore, the deflection of the specimen is directly
proportional to chart travel as this is a stiff testing machine. A
load deflection curve can then be constructed, and the area under the
load-deflection represents the energy dissipated in fracturing the
specimen. A typical load deflection curve of a three-point bend test
on a composite material is shown in Figure IV-7.

The notched composite bar fractures discontinuously, as shown by
the saw-tooth form of the load deflection curve. Acoustical bursts
can be heard at each load drop; presumably this is a result of groups
of filaments breaking as the crack progresses.

The following mechanical properties can be extracted from the
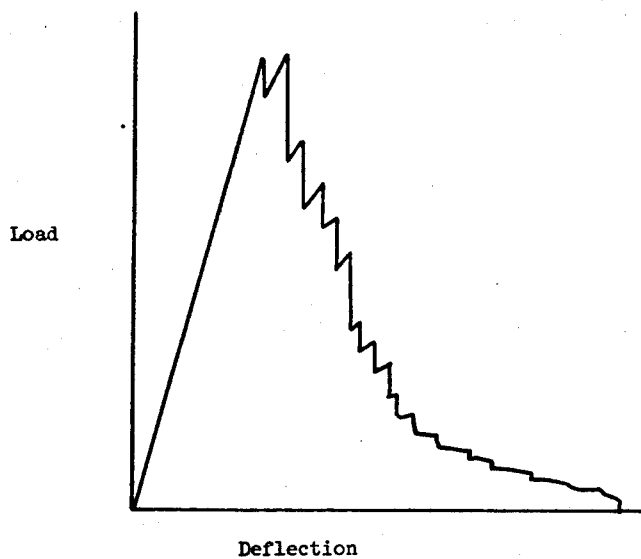
Figure IV-7. Typical load-deflection curve for a three point
bend toughness test.

load deflection curve: flexural modulus, flexural strength and

fracture toughness. The flexural modulus can be determined using

the following formula:

$$E = 2280 \ (Kt/1 - Kt/Km) \ psi \qquad (IV-7)$$

where Kt is the stiffness of the uncracked specimen and Km is the

stiffness of the testing machine. The constant factor, 2280, is

derived from an energy analysis using simple bending theory. (This

theory can be found in the Appendix.) The machine stiffness is

accounted for by the correction (Kt/1 - Kt/Km).

The flexural strength is determined from the simple bending

stress equation

$$\sigma = 6X1/bh^2 \qquad\qquad (IV-3)$$

where X is the maximum load, 1 is the total length of the specimen (35 mm), b is the thickness, and h is the height of the specimen.

The fracture toughness can be determined by graphically integrating the load-deflection curve. Two methods were employed for the graphical integration, the first consisted of an approximation of the area using a series of triangular sections, the second involved measuring the area with a polar planimeter (Keuffel and Essor model 4236). The planimeter readings, rated accurate to within one percent, were within three percent of the triangular approximation method. Routinely, three readings were taken with the planimeter and an average taken on the three. The work of fracture, Y , is simply the area of the curve divided by the cross sectional area. (This is the integrated average work of fracture.)

The interlaminar shear strength, T , was determined with a short span unnotched composite beam loaded in three point bending. Figure IV-8 represents the load deflection curve of a typical short beam specimen. The curve has an ultimate load which is associated with the interlaminar shear failure. The load drops off after ultimate due to tensile failure of the outer filaments. The shear strength is determined with the following equation:

$$\tau = 3X_{max}/4bh \qquad\qquad (IV-9)$$

where X_{max} is the ultimate load, b and h are the base and height of the specimen respectively.
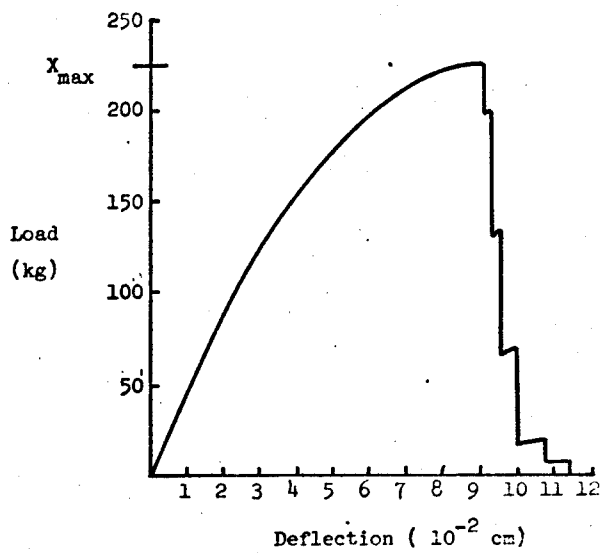
Figure IV-8. Typical load-deflection curve for an ILS test.

The test series consisted of composite bars containing as-received filaments, filaments boiled in methanol, filaments fully coated with SVG, filaments intermittently coated with SVG and then coated with epoxy dissolved in acetone, and filaments simply intermittently coated with SVG.

Table IV-5 summarizes the results of this test series.

TABLE IV-5

Mechanical Properties of the Fracture Toughness Bend Specimens
As A Function of Surface Treatment

Condition	Work of Fracture			Strength			Modulus			Shear Strength
	Mean	High In-lb/in²	Low	Mean	High Ksi	Low	Mean	High Msi	Low	Mean Ksi
		KJ/m²			GN/m²			GN/m²		MN/m²
As-Received	199	206	195	173	176	170	26.0	28.0	23.9	9.56
	34.8	36.1	34.1	1.19	1.21	1.17	179	193	165	65.9
100% Coated	185	220	143	155	175	145	22.2	22.2	22.2	---
	32.4	38.5	25.0	1.07	1.21	1.00	153	153	153	---
Methanol Boil	182	192	172	165	171	160	24.2	24.8	23.1	8.81
	31.9	33.6	30.1	1.14	1.18	1.10	176	171	159	60.8
50% Acetone	142	165	116	120	132	111	20.0	23.9	14.7	8.63
	24.9	28.9	20.3	0.83	0.91	0.765	138	165	101	59.3
50% w/o Acetone	150	174	121	153	177	129	22.3	26.3	18.4	---
	26.3	30.5	21.2	1.06	1.22	0.89	154	181	127	---
50% Wrapped	175	177	173	171	184	161	22.9	24.8	21.5	8.20
	30.6	31.0	30.3	1.18	1.27	1.11	158	171	148	56.6
Ends	251	291	227	142	163	132	20.6	24.8	18.4	---
	43.9	50.9	39.7	0.98	1.12	0.91	142	171	127	---

IV.A.6.b. Incremental Work of Fracture

The preceding values of the work of fracture were the inte-
grated average values, namely the total energy consumed divided
by the net cross section. It was of interest to determine the
incremental work of fracture γ_i as a function of crack area since
this would demonstrate the consequence of the specimen shape on
fracture toughness.

There are two procedures for obtaining the incremental work
of fracture: the first is a modification of Irwin's method (Beaumont
et al., 1972), and the second is the energy method. Both processes
require the functional relationship between the specimen compliance
(1/k) and crack area (A) be known. The relationships were
determined experimentally in the following manner. An uncut speci-
men (A=0) was loaded in three-point bending to determine its compli-
ance. The specimen's test section was then cut to a depth of 0.13 mm
(.005 in) with a diamond saw and its compliance was measured. This
process of removing 0.13 mm (.005 in) of the test section and measur-
ing its compliance was continued through the test section. Care was
taken during the loading of the "cracked" specimen to avoid fracturing
any uncut filament; the load was raised until the load deflection
curve became linear. The crack depth was converted to crack area
and the following graphical relationships (Figure IV-9) between com-
pliance and crack area were generated.

In order to determine the work of fracture from Irwin's relation-

$$\gamma = G_c/2 = X^2 \partial(1/k)/ 4\partial A \qquad \text{(IV-10)}$$

Figure IV-10. Load-deflection curve (see text for details).

Figure IV-9. Compliance (1/k) - crack area (A) curve for the composite fracture toughness specimen.

ships, it was necessary to determine the load X and the differential of compliance with respect to crack area $\partial(1/k)/\partial A$. Two methods were used to determine ($\partial(1/k)/\partial A$), one being an nth order polynominal regression formula and the other a simple graphical slope ($\Delta(1/k)/\Delta A$) of the compliance curve. Since the computer program for the regression formula was never fully operative and given the accuracy of the graphical method, the latter was considered sufficient. Figure IV-10 depicts a typical load deflection curve, showing the various compliances ($1/k_i$) and their corresponding maximum loads (X_i). The work of fracture is then equal to:

$$\gamma_i = X_i^2/4 \; \{\Delta(1/k)/\Delta A\}_i \qquad\qquad \text{(IV-11)}$$

The energy method is related to the integrated average in the sense that it measures the energy dissipated by the crack as it advances over a determinable area. One of the assumptions made in this procedure is that a cracked member will return to zero deflection when the cracking load is removed. This is delineated by the line B-C in the sector area of Figure IV. The line A-B gives the compliance, hence the area (from Figure IV-9) can be deduced. The line B-C gives the compliance and the area after the cracks stops. The integrated area of the sector A-B-C represents the energy dissipated with the crack advancement from area (A_1) to area (A_2) and is measured using a polar planimeter. The incremental unit of fracture, γ_i, is therefore, equal to $\dfrac{\text{Area (Energy)}}{A_2 - A_1}$, where area is representative of the energy associated with the sector area, and A_2, A_1 is the crack area before and after crack advancement. It should

be realized that this procedure gives an average work of fracture over the area of crack advancement.

A comparison of the two techniques for determining γ_i using one sample is included in Table IV-6.

TABLE IV-6

Incremental Work of Fracture Values Computed Using the
Energy Method and the Modified Irwin Method

Region	Work of Fracture		Area of Region in^2
	Energy $in-lb/in^2(kJ/m^2)$	Irwin $in-lb/in^2(kJ/m^2)$	
1	198(34.7)	126(22.2)	.0016
2	233(40.8)	211(27.0)	.0007
3	276(48.3)	310(54.3)	.0014
4	283(49.5)	312(54.5)	.0016
5	203(35.6)	272(47.6)	.0037
Remainder	129(22.6)	170(29.6)	.0085
Total	181(31.7)	181(31.7)	.0175

The energy method was used to delimit the incremental work of fracture for several specimens. Figure IV-11 is a plot comparing the work of fracture of several types of specimens.

IV.A.6.c. Electrical Resistance Method

An attempt was made to utilize the electrical resistance measurement of a specimen as a crack area indicator. This is possible because the boron filaments (actually the tungsten boride core) is a conductor and the epoxy matrix is an insulator. The filaments can
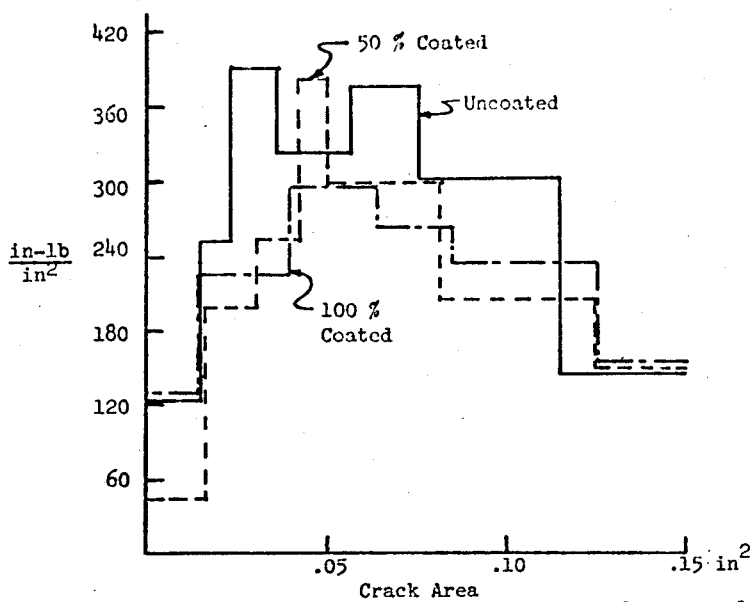
Figure IV-11. The incremental work-of-fracture for several
different filament conditions.

be considered as parallel resistors and the following relationship

between crack area and measured resistance is obtained:

$$A_{c_i} = (1-(R_o/ R_i))A_o \qquad\qquad (IV-12)$$

where A_{c_i} is the instantaneous crack area, A_o is the net area,
R_o is the initial resistance and R_i is the instantaneous resis-
tance.

The electrical connection between the filament was made by

polishing the ends of the specimens to expose the conducting cores;

the ends were painted with conducting paint and leads attached to

the ends of the specimens. The electrical resistance was measured

with a digital ohmmeter accurate to within $\pm 0.1 \Omega$ (Weston model

1241 VOM).

The resistance measurements were recorded at each load drop and the corresponding crack area increase was calculated. The energy dissipated was related to the sector area (see previous section). Table IV-7 gives the pertinent data for the resistance technique for the identical specimen quoted in Table IV-7.

TABLE IV-7

Incremental Work of Fracture

(Electrical Resistance Method)

Region	Ro/R	A crack	Energy in-lb	$\frac{\text{in-lb}}{\text{in}^2}$
1 & 2	.995	.00009	.479	5322
3	.990	.00009	.3911	4345
4	.983	.00021	.447	2128
5	.877	.000961	.740	377
Remainder	0	.015685	1.10	70

IV.B. Fractographic Analysis

This section of the Experimental Results is a summary of the microscopic analysis of fracture using scanning and optical microscopy (see section II-3). Fractography was used to investigate filament-matrix interaction, crack filament interaction, interfacial and filament changes due to coating, etc.

IV.B.1. Tensile Fracture Surfaces

A typical fractograph of a composite material appears in Figure IV-12. The surface can be divided into three main areas, the fracture initiation point, the slow growth ($v < 0.38$ c, where ċ is the velocity of propagation of an elastic disturbance) region, and the fast growth ($v \sim 0.38$ c) region. The fracture initiation point (an interface defect) appears in Figure IV-12 as the dark circled area in the left center of the fractograph. The row of darkened spots represent the row of filaments; they appear dark because their fracture surfaces are out of the plane of focus. The slow growth region is characterized by a bright nearly specularly reflective surface (sometimes called the mirror region). In Figure IV-12, the slow growth region extends for about seven filaments either side of the initiation point. The remainder of the fracto-graph is the fast growth region. It is characterized by a roughened surface due to crack branching and/or parabolic formation. If the reader is unfamiliar with fracture surface characteristics in poly-meric materials, two review papers, one by Berry (1964) and the other by Wolock and Newman (1964), would provide excellent background information in this area.

The three regions discussed above always appeared on the frac-ture surface in this research, but the size and number of each was found to vary. Some of the more ductile specimens had multiple initiation sites. Qualitatively, the larger the slow crack growth region, the higher the strength of the material.
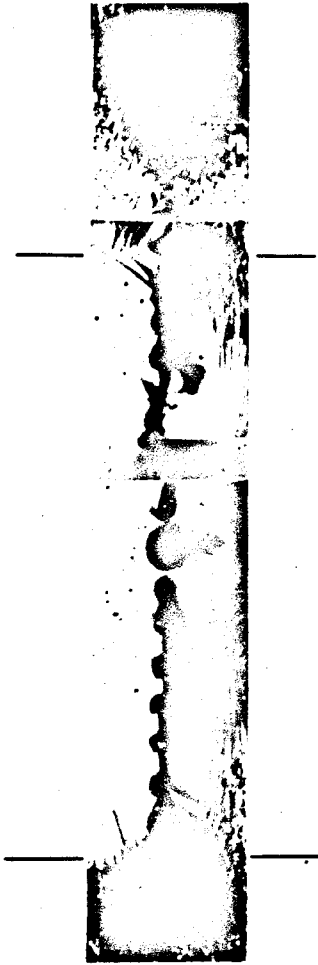
Fig. IV-12 Optical micrograph (27X) of a complete fracture surface. The point of fracture initiation is indicated by an arrow, the mirror region is delineated by vertical lines and the fast growth region is the remaining portion.

IV.B.1.a. Fracture Initiation

The initiation of a fracture in a composite material is most often associated with filament fractures (see section I-C). The three fractographs, IV-13, 14, 15, demonstrate the most common form of fracture initiation, viz: a filament failure generating a matrix crack, i.e. mode III type of behavior (section I-C). Initiations of this type possess three common characteristics, (i) a planar type of filament fracture where, (ii) that plane of filament fracture is coincidental with the main crack plane, and (iii) no perceivable interfacial separation between the matrix and the filament. The nature of the filament failure can be classified as either a tungsten-boride core defect, or as a surface defect resulting from the vapor deposition process. Figure IV-13 is an example of a core defect causing the filament to fracture, as shown by the fragmented core in the center of the filament. The matrix fracture initiated from the ten o'clock portion of the fracture filament and swept around the filament. Notice the small size of the slow growth region in this specimen relative to that of Figure IV-12. Figure IV-14 demonstrates how a surface defect in the filament can result in fracture initiation. The matrix fracture was generated all about the filament as illustrated by the transfer of the fracture surface markings of the filament onto the matrix fracture. Defects of this type result from impurities in the boron-trichloride gas during the deposition process.

The third fractograph (Figure IV-15) shows a defect near the core of the filament formed early in the deposition process. The filament
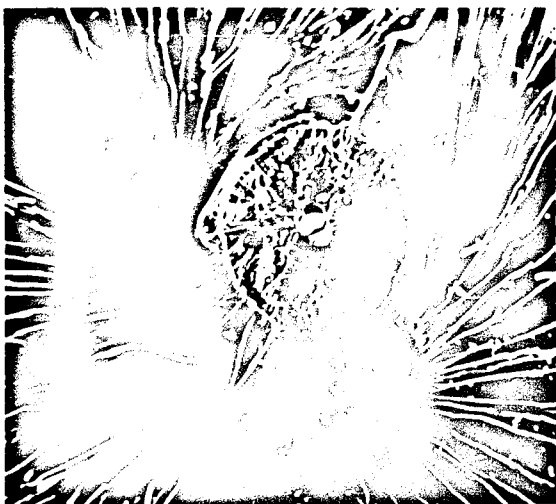
Figure IV-13. SEM fractograph (400x) of a
fracture initiating filament with a
defect in the tungsten boride core.
Note the planar fracture surface and the
absence of separation between the matrix
and the filament..
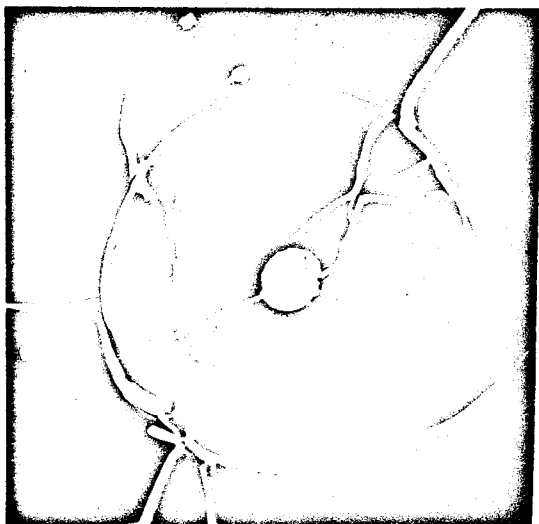
Figure IV-14. SEM fractograph (750x) of a
fracture initiating filament with a
defective boron sheath. Note the
planar fracture surface and the trans-
ferral of fracture markings.
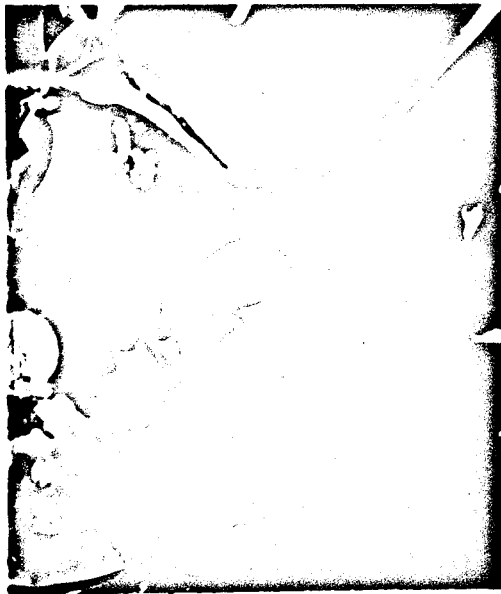
Figure IV-15. SEM fractograph (1000x) of a fracture initiating
filament with both an internal defect and an interface defect.
The internal defect is indicated by an arrow and the inter-
face defect is circled.

fracture initiated just beyond the light colored core near the five o'clock position; (this can be determined by following the fracture markings back to their origin). One peculiar aspect of this failure was the origin of the matrix crack. It appears to have originated at a defect point in the interface, possibly due to an impurity introduced before the casting process. However, the filament failed before the matrix crack began.

Although the vast majority of the composite fractures originated with filament failure, some did not. The most common of the latter group began from defects in the interface. In contrast to the filament initiated failures, the interfacial type of failure was characterized by an out of the crack plane filament failure (or pull-out), indicating that it was not the source of the fracture.

Even though each filament was cleaned by blasting it with dry air, some dust particles would adhere and produce gross discontinuities in the interface after the epoxy was cast. An interfacial failure specimen appears in Figure IV-16; note the appearance of the shear type of filament failure. The defect can be seen at the top of the radial fracture marking emanating from the lower portion of the filament. Figure IV-17 illustrates another specimen that failed from an interfacial defect. The filament occupies the upper left third of the photograph. The defect can be clearly seen, but its composition seems to be similar to that of the matrix material. The defect could be a bit of curing agent which 'crystallized' and adhered to the filament rather than chemically reacting with the epoxy resin. This figure clearly illustrates the matrix-filament separation.

Figure IV-17. SEM fractograph (1300x) of another interfacial defect initiating fracture. The filament appears in the upper left third of the picture.

Figure IV-16. SEM fractograph (300x) of a fracture initiating interfacial defect, indicated by an arrow. It should be noted that the filament fracture and the composite fracture are non-coplanar.

There was only one exception to the above mentioned fracture
initiations, i.e. filament and interfacial fracture, that exception
occurring in a specimen containing fully coated SVG filaments. The
final composite fracture was caused by a defect in the matrix mater-
ial. Figure IV-18 is a low magnification fractograph of this sample.
The fracture originated from the inclusion near the bottom center
of the specimen. The long pullout of the filaments should be noted
and also the remarkable similarity of this fracture surface to that
of a plain epoxy specimen (Figure IV-2). The presence of the weakly
bonded filaments has little effect on the fracture sequence. All
this, along with this specimen's strain to failure (three times that
of the filament), indicates that SVG reduces the interfacial strength
to a very low quantity.

IV.B.1.b. Fracture Sequence

The intermittent bond concept is predicated on the assumption
that a crack propagates from filament to filament via the matrix, or
simply the filaments do not fracture before the main crack front
reaches them. One feature that appears in the slow growth region of
the crack propagation is the presence of striations on the fracture
surface resulting from filament fractures. The striations are pro-
duced by the interaction of the filament fracture strain pulse with
the main crack. Explanations of the striation will help substantiate
the fracture sequence hypothesis. In Figure IV-19, one of the stria-
tions appears as a light colored band running from the left-hand
corner to the left edge of the right filament. Only one striation

Figure IV-19. SEM fractograph (300x) showing a striation in the slow growth region of a composite fracture surface. Fracture is moving from right to left.
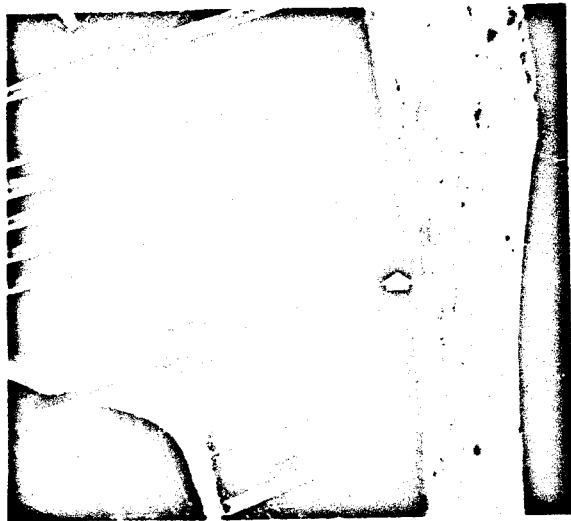
Figure IV-18. SEM fractograph (30x) of a fully SVG coated composite. The fracture initiation point (arrow) is not associated with the filaments. The extremely long pullout should be noted.

emanates from the filament due to the lack of symmetry of the crack
front. Figure IV-20 is a detailed photograph of a typical situa-
tion, demonstrating that striation is actually an interruption in
the river markings. Qualitatively, the smoother the fracture
surface, the slower the propagation velocity of the crack. Like-
wise, the river markings disappear because the main crack is re-
tarded when the stress field encounters the rigid unbroken filament.
When the filament fractures, the crack accelerates for two reasons,
namely the introduction of the filament fracture energy pulse and
the encounter of the stress field with the lower strength of the
matrix. Figure IV-21 features a fracture surface showing both a
slow growth region with striations and a fast growth region without
striations. The crack is moving from right to left. At the center
of the picture, the fracture topography changes abruptly due to the
transition from stable to unstable crack propagation. This transi-
tion results from the incapacity of the remaining (uncracked) material
to support the stress imposed on it. The shape of the ridge deline-
ates the main crack shape at the time of instability. It is not
determinate which striation is associated with each filament fracture
in the slow growth region. Figure IV-22 features the left hand fila-
ment in Figure IV-21, detailing the fast growth crack sequence. It
is evident from the fracture markings that the crack moved from right
to left and ran directly from the matrix into the filament. The
fracture sequence in the unstable region is filament-matrix-filament
as originally proposed. Figure IV-23 confirms the fracture sequence
in the stable region as identical to that in the unstable region.

Figure IV-20. SEM fractograph (750x) showing the makeup of a striation. The striation is the smooth region between the river markings on the right and on the left.

Figure IV-21. SEM fractograph (150x) showing the transition from slow growth region to unstable fracture on a composite fracture surface.

Figure IV-23. SEM fractograph (200x) showing conclusively the fracture sequence. See text for explanation.

Figure IV-22. SEM fractograph (1500x) showing the left hand filament in Figure IV-21 in detail. It should be noted how the fracture proceeds directly from the matrix to the filament.

The crack enters from the right side of the fractograph and slows down as its stress field encounters the rigid filament, producing striations. The right filament fractures causing both an acceleration of the main crack and a secondary fracture front to form away from the main crack front. The secondary fracture is initiated before the main crack front reaches it, because the strain pulse propogates through the filament approximately ten times faster than through the matrix. (The propagation velocity of an elastic disturbance c in an isotropic solid is equal to $[E/\rho]^{1/2}$ where E is the absolute modulus and ρ is the density and so $c_{fil} = 1.4 \times 10^6$ m/s and $c_{mat} = 1.5 \times 10^5$ m/s). The secondary fracture sweeps out from the filament and intersects the main fracture front, generating a ridge at this intersection. This conclusively identifies the striation with the filament which is in closest proximity to it. The normal fracture sequence in both the stable and unstable propagation is for matrix cracks to cause filaments to fracture when encountered. This is the fracture sequence necessary for the intermittent bond concept to function.

As stated before in section IV-B-1, there can be more than one main fracture initiation point. Figure IV-24 illustrates the complexity of the interaction of the main crack fronts, one moving from the left and one from the right. Striations are associated with both cracks, and the right hand crack goes unstable first as evidenced by the last striation being complete. The left hand crack instantaneously changes direction perpendicular to main crack plane. Finally, the right hand crack is slowed by the presence of the then unbroken filament (third from the right).

Figure IV-24. SEM fractograph (80x) of a doubly initiated composite
fracture. One fracture front is moving from the
right and one from the left. See Figure IV-25 and
the text for details.
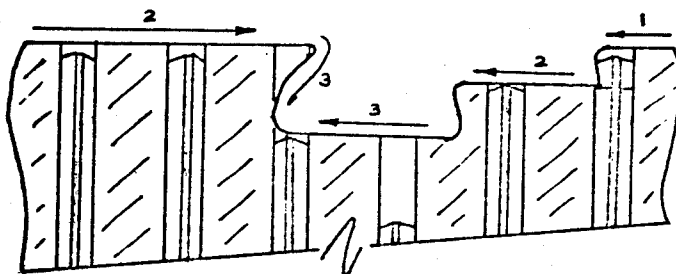
Figure IV-25. Schematic drawing of the fracture surface shown
in Figure IV-24. A sectional view through the
filaments show the relative positions of the
surfaces and the crack directions.

Figure IV-25 is a sectional view taken through the row of filaments to show the relative position of the fracture surfaces and to aid the interpretation of Fig. IV-24. The numbers in Fig. IV-25 give an idea of the fracture sequence, e.g. 1 being first, etc.

IV.B.1.c. Filament Fracture

The most prevalent mode of filament fracture is the double cone type whose schematic appears in Figure IV-26. The double cone fracture initiates from the core region which has a lower strain to failure than the outer boron sheath. The double core fracture is generally associated with filaments having mean strength, as opposed to the planar type of failure associated with low strength filament fractures discussed in section IV.B.1.b. The conical fracture is, therefore, more energetic than the planar fracture, but some of the energy is dissipated in shattering the central portion between the conical surfaces, and is less likely to initiate a matrix fracture. Figure IV-27 shows one-half of this particular type of filament fracture.

Another filament failure mode associated with the small (100 μm) diameter boron filaments is the longitudinal splitting mode. The splitting is caused by the residual tensile stress induced in the outer boron sheath by the tungsten-boride core during fabrication (see section I.A). This longitudinal splitting can be seen in Figure IV-28. The filament has simultaneously fractured in a conical manner and split longitudinally. The splitting mode of failure in the 100 μm filaments has been shown by other workers
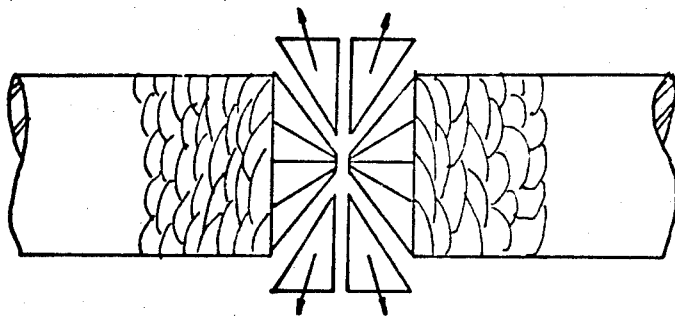
Figure IV-26. Schematic representation of the typical double
conical fracture of boron filaments.
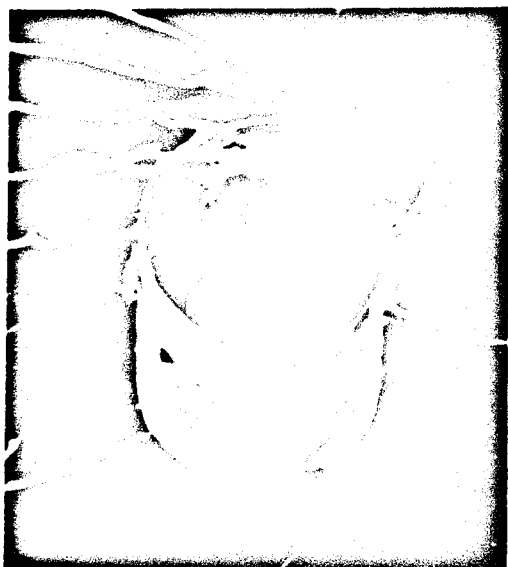
Figure IV-27. SEM fractograph (500x) of a typical conical boron
filament. The separation of the matrix from the
filament should be noted.

Figure IV-28. SEM fractograph (700x) of longitudinally split boron filament. The split tungsten core is clearly revealed.

to be the cause of low transverse tensile strengths in both poly-
meric and metallic matrix composites. This splitting has been
avoided in the larger 140 μm diameter filaments presumably by
St. Venant's principle.

IV.B.1.d. Interface Study

The interface performs a critical role in the intermittent
bond theory so it was crucial to observe the changes in the inter-
facial topography as a function of the treatment. In section I-A
the interfacial bond in a conventional boron-epoxy composite is
described as predominately mechanical in nature resulting from
the interference and interlocking between the matrix and the fila-
ment. As a result of this, any changes in the interfacial strength
should be accompanied by a change in the topography of the inter-
face. Figures IV-29 of the epoxy side and IV-30 of the boron side
of the interface demonstrate the close approach or wetting of the
boron surface by the epoxy, resulting in an accurate replica of
the "corn-cob" filament surface after the cure cycle. The epoxy
surface of IV-29 does not correspond to the boron surface in IV-30
as it appears, because the nodular surface of a boron filament is
very uniform. Figure IV-31 is a micrograph of a composite fracture
surface showing a hole left after a filament has pulled out during
the fracture process. The surface of the hole (which was the inter-
face) is very similar to that in Figure IV-29; the depth of the
cavity is approximately 0.25 mm. The surface has experienced very
little damage from the filament movement, indicating that the matrix
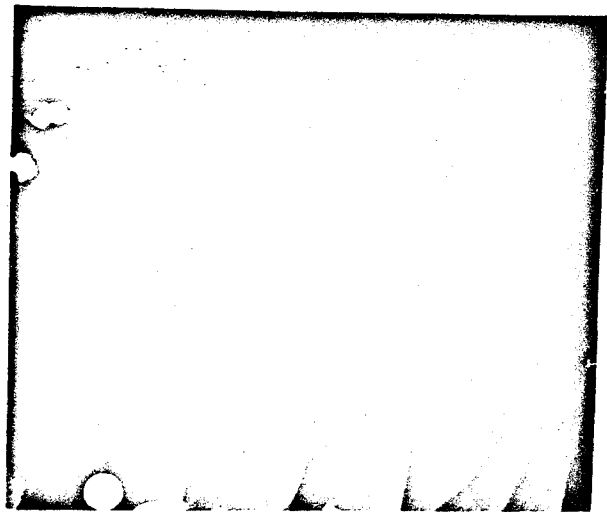
Figure IV-30. SEM micrograph (3000x) of a boron filament surface. The corn cob type surface is clearly shown.
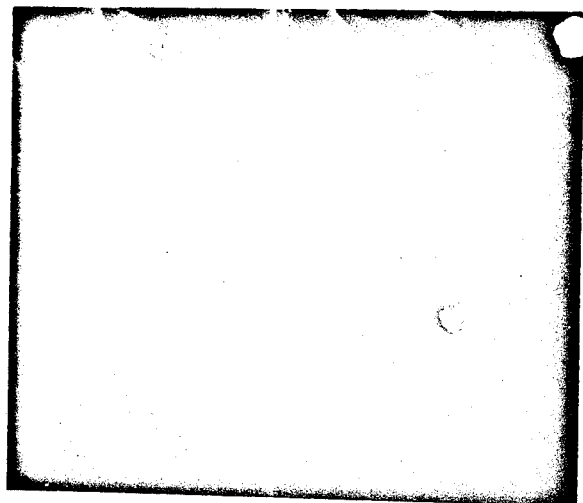
Figure IV-29. SEM micrograph (3000x) of the matrix side of a boron-epoxy interface. Compare this surface topography with that of Figure IV-30.

Figure IV-31. SEM fractograph (500x) showing the uncoated boron-epoxy interface. The filament has pulled-out revealing the epoxy replication of the boron surface.

has relaxed away from the filament at fracture providing clearance
for the filament during pullout.

As explained in section IV.A.4, the organic wetting agent
WD-40 was found to be an effective bond strength reducer and was
used in this study; Figure IV-32 depicts the interfacial appear-
ance of a WD-40 coated composite. The surface is characterized
by a ubiquity of small cavities (approximately 1.0 μm in diameter)
at the interface.

The filament has fractured in the typical double cone manner
(IV.B.1.d) with some of the shattered central portion remaining
on the conical fracture surface. A more detailed view of the
interface (Figure IV-33) shows the cavities which are caused by
vaporization of the WD-40 during cure, but also reveals a suppres-
sion of the replication of the modular boron surface, indicating
that the close approach of the epoxy has been reduced by the wetting
agent.

Coating the filaments with SVG lowered the interfacial strength
most significantly and drastically altered the interfacial appear-
ance. The following micrographs compare the coated and uncoated
interfaces of an intermittently coated tensile specimen. Figure IV-
34 reveals the near total suppression of the replication of the
boron surface implying that wetting has been minimized. The cavities
(approximately 10 μm in diameter) are a direct result of the dual
application of SVG in layer and globular form.

The uncoated interface (Figure IV-35) is very similar to Figure
IV-31 except for the presence of the rows of cavities running along
the axis of the filament. The cavities are micron to sub-micron in
size and seem to be an artifact of the coating process. The effects

Figure IV-33. SEM fractograph (4500x) of the interface shown in Figure IV-32. The cavities in the epoxy result from vaporization of WD-40. Notice the poor replication of the boron surface in the interface.

Figure IV-32. SEM fractograph (1000x) showing a WD-40 coated filament. Notice the fragments of boron lying on the filament fracture surface.
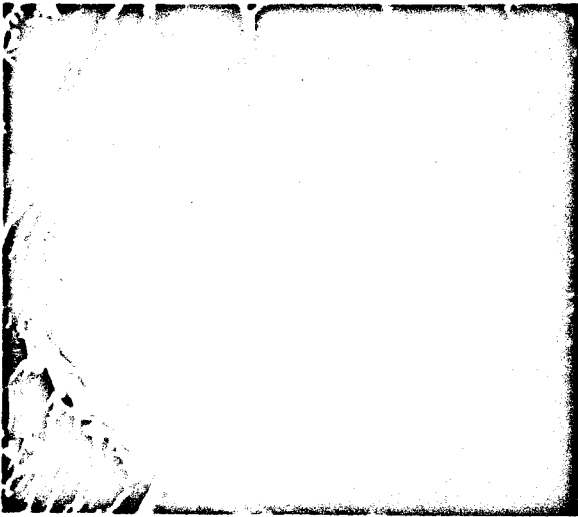
Figure IV-35. SEM fractograph (900x) of an uncoated interface in an intermittently coated composite. The interface appears to be similar to the one in Figure IV-31 except for the line of bubbles (arrow).
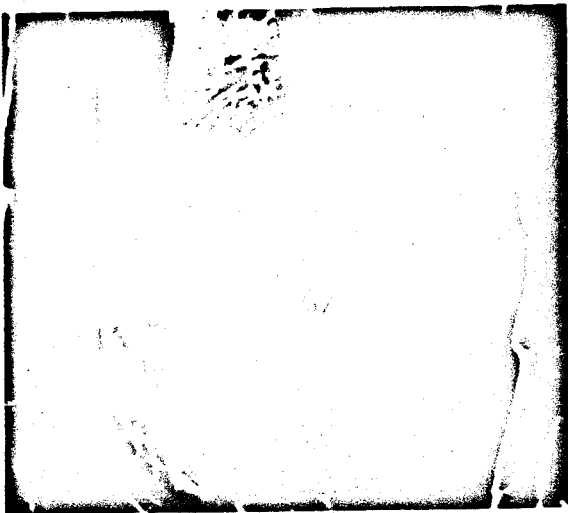
Figure IV-34. SEM fractograph (900x) of a coated interface in an intermittently coated composite.

of the cavities are not considered significant because of their sparsity, wide distribution and small size.

IV.B.1.e. Filament Coating

It was necessary to record the change in the surface appearance of a coated filament both before and after encapsulation in the epoxy to determine the effect, if any, the curing process has on the stability of the coating. The first micrograph (Figure IV-36) shows a coated filament which has been mounted in the SEM for observation. The particular area shown is the juncture of the coated and uncoated regions. The imprint of the coating rollers can be seen in the coating layer as indicated by dashed lines. The coating appears smooth with some evidence of globulation. It was only possible to remove the filaments from the cured epoxy by pyrolysis which would have certainly destroyed the SVG, therefore, the coating could only be investigated after fracturing the specimen. As shown in Figure IV-37, very little damage is done to the coating except for some streaking incurred during extraction. The globules of SVG are not apparent but the cavities indicate that they were present during the cure cycle. The SVG appeared to withstand the cure cycle without significant change.

IV.B.2. Fracture Toughness
IV.B.2.a. General Appearance

The bend-type fracture toughness specimens are high volume fraction composites ($v_f > 40\%$) and their corresponding fracture surfaces are complex and enigmatic. The complexity of the fracture process is
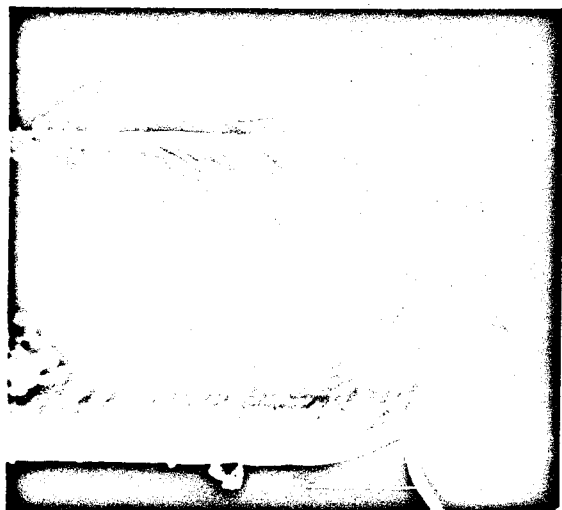
Figure IV-37. SEM fractograph (650x) shows the coating condition after fracture.

Figure IV-36. SEM micrograph (1000x) showing the junction of the coated and un-coated region of a boron filament. The lines display the outline of the coating rollers.

illustrated in Figure IV-38a, b in the form of a typical fracture surface. Both halves of the surface are included to show the pulled out filament and the holes left on the apposite surface. The abrasion marks on the side of the triangular section result from cutting with a diamond saw. The number of damaged filaments can readily be seen, also. This particular test was terminated before the crack propagated through the complete test section. This explains the change in the fracture appearance in the left portion of Figure IV-38a.

IV.B.2.b. Filament Distribution

The filaments, although initially placed randomly, are well distributed in the composite bar as shown in Figure IV-39. The filaments are touching in various places and this can have detrimental effects on the filament behavior as illustrated in the next micrograph (Figure IV-40). The central filament has split as a result of contacting the adjacent filaments and causing a severe stress concentration in the transverse direction. Commercially made prepreg tape is carefully collimated to reduce the chance of filament to filament contact.

Figure IV-38-a. SEM fractograph (45x) of a typical triangular notched fracture toughness specimen. The fracture moved from right to left.
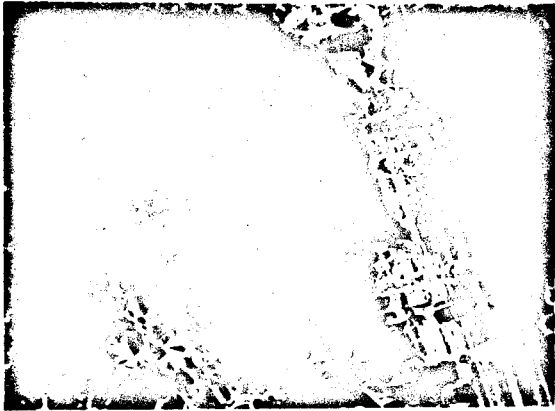
Figure IV-38-b. SEM fractograph (45x) of the upper portion of the fracture surface depicted in Figure IV-38-a. The filament marked "A" in IV-38-b, has pulled out from hole "A" in IV-38-a.

Figure IV-40. SEM fractograph (400x)
showing the detrimental effect of
filaments in contact. Notice the
crack resulting from the contact
(arrow) with the adjacent filament.

Figure IV-39. SEM fractograph (250x)
showing the typical filament packing
in a fracture toughness specimen.

CHAPTER V

Analysis of Experimental Results

V.A. Matrix Analysis

V.A.1. Tensile Analysis

The epoxy matrix material prepared for this thesis had

somewhat different properties than the manufacturer would suggest

(see Table I-III). The listing below summarizes the pertinent

experimental properties and the supplier's specifications.

TABLE V-I

Property	Experimental	Supplier	% Difference
Tensile Strength (MN/m^2)	66.5 (9.6 ksi)	86.7 (12.6 ksi)	-23
Tensile Strain (%)	2.8	4.8	-46
Elastic Modulus (GN/m^2)	3.21 $(4.65 \times 10^5$ psi)	2.48 $(3.60 \times 10^5$ psi)	+29

Some of the difference between the tensile strengths and strains can

be explained by the presence of Griffith-type flaws (see section IV.

A.1.a). Heimbuch (1970) demonstrates the effect of machining the

cast surfaces of epoxy tensile specimens. He obtained a mean strength

for as-cast specimens of 63.5 MN/m^2 (9.2 ksi), and after machining

a strength of 73.9 MN/m^2 (10.7 ksi) with a reduction of scatter. This

increase in strength and ductility is attributable to the removal of

Griffith-type flaws both of the impurity type and the cracks formed during the demolding procedure. The foreign matter tends to collect at the mold interface. The results from Shell are not specific with respect to data scatter or type of test or even if the strength value listed is an average of a number of tests. The disparity between the moduli cannot be as easily rationalized as it is not sensitive to flaws as is the strength. The higher modulus of the epoxy tested in this research indicates a higher degree of cross-linking than the epoxy listed by Shell. Because the nominal cure agent concentrations are similar, the increase in cross-linking can only be a result of the more severe cure cycle (time and temperature) used in this research. The increase in modulus would account for the remainder of the decrease in failure strain. The differences were not significant to this thesis because only one cure composition and cycle was used throughout, and the properties were consistent.

V.A.2. <u>Griffith Analysis</u>

The values of the work of fracture, δ for various epoxies , calculated from the approximate Griffith analysis were representative of the values found in the literature for the epoxy polymers. Although the literature abounds with data of impact strengths, there are few work-of-fracture data. Table V summarizes the available work-of-fracture values for different epoxies.

Recognizing the approximate nature of the Griffith analysis, the results are surprising. In spite of the finite size specimen and the nonspecific nature of flaw characterization, the work-of-fracture value derived from the Griffith analysis compares favorably

TABLE V-2

Representative Work of Fracture Values

Material	Listed Values	Test	Reference
EPON 828 (Shell Chemical)	1.7 KJ/m^2 (9.6 in-lb/in²)	Griffith	Present
EPON 828	2.6 (15.0)	3 Point Bend	Present
EFON 828	2.7 (15.5)	Unknown	McGarry (1969)
ERL (Union Carbide)	3.0 (17.0)	3 Point Bend	Beaumont (1971)
DER 332 (Dow Chemical)	1.1 (6.1)	Notched Tensile	Corton (1969)

with those derived from other methods.

The use of an integrated average elastic modulus in the Griffith analysis (see section IV.A.1.b.) which has never been advanced in the literature is important when applying any fracture mechanics relations to non-linear elastic materials. For example, in the epoxy analysis the work-of-fracture value obtained using an integrated average modulus was 25% greater than the value obtained using the initial modulus.

V.B. Composite Tensile Properties

V.B.1. Uncoated Monolayer Composite Results

The uncoated monolayer test results justify the premise that boron in the as-received condition bonds well enough to epoxy to produce mode I (see section I-C) fracture behavior. This judgment is

based on a number of experimental observations. The average filament stress corresponding to the average fracture strain (0.582%) is 2.2 GN/m^2 (323 ksi), substantially less than the average tensile strength of the filament. All fracture surfaces indicate only a single primary initiation site, namely a fractured filament. No pre-fracture filament failures are associated with the uncoated composite, no audible emissions were heard before composite failure. All of these observations imply that the first filament failure causes a catastrophic matrix crack to form resulting in the low fracture strain.

The monolayer results are well corroborated by the data from Heimbuch (1970): present tensile strength 65.6 MN/m^2 (9.5 ksi), Heimbuch for the same specimen 63.5 MN/m^2 (9.2 ksi).

These strengths are well below the rule of mixtures (ROM) prediction for 2% volume fraction filament boron epoxy, which is 122 MN/m^2 (17.7 ksi). The ROM analysis is only accurate in higher volume fracture composites, and then predicts upper bound behavior. The ROM does correctly predict that fracture would be filament controlled. The monolayer specimen does represent the behavior of the boron epoxy system in terms of fracture strain.

V.B.2. Coated Tensile Results

The four coating techniques used for this research produced a spectrum of interface strengths and tensile properties. For example, the teflon treatment did not reduce the shear strength from the virgin boron value but increased it. The rubbing action of the teflon on the filament apparently removed surface impurities such as

the absorbed water layer or even oxides which form on the boron sur-
faces. SEM micrographs showed no change in the filament surface
appearance, also indicating that a layer of teflon was not being
deposited as originally proposed. The hydrocarbon oil (Cutmax)
did reduce the interfacial strength but not to the desired extent.
This partial reduction can be attributed to the weak tendency of
the oil to wet the boron surface (i.e. it had a tendency towards
large 'contact angles'). An initially uniform layer of oil would
coalesce into discrete balls along the filament, similar to water's
behavior on a waxed surface. The wetting agent, WD-40, greatly
reduced the interfacial strength, but concurrently produced vapor
products at the interface. The most undesirable feature of this
coating material was its high wettability and its resulting mobility
on the boron surface. The vacuum grease (SVG) altered the inter-
facial strength and remained stable on the filament. The resulting
interfacial strength can be calculated if the linear stress distribu-
tion is assumed. If we assume that the longest observed pulled out
fiber (~ 24 mm) approximates one half the critical transfer length,
then the shear strength of the interface is be less than 3.1 MN/m^2
(0.45 ksi) and the corresponding interfacial tensile strength is
0.39 MN/m^2 (0.056 ksi) (see Chapter II) which are well below the
limits set forth in section I-D.

V.B.3. Intermittently Coated Composites

The intermittent bond concept has proved to be an effective
means for enhancing the tensile properties of a boron-epoxy composite.
The average tensile fracture strain is raised from 0.582% for uncoated

monolayer composites to 0.777% for intermittently coated monolayer composites. This corresponds to an increase of average filament stress in the composite from 2.2 GN/m² (319 ksi) to 3.92 GN/m² (427 ksi). This yields a 35% increase in reinforcement capability. The elastic modulus dropped only 3.1% from 11.0 GN/m² (1.59 x 10⁶ psi) to 10.7 GN/m² (1.45 x 10⁶ psi) as a result of the intermittent coating. The composite tensile strength increased from 65.6 MN/m² (9.5 ksi) for the uncoated specimen to 75.8 MN/m² (11.0 ksi) or an increase of about 16%. The increase in strength is less than one-half the increase in fracture strain due to the low volume fraction percent filament in the monolayer specimen. Each pre-fracture filament failure and its associated drop in reinforcement capacity represented a significant portion of the specimen's total reinforcement. In a high volume fraction composite, each filament failure would have an imperceptible effect on the overall load carrying capability of the composite.

The fracture strain is insensitive to volume percent coated filament in the range tested (38 to 82%). The average fracture strain for each volume fraction coated filament test series proved to be within 3.6% of the average of all the intermittently coated specimens. The variation of average fracture strain from group to group (see Table IV-4) proved to be randomly distributed about the mean overall fracture strain, indicating there is no preferred volume fraction of coated filament.

One test series was conducted to study the effect of decreasing the uncoated length. From the limited test data taken, it became

evident that critical transfer length-over-diameter ratio is less
than fifty. The theoretical critical transfer length ratio for this
system was thirty.

Fractographic and experimental observations support the validity
of the intermittent bond concept. The fractures are generally multi-
initiated, indicating that the average filament stress is near the
average filament tensile strength. The few specimens which are
singly initiated have a slow growth region encompassing over one-
half the specimen area. The filaments fracture well off the crack
plane in intermittent coated composites resulting in low filament
pullout. In all intermittently coated specimens, multiple pre-frac-
ture filament failures were encountered. These pre-fracture failures
were generally concentrated in one area of the test section rather
than randomly distributed throughout the gage section. This localiza-
tion of filament fracture results from a short range stress increase
due to adjacent filament failures, an interaction typical of composite
materials.

V.C. Interlaminar Shear Strength

The interlaminar shear strength (ILS) of a composite material is
a direct function of the interfacial shear strength and ILS tests are
then a measure of the interfacial shear strength. The short span
three-point bend test (described in section III.B.3.) is the oldest
and most disputed of the ILS tests but also the simplest to conduct.
The main objection to the test is the uncertainty of the failure mode.
The bend test is excellent for comparing surface coating effects.

As a rule of thumb, the percent planar fracture area associated with the filaments is the square root of the volume fraction of the filaments. For example, given a 0.43 v_f composite failing in an interlaminar shear mode, 0.66 of the fracture area would be exposed filament as a result of interfacial failure.

The as-received boron-epoxy ILS values compare very favorably with the interfacial shear strength values obtained from other tests (see Chapter II). Qualitatively, the ILS test demonstrated the effects of coatings and treatments. For example, boiling the boron filaments in methanol reduced the interfacial shear strength as Broutman (1969) had determined in another type of test. The ILS tests also showed that acetone reduces the effectiveness of the SVG coating. The ILS values are included in Table IV-5.

The ILS of an intermittent coated composite was thought to be approximated by a ROM analysis using areal percent rather than volume percents. The shear strength equation was:

$$\tau_c = A_m \tau_m + A_{f_c} \tau_c + A_{f_{uc}} \tau_{uc} \qquad (V-1)$$

where A_m, A_{f_c}, $A_{f_{uc}}$ are the areal percent of matrix coated and uncoated filaments and the τ's are the corresponding shear strength. The matrix shear strength was approximated by one-half the tensile strength or 51.5 MN/m^2 (7.5 ksi). The agreement with the measured values is poor, and equation V-1 was not used, but with minor sophistications it might be useful.

V.D. Composite Fracture Toughness Data Analysis

V.D.1. Fracture Toughness Data (General)

The intermittent bond concept originally assumed a direct
correlation between fracture strain (and stress) and fracture
toughness. The experimental data listed in section IV.A.6.a. shows
this assumption to be untrue. This discrepancy is a result of over-
simplifying the parameters affecting the work of fracture (WOF).
The three composite fracture toughness theories found in the litera-
ture indicate that only the interfacial shear strength affects the
work of fracture (see section I.D.2.), but it would seem that the
energy to fracture the interface must also be taken into account.
A new composite fracture toughness theory will be presented in section
V.E. to account for both the shear strength τ and the interfacial
energy γ_{if}.

The notched three-point bend test series was designed to evalu-
ate a coating and/or a treatment effect on a composite's work of
fracture. The as-received boron test established a base-line per-
formance. Methanol boiling resulted in both a reduction of the inter-
face strength and the work of fracture, indicating that the inter-
facial energy was reduced. Fully coated (SVG) composites were fabri-
cated using an epoxy diluted with acetone to facilitate infiltration
of the filament bundle. The specimen bar was cut into individual
specimens which prevented ILS tests from being conducted, but the
work of fracture values show that the coating reduced the interfacial
energy. The untreated filament composites (AR) showed the highest
average work of fracture values of all uniformly treated composites.

Some intermittently coated samples were produced to investigate the WOF as a function of percent coated filament (v_{fc}). The first group tested were 50% coated as it was felt that this would reveal the intermittent bond effect most conspicuously. The epoxy was diluted with acetone (50-50 w/a) to enhance the infiltration of the filament bundle as a result of its lower viscosity. The average WOF values were considerably lower than both the fully coated and the as-received specimens. One particular specimen (50-50 w/a-2) gave extremely low values and a SEM examination showed a "resin-rich" area at the apex of the test section, as shown in Figure V-1. Both the 50-50 w/a and the 100% coated specimen showed a ubiquity of bubbles in the composite resulting from a vaporization of the acetone during the cure cycle in spite of extensive evacuation before sealing the mold. Figure V-2 shows the form of the vapor pockets. It was originally felt that the decrease in WOF was a result of the acetone diluted epoxy, so a series of tests were conducted with undiluted (50-50 w/o) epoxy. The average WOF rose, but not to the as-received values. The coating process was altered to permit coating the filament in one operation instead of five (50-50 Single Wrap). This series gave less scatter and a higher WOF value, but remained 15% less than the as-received values.

A final test group called ENDS gave the highest toughness values. The ENDS' filaments were actually scrap filament from the tensile specimens of varying degrees percent coated. The filaments were placed in an empty bottle for two and a half months before incorporating into composite bars. The "drying time" of 75 days apparently

Figure V-2. SEM fractograph (1000x) showing the vapor pockets formed during cure.

Figure V-1. SEM fractograph (250x) showing the 'resin rich' area in the apex of the test section.

altered the bonding characteristics of the boron epoxy and the re-
sulting interfacial energy. The long term effects of drying on the
SVG coating would be an interesting topic for future research.

V.D.2. Work of Fracture vs Strength Data

The strength property (σ) and the work of fracture property
(γ) of the composites tested in this thesis have a peculiar correla-
tion. All of the bend toughness data were plotted with σ as the
ordinate and γ as the abscissa and are reproduced as Figure V-3.
All of the composite specimens have nominally the same geometry,
number of filaments of the same strength and crack size, the only
intentional difference being in the filament surface treatment. The
strength (measured in bending) initially rises as a function of the
work of fracture γ and this continues until the strength reaches
the rule-of-mixture (RCM) strength. From this point, an _increase_
in toughness is accompanied by a _decrease_ in strength. Intuitively,
the strength is governed by two independent criteria.

Many authors such as Beaumont (1971) or Harris (1971) purport
that composite materials follow a linear elastic fracture mechanics
(LEFM) relationship as long as the plane of crack propagation corre-
sponds to a plane of symmetry. Dense unidirectional composites
possess orthotropic symmetry, i.e. properties are constant in all
directions perpendicular to the filament axis. In the toughness bend
specimens, the crack propagates perpendicularly to the filament which
is a plane of symmetry. The toughness specimens should be amenable
to LEFM.

$\sigma \propto 1/\tau$

$\sigma \propto \gamma^{1/2}$

(ROM)

Strength

Fracture Toughness

Figure V-4. Analytical strength-frac-
ture toughness curve.

ROM

Strength (ksi)

$\gamma = G_c/2$ in-lb/in^2 (X 10)

1 2 3 4 5 6 7 8 9 10 11 12 13 14 15

Figure V-3. Experimental strength-frac-
ture toughness curve.

In Chapter I, it was shown that for anistropic materials the critical stress intensity factor is related to the critical strain energy release rate by $K_c^2 = \frac{1}{\bar{E}}$ Gc where $\bar{E}$ is the effective modulus (see equation I-15). For a fixed volume fraction filament in a unidirectional composite $\bar{E}$ is a constant, and Gc is proportional to the square of Kc. In LEFM, Kc is related to the strength by a specimen factor $[a \pi c]^{\frac{1}{2}}$ where a is a specimen geometry factor (see section I-D) and c is the starting crack length. For a given specimen geometry and crack dimension as we have in the bend toughness specimens, Gc should be proportional to the square of the strength.

The strength of composite materials is a function of the interfacial shear strength as shown by Kelly and Tyson (1966) and Greszczuk (1969). Physically, this is due to the mode of reinforcement; and once the shear strength falls below a certain value for a given filament length, the filaments are no longer reinforcing to their potential degree. The composite strength is bounded upwards by the rule-of-mixtures and once the ROM is reached an increase in shear strength has no beneficial effect. As mentioned in Chapter II and to be discussed in section V-E, the work of fracture of a composite material is inversely proportional to the interfacial shear strength (see, for example, Harris,1971, and Kelly, 1969).

All of this information is incorporated in Figure V-4. The dashed positive slope line represents the LEFM relationship of work of fracture to the square of the strength. (This is a monotonically increasing function.) The abscissa l is also representational of $1/\tau$

and the composite strength as a function of shear strength is de-
noted by the negatively sloped dashed line. The resultant strength
of the composite (solid line) is controlled by the LEFM relation-
ships before it reaches the ROM level, as δ increases (and σ
decreases),the composite strength is governed by the interfacial
strength.

The reasoning behind Figure V-4 is qualitative at best but is
supported by experimental observations. It should be noted that
the strengths are based upon the flexural test, which is a disputed
test to begin with (see Rosen and Dow, 1972) and the stress analysis
uses only approximate bending theory. The stress state of the tri-
angular notch bend specimen has been investigated using approximate
computer techniques and the results show reasonable agreement with
the simple stress analysis in the initial stages of crack propaga-
tion (Atkins and Raghava, 1972).

The physical meaning of Figure V-4 can be explained using the
following rationale. The rising portion of the σ-γ curve is
attributable to the presence of a fabrication flaw such as the resin
rich (filament poor) region shown in Figure V-1 or interfacial defects
due to coating dissolution by solvents such as acetone, or broken
fibers. The negatively sloped portion of the σ-γ curve is more
difficult to explain physically. If the shear strength is lowered,
the propensity of pulled out (rather than fractured) filaments must
increase. This phenomenon should manifest itself on the fracture
surfaces. All of the specimens which fall on the right hand portion
of the plot exhibit extremely long pullout as shown in Figure V-5.
It is not conclusive whether the filaments pulled out intact or frac-
tured.
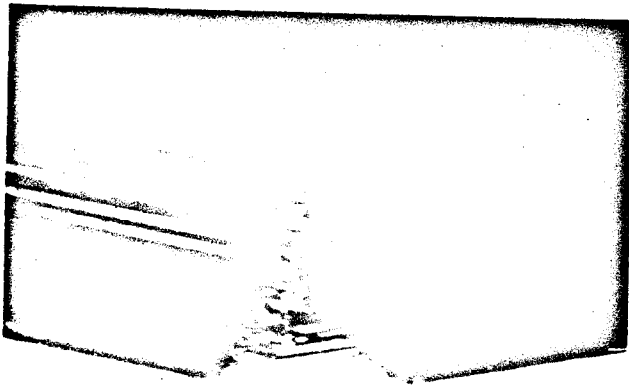
Figure V-5. Optical micrograph (9·2 x) showing the filament pull-out experienced by high fracture toughness specimens.

V.D.3. Incremental Work-of-Fracture Measurement Techniques

Three methods are proposed in Chapter IV for the measurement of incremental work of fracture (WOF), namely the modified Irwin technique, the energy method and the electrical resistance method. Reviewing Tables IV-1, IV-2 reveals that both the Irwin and the energy methods give comparable values and indicate similar trends in the data. The electrical resistance method predicts unrealistic high values for the initial WOF, and the values fall off exponentially to an unrealistic low value. The electrical resistance method for measuring crack area is not amenable to this type of specimen because of the uncertainty of electrical contact between all of the filaments.

The energy method is chosen over the Irwin method for two reasons: one, it requires only the compliance as a function of crack area data rather than the derivative of the compliance-crack area data, and two, the energy dissipated is measured directly off the load deflection plot by graphical integration. The energy method utilizes the fundamental concept of the WOF - the energy dissipated by a crack propagating over an area, divided by that area.

V.D.4. Incremental Work-of-Fracture Distribution

The incremental work of fracture is not constant across the triangular test section of the bend toughness specimens. The work of fracture for all filament conditions rises from one initially low value at the apex of the test section to a maximum at a point about sixty percent of the way into the test section and then decreases the remainder of the way. This distribution is controlled by two independent quantities; the first being the instantaneous stress state and the second being the condition of the filament.

The stress state for a cracked body is almost totally controlled by the section thickness. A thin cracked section will experience a condition of plane stress because one of the principle stresses is no higher than ambient pressure. The resulting stress state is two dimensional and the corresponding strain state is three dimensional. On the other hand, a thick cracked section will undergo a plane strain state because of the almost zero strain in the lateral direction caused by the constraint exerted by the uncracked surrounding material. The strain in this condition is two dimensional and the stress state is three dimensional.

The work of fracture is greatly influenced by the stress state
a material experiences. The plane stress work of fracture is sub-
stantially greater than the plane strain work of fracture for the
same material. Irwin (1960) cites a $3\frac{1}{2}$ times greater work of frac-
ture value for plane stress than for plane strain in a 7075 aluminum
alloy and a seven fold increase for a 2024 T4 aluminum alloy. Apply-
ing the above observation to the composite bend specimen results
in the following hypothesis. The crack (or fracture) always begins
in the apex of the section where the stress state would be plane
stress because of the thin section. The corresponding work of frac-
ture for this apex would be high. As the crack penetrates the test
section, it encounters progressively thicker section material, and
hence, the stress state becomes more plane strain than plane stress.
With this change in stress state goes a drop in the instantaneous
work of fracture. The rate of crack propagation will affect the
local WOF value, but for simplicity the effect is neglected.

This hypothesis is corroborated by the data for boron-epoxy
toughness specimens found in Beaumont (1971). The instantaneous
work of fracture was determined by using the modified Irwin technique
(see section IV.1.c.). Figure V-6 schematically shows the work of
fracture distribution due solely to specimen design (denoted by the
solid line).

The initially low values for the work of fracture result from
a preponderance of damaged filaments in the apex of the test section.
Figure V-7 illustrates the type of damage and clearly shows the frac-
ture was initiated from the damage. The filament damage is a result
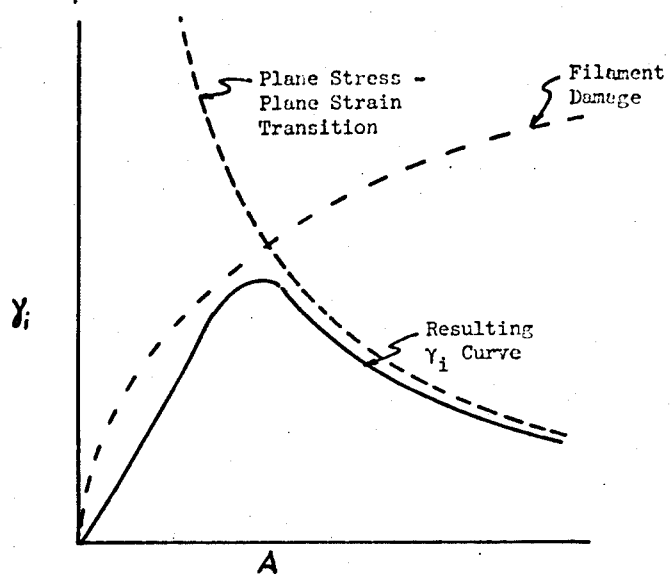
Figure V-6. Analytical incremental work-of-fracture distribution.

Figure V-7. SEM fractograph (250x) showing typical filament damage.

of the non-uniform (on a fine scale) abrasive cutting action of
the diamond wheel. The damage is confined to a depth of 100 μm
and is nearly uniform along both cuts of the triangular test
section. The proportion of damaged filaments is nearly 100% in
the apex and drops to less than 6% in the base of the triangle.
As shown in Figure V-7, the damage can be severe and has a marked
detrimental effect on the local work of fracture. The magnitude
of the damaged filament effect is related to the proportion of
damaged fibers and, therefore, is greatest in the apex and negli-
gible at the base. The dashed line in Figure V-6 represents the
resulting distribution of the work of fracture and is a combination
of the damaged filament effect and the plane stress-plane strain
transformation.

V.D.5. The Anomalous Y_i Distribution

The interpretation of the Y_i distribution is apparently con-
tradicted by specimen AK-4. This virgin boron composite embodies
two maxima in its Y_i distribution. The two maxima could not be
explained from basic principles, therefore an SEM fractograph analy-
sis was made on the specimen. Figure V-8 is a composite figure con-
taining the complete fracture surface, the load deflection curve
divided into region of crack advancement, the incremental WOF plotted
as a function of crack depth (below the fractograph) and the crack
area vs crack depth relationship plotted above the picture. The
vertical solid lines correspond to the approximate crack extension
limits associated with each load drop. Although the crack front
could not be characterized as strictly rectilinear, the line does

Fig. V-3   The anomalous γ_i distribution (see text.)

provide a feeling for the crack boundaries.

The double maxima appear in the 3rd and 5th regions of the surface with the drop in γ_i in the 4th. The 4th region should be the area of highest γ_i , according to the explanation in section V.D.4. and, therefore, is actually more than a 75 $\frac{\text{in-lb}}{\text{in}^2}$ drop in γ_i . A critical observation of this region reveals an anomalous fracture appearance.

The area corresponding to the γ_i drop is distinquishable from the remainder of the fracture surface. The region located by the intersection of the vertical line bounding regions 3 and 4 and the horizontal midline of the specimen is uniquely devoid of pulled-out filaments. This is in contrast to the remainder of the fracture surface which is characterized by pullout averaging five filament diameter in length. The cause of the drop in γ_i and the lack of pullout is presumed to be a result of excessively high interfacial strength. The reason for this localized increase is unknown.

If this condition of high interfacial strength were not present, the drop in γ_i at this point would be replaced by a maximum. Therefore the apparent contradiction of the theory presented in section V.D.4. results from an extraordinary bonding condition between the boron and the epoxy and is independent of the variables controlling the theory.

V.D.6. Fracture Toughness Plate Specimen

The shortcomings of the notched bend specimen can be circumvented by using a compact tensile specimen (described in section III. A.1.e.). The main drawbacks of the bend specimen include: peculiar

stress distribution which is very difficult to analyze, filament
damage resulting from machining the test section, and varying
specimen thickness (the plane stress-plane strain transformation).
The compact tensile specimen has been extensively reviewed by
Brown and Srawley (1968), but only stress distribution data for
isotropic materials are available. One advantage is that the
damage due to machining is present only at the end of the starter
crack. Preliminary compact tensile specimens were fabricated as
described in section III, but no toughness data were obtained. The
specimen suffered from poor filament alignment and lack of infiltra-
tion of the filaments by the epoxy resulting in gross bubbles. The
filament supply was exhausted before the fabrication techniques
were perfected. I have recommended this specimen design for future
fracture toughness studies because of its potentially unambiguous
results.

V.E. Fracture Toughness Theory

I am proposing a new theory for the approximation of the work
of fracture of composite materials. The theory is based on two
experimental observations. The first is deduced from the observation
that there is no pre-fracture debonding between the filament and the
matrix; the second involves fracture and the fact that the matrix
material relaxes away from the filaments thus minimizing the normal
force and frictional force between the filament and the matrix.
(This has never been recorded in the literature.) These two observa-
tions essentially refute the pullout theory of Kelly (equation I-10)
and the debonding theory of Outwater and Murphy (equation I-17).

The present theory accounts for the energy absorbed in creating new surfaces during the fracture of a composite material which the others don't. There are three types of surfaces created during fracture: 1) cross sectional filament surfaces resulting from filament fractures, 2) cross sectional matrix surfaces resulting from matrix fractures, and 3) surfaces created between the filament and the matrix as a result of interfacial failures. Associated with each type of surface is an energy needed to create the condition labeled 'surface energy' when no irreversibilities are present and 'work of fracture' when they are. In order to predict the total energy absorbed, it is necessary to account for both the area created and the total work done to create a unit of that area. The total energy is simply the sum of the products of the areas and their associated energies.

The area of newly created filament area can be approximated by:

$$A_f = N\pi d^2/4 \qquad\qquad (V-2)$$

where N is the total number of filaments fracturing and d is the filament diameter. This assumes a planar type of filament fracture, and is not strictly correct for the double conical fracture present in the boron system. γ_i' is the surface free energy of the filament.

The second type of surface formed is the matrix area which can be approximated by the equation

$$A_m = A_{nominal} - A_f \qquad\qquad (V-3)$$

where A-nominal is the nominal cross sectional area. This equation

neglects the small order deviation from a planar fracture surface

such as branching, parabola formation, etc. The work of fracture

for the matrix material Y_m is determined experimentally with a

suitable specimen.

The third type of newly formed surface is by far the greatest

with respect to the dissipation of fracture energy. The surface

area created by interfacial fracture and subsequent filament pull-

out (with near-zero frictional work) can be approximated by:

$$A_{if} = N\pi d\overline{\ell} \qquad (V-4)$$

where $\overline{\ell}$ is the average exposed length of filament on both halves

of the fracture surface. If the filaments fracture randomly, the

average length of exposed filament will be one-fourth the critical

transfer length, since the longest exposed filament will be one-half

the critical transfer length and the shortest will be zero length

(see section I.B.1.). Kelly (1970) proposes a theory for the random-

ness of filament fracture. He states that if the elastic strain

energy stored in the matrix at the time of fracture time is much

less than the strain energy of the filament, then the filaments will

break randomly. Mathematically, this is expressed as:

$$\tau < \sigma_f \{G_m / E_f \}^{1/2} \qquad (V-5)$$

where τ is the shear strength of the interface, E_f is the modulus

of filaments with strength σ_f , and G_m is the shear modulus of
the matrix. Approximate values for the boron epoxy system are
G_m = 4.62 GN/m^2, E_f = 3.79 GN/m^2, and σ_f = 3.00 GN/m^2 and the
shear strength is required to be less than 0.311 GN/m^2. The high-
est observed shear strength is 0.106 GN/m^2 (Avco, 1972). It can
be assumed that the filaments fail in a random fashion as fracto-
graphic evidence would corroborate. Equation V-4 becomes

$$A_{if} = N\pi d \ell_c / 4 \qquad (V-6)$$

The energy associated with the interface is γ_{if} . The total energy
consumed is equal to

$$U_{total} = N\pi d^2 \gamma_f'/4 + (A_{nom} - N\pi d^2/4)\gamma_m + N\pi d\ell_c\gamma_{if}/4 \qquad (V-7)$$

The work of fracture is defined as simply the total energy dissipated
divided by the area of dissipation or:

$$G_c = 2\gamma = U_{total}/ A_{nom} \qquad (V-8)$$

The nominal (or cross-sectional) area can be accounted for in the
definition of volume fracture filament:

$$v_f = N\pi d^2/(4A_{nom}) \qquad (V-9)$$

Rearranging gives:

$$A_{nom} = N\pi d^2 / 4v_f \qquad (V-10)$$

Substituting equations V-7, 10 into equation V-8 gives:

$$G_c = 2\gamma = v_f\gamma_f' + (1-v_f)\gamma_m + v_f^2{}_c\gamma_{if}/d \qquad (V-11)$$

The definition of the critical transfer length equation (I-6)

$$\ell_c = \sigma d/2\tau \qquad (V-12)$$

can be incorporated into V-11 giving:

$$G_c = 2\gamma = v_f\gamma_f' + (1-v_f)\gamma_m + v_f\sigma\gamma_{if}/2\tau \qquad (V-13)$$

In order to approximate the work of fracture, γ_{if} must be known. The following sample argument is advanced to approximate the value of γ_{if} with the matrix toughness γ_m in an uncoated boron epoxy composite. If the interfacial surface energy were much less than the matrix surface energy, the interface would fracture along the filament simply from the Poisson effect. Conversely, if the γ_{if} were greater than γ_m the filament would be coated with adhering matrix material after fracture, which the fractographs never reveal. From these arguments, the first approximation of γ_{if} is γ_m and equation V-13 becomes

$$G_c = 2\gamma = v_f\gamma_f' + \{(1-v_f) + v_f\sigma/2\tau\}\gamma_m \qquad (V-14)$$

γ_f' is generally much smaller than γ_m and when multiplied by a fractional number becomes insignificant and can be disregarded. In the boron epoxy system, $\gamma_f' = 3.5$ J/m^2 (0.0185 in-lb/in^2) and $\gamma_m = 2.6$ KJ/m^2 (15 in-lb/in^2). The final approximation equation for the work of fracture for an uncoated composite material is:

$$G_c = 2\gamma = ((1-v_f) + v_f \sigma/2\tau)\gamma_m \qquad (V-15)$$

A similar theory can be developed for an intermittently coated composite, as long as the interfacial energies of the coated and uncoated regions are differentiated. The energy of the uncoated segment is assumed to be equal to the energy of the matrix as before. The intermittent theory is described mathematically as:

$$G_c = 2\gamma = (1-v_{f_c} -v_{f_{uc}})\gamma_m + v_{f_c} \sigma/2\tau_c \gamma_{if_c} + v_{f_{uc}} \sigma/2\tau_{uc}\gamma_m \qquad (V-16)$$

if the coated length L_c is greater than the coated critical transfer length l_c. If the coated length L_c is less than l_c, the average exposed length will be $L_c/2$ and the contribution for the coated segment will be $v_{f_c} 2L_c\gamma_{if_c}/d$ rather than $v_{f_c} \sigma/2\tau_c(\gamma_{if_c})$.

The following table compares the four theories of fracture toughness based on the experimental data obtained in this research. The required data for the uncoated boron epoxy system includes:
$\sigma_f = 430$ ksi (2.96 GN/m^2), $E_f = 55$ Msi (380 GN/m^2), $\tau = 10$ ksi
$\tau = 69$ MN/m^2, $v_f = 0.42$.

tho critical transfer length l_c is .086 in (2.18 mm). For tho Outwater-Murphy Theory, a value of $1\ l_c$ will be assumed for D (see section I.D.2.). The work of fracture for the epoxy will be assumed to be 15 in-lb/in^2 (2.67 KJ/m^2).

TABLE V-3

Comparison of the Four Toughness Theories
for Composite Materials

Theory	Formula	Prediction in-lb/in^2 (KJ/m^2)	Experimental in-lb/in^2 (KJ/m^2)
Kelly (sec. I.D.2.)	$G_c = v_f \sigma_f \ell_c /12$	1300 (228)	199 (35)
Outwater-Murphy (sec. I.D.2.)	$G_c = v_f \sigma_f^2 D/2E_f$	61 (10.5)	199 (35)
Relaxation (sec. I.D.2.)	$G_c = v_f \sigma_f^2 \ell_c /3E_f$	40 (7)	199 (35)
Marston Interfacial Energy (sec. V.E.)	$G_c = (v_m + v_f \sigma/2\tau)\gamma_m$	162 (29.0)	199 (35)

* $G_c = 2\gamma$

For each composite system, there is a predominant energy dissipation mechanism contributing to the work of fracture. This does not mean that it is the only operating mechanism. In the glass-polyester system (fiberglass), the predominant mechanism is debonding (see

Table I), but the relaxation phenomenon is also absorbing energy.
It is not possible to have both the debond mechanism and the surface
energy mechanism acting in one system, because they both account for
fracturing the interface. In the boron-epoxy system, the major
energy dissipation is the surface energy, but relaxation is also
present. Debonding and pullout are not effectual as discussed in
section V.E. p. 137. The total work of fracture for the boron epoxy
composite should be the sum of the energies dissipated by the forma-
tion of new surfaces and the relaxation of stresses. From Table V-3,
the sum is (162 in-lb/in^2 + 40 in-lb/in^2) = 202 in-lb/in^2 which is
within 2% of the measured value of 199 in-lb/in^2.

This approach of accounting for all the various mechanisms can
be applied to the carbon polyester system. This system is chosen
for two reasons; the first being the principal energy dissipation
mechanism is filament pullout (in contrast to the boron-epoxy system)
and the second being the availability of information as a result of
P.W.R. Beaumont's data (Harris, et al., 1971), which are: σ_f =
1.58 GN/m^2 (249 ksi), V_f = 0.44%, E_f = 360 GN/m^2 (52 msi), l_c/d
120, d = 8 μm (.0032 in), τ = 20 MN/m^2 (4.34 ksi), γ (polyester) =
1.32 KJ/m^2 (McGarry, 1968), (4.0 in-lb/in^2), and γ = 34 (KJ/m^2
(194 in-lb/in^2).

Since the principal contributor to the work of fracture is due
to pullout, the Kelly equation for this system is:

$$\gamma = v_f \sigma_f l_c /24 = \frac{0.4 \times 1.6 \times 10^9 \times 120 \times 8 \times 10^{-6}}{24} \qquad (V-17)$$

$$= 25.6 \text{ KJ/m}^2$$

This is 8.4 KJ/m^2, lower than the experimental value. Relaxation and the surface energy mechanism are also operating. The debond mechanism is precluded because of the small fracture strain of the filaments (see section I.D). The work of fracture due to relaxation can be approximated by equation V-17

$$\gamma = v_f \sigma_f^2 \ell_c / 6E_f = \frac{0.4 \times (1.6\times10^9)^2 \times 120 \times 8\times10^{-6}}{6(3.6)\times10^{11}} \qquad (V-18)$$

$$= 0.45 \text{ KJ/m}^2$$

The surface energy mechanism is predicted by:

$$\gamma = G_c/2 = (v_f/2)\sigma_f \gamma_m / 2 = \frac{0.4 \times 1.6\times10^9 \times 1.32}{2(4.0\times10^7)} \qquad (V-19)$$

$$= 9.5 \text{ KJ/m}^2$$

The total work of fracture for the carbon-polyester system is:

$$\gamma_{total} = \gamma_{pullout} + \gamma_{relax} + \gamma_{surface \ energy}$$

$$= (25.6 + 0.45 + 9.5) = 35.6 \text{ KJ/m}^2$$

This is within 5% of the measure work of fracture value.

CHAPTER VI

Conclusions

1.- The fracture toughness Gc of the epoxy matrix material Epon 828
with 25 pph Shell Z hardener can be approximated from unnotched
tensile tests using fractography to measure the flaw size and the
Griffith analysis for brittle materials. The value is 1.7 kJ/m^2.

2.- An integrated average modulus is more appropriate for fracture
toughness calculations for non-linear elastic materials such as
epoxy or cast iron rather than the traditional initial tangent
elastic modulus.

3.- The fracture strain of composites containing a higher percentage
of filaments than the critical volume percent is an inverse function
of the interfacial shear strength τ but is bounded upwards by the
average filament fracture strain ε_f .

4.- A silicon vacuum grease (SVG) coating effectively reduces the
interfacial bond between the boron filament and the epoxy matrix
resulting in a reduction of the shear strength from a virgin value
of approximately 67.5 MN/m^2 (9.8 ksi) to a coated shear strength
value of 3.1 MN/m^2 (0.45 ksi).

5.- The intermittent bond concept is a viable means for improving the
tensile properties of a boron-epoxy composite. The average fracture
strain of the intermittently coated composites is 135% of the average
fracture strain of the uncoated composite and is equal to the average
filament fracture strain.

6.- The fracture strain of the intermittently coated composites is insensitive to the percent of coated filaments in the range from 38% to 82% coated because the fracture strain is bounded by the average filament fracture strain.

7.- The scanning electron microscope (SEM) is the most successful means for investigating composite fracture surfaces because of the intrinsic depth of field of the machine. From SEM fractography, the fracture sequence in both coated and uncoated composites is deduced as being that the fracture proceeds from filament to filament by way of a matrix fracture rather than directly from filament to filament.

8.- The fracture toughness G_c of a boron epoxy composite is more than an order of magnitude greater than the weighted sum of the toughness of its constituents. The average G_c for virgin, 42% volume filament composite is 34.8 KJ/m^2 (199 in-lb/in^2), and the fracture toughness of the epoxy matrix is 2.64 KJ/m^2 (15 in-lb/in^2) and the fracture toughness of boron is less than 3.25 J/m^2 (0.0185 in-lb/in^2).

9.- Linear elastic fracture mechanics (LEFM) is useful for predicting the toughness-strength relationship as long as the strength is mono-tonically increasing and the strength is less than the RCM strength, which is the upper bound for composite strength. If these criteria are not met, the toughness is inversely proportional to the strength.

10.- The fracture toughness of boron epoxy is not strictly a function of the interfacial shear strength as predicted by the pullout, debond-ing and relaxation theories, but a combined function of the inter-

facial shear strength and the fracture energy of the interface.

11.- The fracture toughness contribution from interfacial energy dissipation in a uniform bond strength composite is approximated by the equation

$$G_c = (1-v_f+v_f\sigma/2\tau)\gamma_m$$

where v_f is volume percent filaments, σ_f is the average filament strength, τ is the interfacial shear strength and γ_m is the energy needed to fracture a unit area of the interface. The γ_{if} for an uncoated boron epoxy composite can be approximated by the fracture toughness of the matrix γ_m.

12.- The interfacial energy contribution of an intermittently coated composite is controlled by both the shear strengths and the interfacial energies of the coated and uncoated regions. The toughness of the intermittently SVG coated boron epoxy composites was less than that of the as-received filaments composites, since the γ_{if} was reduced to a greater degree than the shear strength.

13.- The fracture toughness of a composite material reflects the combined total dissipative mechanisms of interfacial fracture (or debonding depending upon the ratio of the filament fracture strain to the matrix fracture strain), relaxation of the stresses and filament pullout. Acknowledging all these contributions (which has not previously been done), the toughness of boron epoxy composites is predicted to within 3% of the experimental value and the fracture toughness of carbon-polyester composites is predicted to within 4.7%.

14.- The notched three point bend specimen is not the ideal specimen design for composite fracture toughness measurement. The values obtained with these specimens are affected by the increasing section thickness of the test section and damage incurred during the fabrication process. Local fracture toughness values can be three times as high as the integrated average value.

CHAPTER VII

Recommendations for Future Research

The shortcomings of the notched three-point bend specimens for making fracture toughness measurements are discussed in Chapter VI and suggestions for new specimen design are in order. The compact tensile specimen (also called the composite plate specimen) has been described in section III.A.1.e. and its advantages will be summarized below. The filament spacing can be carefully controlled and no handling of coated filament is required. The stress state of the tensile specimen closely approximates that of a cracked composite skin section under tension. There is no thickness change as the crack propagates, and more importantly filament damage is restricted to the end of the starter crack. One suggested change in the original design is to machine the starter notch with as thin a diamond wheel as possible in order to approximate a natural crack. One problem in this specimen design is the presence of transverse cantilever stresses due to the finite size of the specimen (see Atkins et al., 1972). It may be necessary to strengthen the specimen in the transverse direction with a cross-plied outside layer. The preliminary specimen refinement should be conducted with commercially available Prepreg tape to save time.

A second possible specimen design is a composite in the form of an internally pressurized cylinder. The tube can be wrapped on a polymeric mandrel with the present apparatus. The filament spacing

can be accurately controlled and handling of the filament is again
unnecessary. One advantage of this specimen is the variety of
stress states available by simply varying the ratio of axial to
hoop stress ratio. Adequate testing apparatus is also available
through the Mechanical Engineering Department at The University of
Michigan.

The interfacial energy theory (see section V.E.) clearly demon-
strates the importance of the interfacial surface energy with re-
spect to fracture toughness of composite materials. The fracture
toughness results of Chapter IV clearly reveal that SVG reduces
this energy proportionately more than it reduces the interfacial
shear strength. I am suggesting that the shear strength criterion
of Chapter II be relaxed and less effective bond reducers be tested.
Graphite would be one possible candidate (see Mullin et al., 1970).
Coating materials should be screened using a fracture toughness test
rather than a tensile test. Once the coatings are selected, a
tensile test program using intermittently coated filament should be
conducted.

The bend toughness test is generally conducted at very low
strain rates because of limitations in the cross head velocity and
load deflection measuring devices. The effect of high strain rates
can be deduced from the instrumented Charpy impact test. This test
has proved to be a valuable means of fracture toughness testing of
metals at high strain rates. It would be ideal for testing inter-
mittently coated composites. Work by Ireland and Wullaert (1972)
should be investigated before a decision is made to acquire or build

an instrumented Charpy machine. The machine is not restricted to metals or composites, but is ideal for polymers, ceramics, etc.

I am suggesting that new materials should be tested to further evaluate the fracture toughness theory presented in Chapter V. Two systems from which valuable information can be derived are the carbon (or graphite) fiber-epoxy system and the glass filament-polyester system. Both composites are relatively inexpensive, easy to fabricate and are commercially important. The intermittent bond concept should be applied to the carbon-epoxy composite, but in reverse to the boron-epoxy system. The as-received carbon-epoxy interfacial bonding is weak and a coating or surface treatment is needed to produce the requisite high interface strength regions along the fibers. This would require the designing of new equipment for the treatment and fiber handling.

Knowledge of the interfacial surface energy is necessary for the prediction of fracture toughness values in composites. A suitable test must be designed to quantify the interfacial energy of both coated and uncoated filaments. A refinement of the pullout test (section III.A.1.) is a possible approach to this test.

Considerable commercial interest is concentrated on the high temperature (300-400° F) effects with respect to the tensile properties and fracture toughness of composite materials. The recently acquired Instron environmental chamber facilitates testing at temperatures below 200 C (400° F). Lower temperatures (below RT) may prove to be a means for synthesizing high strain rate effects in composite materials.

All of the tensile tests conducted in this research are of
the low value fraction filament variety and the composite frac-
ture strain is used as the merit index. It is assumed that an
increase infracture strain will be accompanied by a proportional
increase in fracture strain will be accompanied by a proportional
utilized. The production of high volume fraction filament com-
posites with intermittently coated filaments would prove (or
disprove) the assumption and permit strength to be used as a merit
index.

—

APPENDICES

APPENDIX A

TABLE 1-A Epoxy Tensile Properties

Specimen	Strain %	Strength MN/m²	ksi	Modulus GN/m²	10⁶ psi	Area x 10⁻⁶ m²
E1 (IX)	1.58	43.53	6.31	2.86	4.15	10.86
E2 (X)	1.95	49.93	7.24	2.69	3.90	11.37
E3 (XIII)	3.00	72.00	10.44	3.32	4.81	11.96
E4 (XIV)	2.28	59.32	8.60	2.94	4.26	11.96
E5 (XV)	2.45	67.29	9.76	3.27	4.74	12.13
E6 (XVIII)	2.61	68.70	9.96	3.68	5.34	11.66
E7 (XIX)	5.12	92.45	13.41	3.27	4.74	12.90
E8 (XX)	3.54	80.05	11.61	3.06	4.43	11.71
E9 (XXI)	3.22	76.68	11.11	3.22	4.67	11.81
E10 (XXII)	2.02	54.52	7.91	3.02	4.38	11.30
E11 (XXVIII)	2.13	54.83	7.95	2.99	4.34	11.39
E12 (XXX)	2.64	70.72	10.25	3.29	4.77	12.03
E13 (XXXIII)	1.54	53.54	7.76	3.73	5.41	12.00
E14 (XXXV)	4.70	87.55	12.70	3.43	4.97	12.16

APPENDIX A

TABLE 1-B

Griffith Analysis
(using English Units)

Specimen	Crack Radius C in	$\frac{1}{C}$ in^{-1}	f^2 x 10^7 (psi)^2
E1	DID NOT EXAMINE		- -
E2	.017	59.2	5.24
E3	.012	85.3	10.90
E4	.016	63.7	7.40
E5	.015	67.8	9.52
E6	.009	115.0	9.90
E7	.007	144.0	18.00
E8	.009	114.0	13.50
E9	.009	113.6	12.40
E10	.015	68.4	6.25
E11	.017	60.5	6.30
E12	.012	82.7	10.50
E13	.014	73.7	6.03
E14	DID NOT EXAMINE		- -
E15	.005	188.4	19.20

APPENDIX A

TABLE 2

As-Received Monolayer Boron-Epoxy Tensile Properties

Specimen	Strain %	Strength MN/m^2	ksi	Modulus GN/m^2	10^6 psi
M-1	.658	72.4	10.5	11.0	1.60
M-2	.670	74.4	10.8	11.0	1.60
M-3	.480	52.8	7.7	11.0	1.60
M-4	.560	62.0	9.0	11.0	1.60
M-5	.610	67.4	9.8	11.0	1.60
M-6	.488	55.0	8.0	10.8	1.56
M-7	.616	68.8	10.0	10.4	1.51
M-8	.448	57.5	8.3	12.8	16.9
M-9	.643	66.7	9.7	10.4	15.1
M-10	.576	64.3	9.4	10.9	15.5
M-11	.580	68.4	9.9	11.9	17.3
M-12	.612	68.3	9.9	10.7	15.6
M-13	.642	72.4	10.5	11.0	16.0
M-14	.565	67.6	9.8	11.1	16 1

APPENDIX A

TABLE 3

Tensile Properties of Intermittently Coated Composites

Specimen (vf %)-No.	f %	Strength		Modulus	
		MN/m²	(ksi)	GN/m²	(x 10⁶ psi)
38-1	0.700	74.18	10.75	10.83	1.57
38-2	0.735	67.93	9.85	10.69	1.55
38-3	0.780	76.55	11.10	10.69	1.55
38-4	0.875	76.55	11.10	10.76	1.56
45-1	0.815	75.17	10.90	11.03	1.60
45-2	0.820	74.83	10.85	11.03	1.60
45-3	0.775	78.28	11.35	10.48	1.52
45-4	0.785	74.83	10.85	10.48	1.52
50-1	0.820	86.89	12.60	10.55	1.53
50-2	0.760	81.38	11.80	10.34	1.50
50-3	0.710	80.00	11.60	11.03	1.60
50-4	0.710	78.62	11.40	11.03	1.60
50-5	0.760	77.24	11.20	10.00	1.45
50-6	0.725	74.48	10.80	11.03	1.60
50-7	0.700	72.75	10.55	10.34	1.50
55-1	0.710	77.24	11.20	11.03	1.60
55-2	0.825	79.31	11.50	10.69	1.55
55-3	0.745	73.79	10.70	10.34	1.50
55-4	0.850	75.51	10.95	11.03	1.60
65-1	0.785	80.00	11.60	10.69	1.55

TABLE 3, contd.

Specimen (vf %)-No.	f	Strength		Modulus	
		MN/m^2	(ksi)	GN/m^2	($\times 10^6$ psi)
65-2	0.780	81.03	11.75	10.34	1.50
65-3	0.740	81.03	11.75	11.03	1.60
65-4	CRACKED	DURING	DEMOLDING		
75-1	0.945	68.97	10.00	10.34	1.50
75-2	0.890	77.24	11.20	10.34	1.50
75-3	0.830	78.62	11.40	10.34	1.50
75-4	0.770	77.53	11.25	10.34	1.50
75-5	0.730	73.79	10.70	10.34	1.50
75-6	0.670	68.28	9.90	10.34	1.50
75'-1	0.780	74.14	10.75	10.83	1.57
75'-2	0.760	71.72	10.40	10.69	1.55
81-1	0.840	74.83	10.85	10.34	1.50
82-2	0.775	71.72	10.4	10.34	1.50
82-3	0.715	77.24	11.2	11.03	1.60
82-4	0.735	73.10	10.6	10.34	1.50

Indicate l/d = 50 rather than l/d = 100.

APPENDIX A

TABLE IV Three Point Bond Fracture Toughness Results

Specimen	V_f Actual	Flexural Strength GN/m²	ksi	Fracture Toughness Gc KJ/m²	in-lb/in²	Specimen Stiffness (KT) lb/in	Modulus GN/m²	10⁶psi	V_f Indicated %
AR-1	42.3	1.19	173	35.5	203	2009	178	25.8	47
-2	42.3	1.18	171	36.0	206	2189	193	28.0	51
-3	42.3	1.21	175	38.3	219	1860	165	23.9	45
-4	42.3	1.17	170	36.9	211	2050	181	26.2	48
METH-1	41.8	1.10	160	30.1	172	1793	159	23.1	42
-2	41.8	1.12	163	30.8	176	1932	171	24.8	45
-3	41.8	1.18	171	33.6	192	1932	171	24.8	45
-4	41.8	-	-	-	-	-	-	-	-
100%-1	41.3	1.07	155	38.5	220	1731	153	22.2	40
-2	41.3	1.08	157	29.1	166	1731	153	22.2	40
-3	41.3	1.00	145	25.2	144	1619	143	20.7	36.7
-4	41.3	1.21	175	37.1	212	1731	153	22.2	40
50/50%A-1	40.5	0.81	117	28.9	165	1673	148	21.5	39
-2	40.5	0.45	65	15.5	88	765	62	8.99	16
-3	40.5	0.91	132	25.2	144	1660	165	23.9	44
-4	40.5	0.77	111	20.3	116	1114	101	14.6	27

TABLE IV, contd.

Specimen	V_f Actual	Flexural Strength GN/m²	ksi	Fracture Toughness G_c KJ/m²	in-lb/in²	Specimen Stiffness (KT) lb/in	Modulus GN/m²	10⁶ psi	V_f Indicated %
50-50W/A-1	42.3	1.11	162	29.1	165	1660	165	23.9	44
-2	42.3	1.22	177	30.5	174	2050	181	26.2	48
-3	42.3	0.97	141	24.0	137	1619	143	20.7	38
-4	42.3	0.89	129	21.2	121	1433	127	18.4	33
50/50 SW-1	41.9	1.13	164	30.5	174	1731	153	22.2	40
-2	41.9	1.11	161	30.8	176	1793	159	23.1	42
-3	41.9	1.27	184	30.8	176	1932	171	24.8	51
-4	41.9	1.19	173	30.5	174	1673	148	21.5	39
ENDS-1	42.5	1.12	163	39.7	227	1932	171	24.8	45
-2	42.5	0.91	132	41.3	236	1433	127	18.4	33
-3	42.5	-	-	-	-	-	-	-	-
-4	42.5	0.91	132	50.8	290	1433	127	18.4	33

APPENDIX A

TABLE V SEM Pictures

Fig. No.	Negative No.	Magnification	Tilt	Accelerating Voltage KV
IV-2	6878	X	20°	15
-13	3141	400 X	41	5
-14	2525	750 X	26	15
-15	2770	1000 X	15	15
-16	3146	300 X	45	15
-17	5158	1300 X	10	25
-18	2595	30 X	24	5
-19	2321	300 X	23	15
-20	7014	750 X	30	15
-21	2327	150 X	24	15
-22	2328	1500 X	24	15
-23	3143	200 X	41	5
-24	7020	80 X	17	15
-27	2323	500 X	23	15
-28	2522	700 X	29	15
-29	6452	3000 X	45	15
-30	6453	3000 X	45	15
-31	2327	500 X	28	15
-32	2589	1000 X	45	15
-33	2590	4500 X	45	15
-34	3084	900 X	25	5
-35	3079	900 X	26	5
-36	7366	1000 X	41	15

TABLE V, contd.

Fig. No.	Negative No.	Magnification	Tilt	Accelerating Voltage KV
-37	5697	650 X	36	15
-38	6456, 7, 8	45 X	42	15
-39	5702	250 X	0	25
-40	5154	400 X	45	15
V-1	5473	250 X	45	25
-2	5484	1000 X	35	25

Appendix B-1
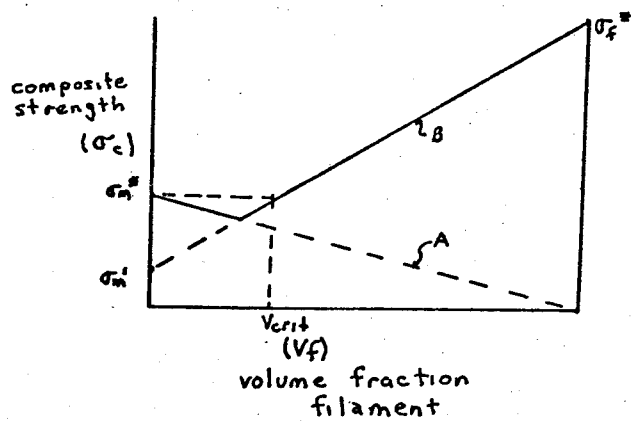
Calculation of the Critical

Volume (v_{CRIT})

See Sec. I.B.1 for the significance of v_{CRIT}.
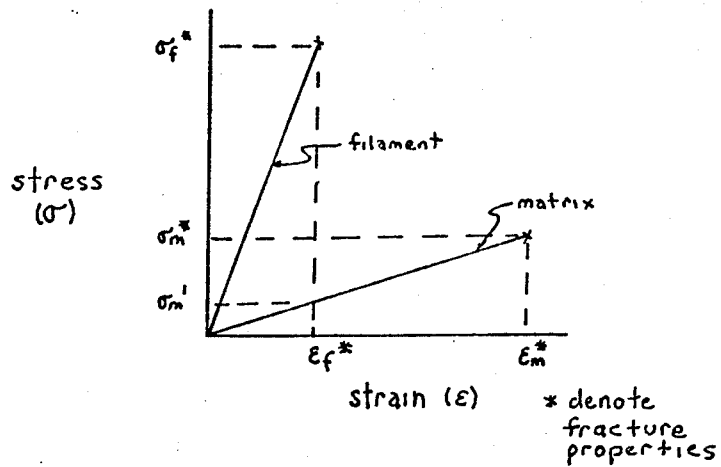
Graphical Representation of the Rule-of-Mixtures

Equation for Line A

$$\sigma_c = \sigma_m{}^* (1 - \nu_f)$$

"Matrix + Holes"

Equation for Line B

$$\sigma_c = (1 - \nu_f)\sigma_m{}^1 + \nu_f\sigma_f{}^*$$

"Matrix + Filaments"

ν_{CRIT} is defined as the ν_f

$$\sigma_m{}^* = \sigma_c = (1 - \nu_{CRIT})\sigma_m{}^1 + \nu_{CRIT}\sigma_f{}^*$$

Rearranging gives

$$\nu_{CRIT} = \frac{\sigma_m{}^* - \sigma_m{}^1}{\sigma_m{}^* - \sigma_m{}^1}$$

For the Boron-Epoxy System

$$\sigma_f{}^* = 430 \text{ ksi}$$

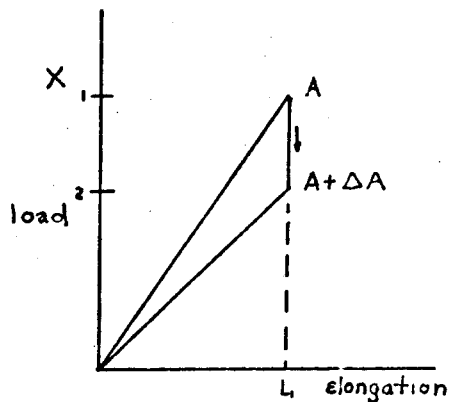$$\sigma_m{}^* = 10 \text{ ksi}$$

$$\sigma_m{}^1 = 3.48 \text{ ksi}$$

$$\nu_{CRIT} = \frac{10 - 3.48}{430 - 3.48} \qquad \% = 1.58\%$$

Appendix B-2

Experimental Determination of Gc

(From Irwin, 1962)

Fixed grip condition exist

e.g. dL = 0

$\delta A = + \delta A$ (Unit Thickness)

Strain energy $U \equiv \frac{1}{2} \cdot X\varepsilon \cdot$

Define $G_{Ic} = \lim_{\delta A \to 0} (U_1 - U_2) = - \frac{\partial u}{\partial A}$

$U = \frac{1}{2} X\varepsilon = \frac{1}{2} X (X \frac{1}{k})$ (1)

$1/k$ = compliance $X = \frac{\varepsilon}{k}$

Defferentiate (1) w.r.t. A

$\frac{\partial u}{\partial A} = \frac{1}{2} (X/k) \frac{\partial X}{\partial A}$ (2)

We know that L = constant = X/k   (3)

Differentiate (3) w.r.t. A

$X \frac{\partial (\frac{1}{k})}{\partial A} + \frac{1}{k} \frac{\partial X}{\partial A} = 0$

$$\frac{\partial X}{\partial A} = - X k \frac{\partial \left(\frac{1}{k}\right)}{\partial A} \quad (4)$$

Substituting (4) into (2)

$$\frac{\partial U}{\partial A} = - \frac{1}{2} \left(\frac{X}{k}\right) (X k) \frac{\partial (1/k)}{\partial A} = - \frac{1}{2} X^2 \frac{\partial \left(\frac{1}{k}\right)}{\partial A}$$

$$G_{Ic} = - \frac{\partial U}{\partial A} = \frac{1}{2} X^2 \frac{\partial \left(\frac{1}{k}\right)}{\partial A}$$

$\frac{\partial (1/k)}{\partial A}$ Can be determined experimentally by measuring $(1/k)$; at

various A.

Appendix B - 3

Gurney Method (1964)

(graphical representaion)
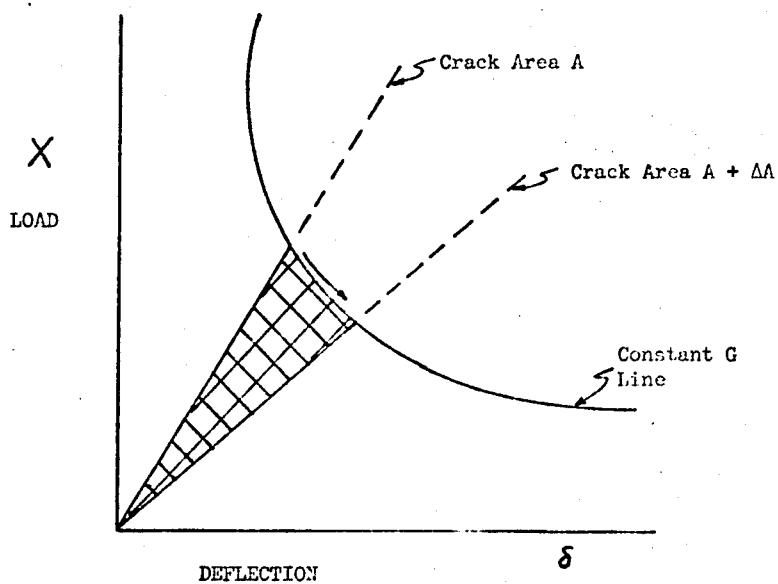
In the simplest case, the quai-static crack propagation

$X - \delta$ trace will follow a constant G line as shown above.

The fracture toughness can be determined from the following

relationship:

$$G \equiv \frac{\text{Sector Area}}{\Delta A} \quad \begin{array}{l} (\text{ cross-hatched region}) \\ (\text{ change in crack area}) \end{array}$$

Appendix B - 4

Development of the pullout equa-
ation.
(see Kelly, 1971)

Assumptions:
Shear stress τ is numerically equal to the interfacial
shear strength and is maintained during extraction of the
filament.
Filaments fracture randomly.

Work of extraction (pullout) for one filament:

$$w = Fd$$

$$F = \tau \pi d(L - x)$$

$$w = \int \tau \pi \, d(L - x) \, dx \quad \text{from 0 to L}$$

$$= \tau \pi dLx - \tau \pi dx^2/2 \quad \text{from 0 to L}$$

$$= \tau \pi dL^2/2 \tag{1}$$

Total work is the sum of (1) over all filaments N.

$$= N\tau \pi dL^2/2$$

From the definition of the volume fraction filament.

$$v_f = N\pi d^2/4A \quad \text{where A is the cross-sectional area}$$

$$N = v_f 4A/\pi d^2 \tag{2}$$

Total work W is by combining (1) and (2)

$$W = 2v_f A\tau L^2/d$$

The average length L of pulled-out filaments is $l_c/4$

$$W = v_f A\tau l_c^2/8d$$

From the defintion of the critical transfer length.

$$l_c = \sigma d/2\tau$$

and the definition of work-of-fracture

$$\gamma = W/2A$$

The work-of-fracture becomes

$$\gamma = v_f \sigma l_c/24 \ .$$

Appendix B-5

Derivation of the Debonding Theory

(Outwater and Murphy, 1967)

Assumption -

equate the energy of debonding with the elastic energy stored in the fiber after debonding.

If debonding occurs over a length x, the strain energy in the filament is

$$W = w_d \pi x = \frac{d^2}{8E_f} \int (\sigma - 4 x/d)^2 dx \qquad (1)$$

The maximum value of this work occurs if σ reaches the filament breaking strength σ which occurs at a distance

$$x = d\sigma_f / 4\tau \qquad (2)$$

substituting (2) into (1) and integrating gives

$$W_d = \frac{d^3}{24E} \frac{\sigma^3}{\tau} = \pi d^2 (\sigma_f^2/E)\sigma_f x/24$$
$$= \pi \sigma_f d^2 x/24E$$

(X and D are used equally in the literature.)

This is for one filament and if the WD is summed over N filaments

$$\gamma = W_{total} / 2A = v_f \sigma_f^2 D / 4E$$

Appendix B - 6

Derivation of the Stress Relaxation Theory

(Beaumont, 1972)

The amount of stress relaxed or strain energy lost to the matrix from the filament is $\frac{1}{2} \bar{\sigma}\varepsilon$ (where $\bar{\sigma}$ is the average stress) and it acts over a distance of $2 (\frac{2}{3} l_c)$ see Fig. I-9.

Therefore, for each filament

$$w_r = (\pi d^2/4)(1/2)(\sigma_f/E_f)(\sigma_f/2)(4 l_c/3)$$

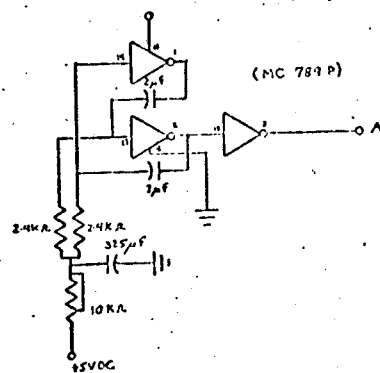$$= \pi d^2 \sigma_f^2 l_c / 12 E_f$$

Summing over N filaments

$$W_r = (v_f 4A/ \pi d^2)(\pi d^2 \sigma_f^2 l_c/ 12 E_f)$$

$$G_c = v_f \sigma_f^2 l_c/3 E_f$$

Appendix B - 7

Variable Width Pulse Generator
(timer circuit)

Astable Oscillator Circuit

Decade Divider Circuit
(each 7490 divides by ten)
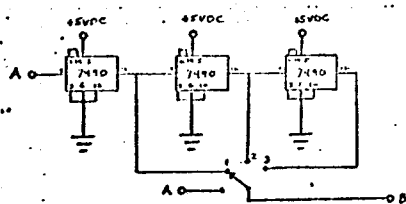
Differentiator Circuit
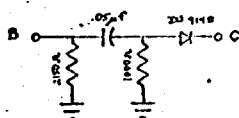
Monostable Vibrator
Circuit
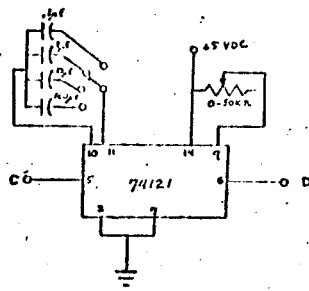
Calibration Data

1/frequency		Width	
X1	3.9 – 39 ms	X1	0.2 – 4.2 ms
X10	39 – 390 ms	X10	2.0 – 55 ms
X100	.39 – 3.9 s	X100	20 – 640 ms
X1000	3.9 – 39 s	X1000	0.2 – 7 s
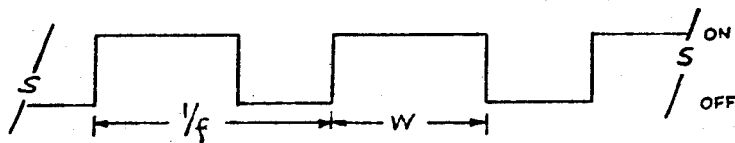
Solid State Relay

(for air valve)
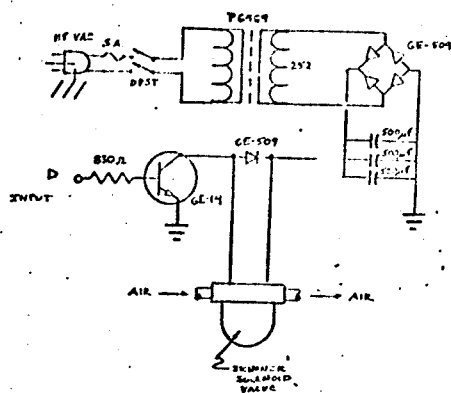
Power Supply
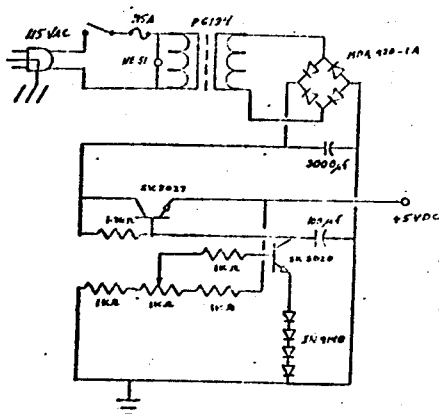
Appendix B - 8

Coater Detail

Stationary Frame

Wiper Seal

Pawl

Soft Rubber Rollers

Teflon-
lined
Bearings

Rachet

SVG

Aluminum Case

Movable Frame

Specimen Jig Detail

Cut-off Slot

Clamping
Bolt

Δ 63.5 °

A

B

A- Specimen in notching position
B- Specimen in cut-off position
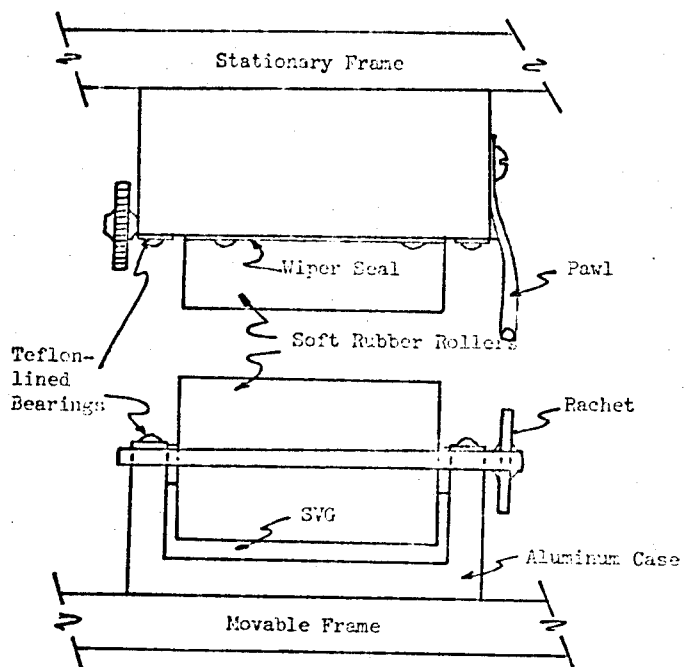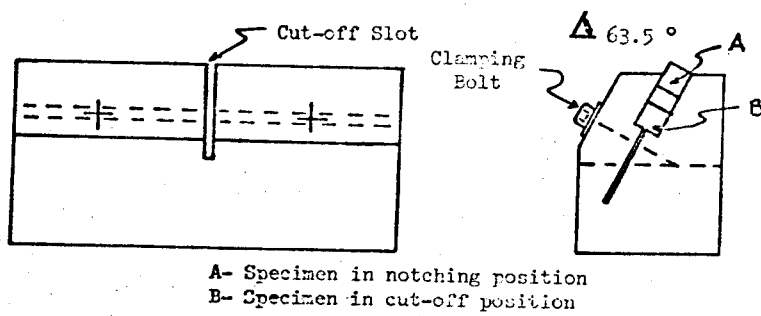
Appendix B - 9

Winding Jig Detail

- Mold
- End Cap
- .740
- 0.5 R
- Aluminum Spacer
- Clamp
- 1.25
- 7.13
- 9.75
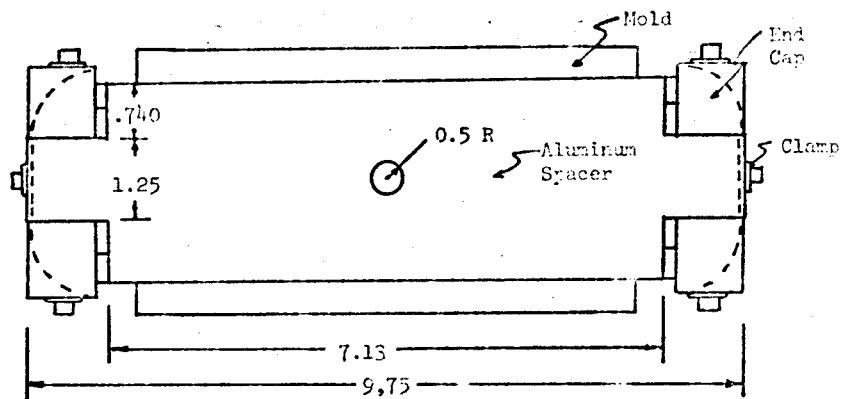
End Cap Detail
(Heimbuch, 1970)

.870 Reference to First Groove[a]

.240

.9570

.9583 Base to Center-line of First Filament

.34

1.22

~2.00

.44

.31

.75

~1.00
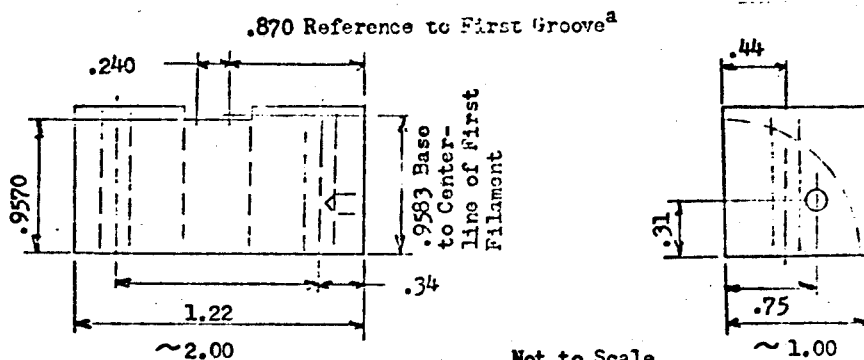
Not to Scale

[a] Does not include shims.

All Dimensions Inches

Appendix B - 10

Load-deflection curve for Instron
tensile machine
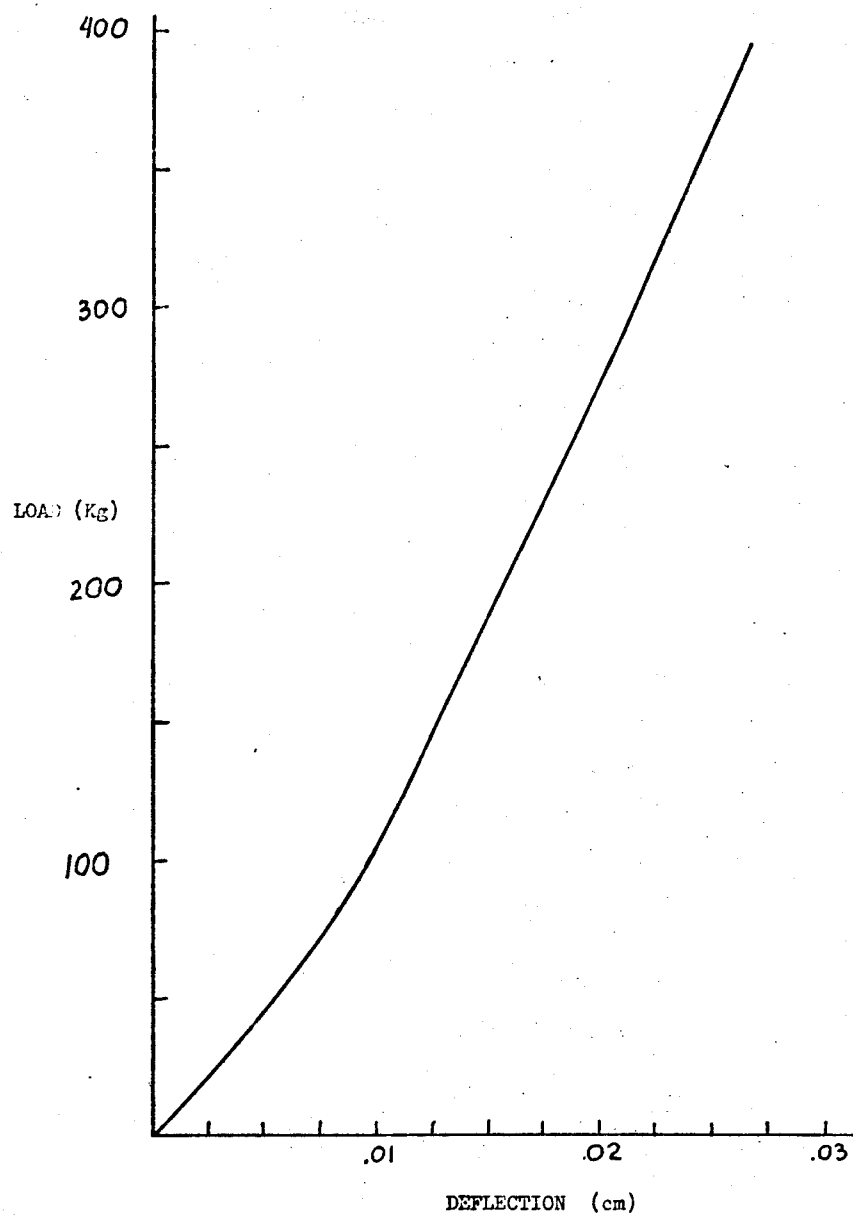
Appendix B-11

Table of Conversion Factors and Multipliers

Conversion Factors

1 GN/m^2 . . . . 145,037 lb/in^2

1 MN/m^2 . . . . 145.037 lb/in^2

1 m^2 . . . . 1549.997 in^2

1 J . . . . 8.856 in-lb

1 kJ/m^2 . . . . 5.714 in-lb/in^2

1 N . . . . 9.807 kg (sea level)

1 kg/mm^2 . . . . 1422.330 lb/in^2

1 m-kg . . . . 86.614 in-lb

1 in-lb/in^2 . . . . 2.71 X 10^4 ergs/cm^2

1 Ns/m^2 . . . . 10 poises

1 dyne/cm^2 . . . . 1.450 X 10^{-5} lb/in^2

1 Mg/m^3 . . . . 1 g/cc   0.03612 lb/in^3

1 m^2/s^2 . . . . 4 X 10^{-4} in

Multiplier (S.I. Units)

Symbol	Prefix	Multiplier
T	tetra	10^{12}
G	giga	10^9
M	mega	10^6
k	kilo	10^3
m	milli	10^{-3}
μ	micro	10^{-6}
n	nano	10^{-9}
p	pico	10^{-12}

REFERENCES

Atkins, A. G., personal communication, 1971.

Atkins, A. G. and Raghava, R., unpublished research, University of
    Michigan, 1972.

Avco, Materials Matter, Vol. 1, No. 1, Avco Systems Division,
    Lowell, Massachusetts, Oct. 1972, p. 1.

Beaumont, P. W. R., Fitz-Randolph, J. M., Phillips, D. C. and
    Tetelman, A. S., "Acoustic Emission Studies of a Boron-Epoxy
    Composite," J. of Composite Materials, Vol. 5, Oct. 1971,
    pp. 542-548.

Beaumont, P. W. R., Fitz-Randolph, J., Phillips, D. C. and Tetelman,
    A. S., "The Fracture Energy and Acoustic Emission of a Boron-
    Epoxy Composite," J. of Materials Science, 7, 1972, pp. 289-
    294.

Berry, J. P., "The Brittle Behavior of Polymeric Solids," Fracture
    Processes in Polymeric Solids, ed. by Rosen, B., Interscience,
    New York, 1964, pp. 195-234.

Boller, K. H., "Fatigue Fundamentals for Composite Materials,"
    Composite Materials: Testing and Design, ASTM STP-460,
    American Society for Testing and Materials, 1969, pp. 217-235.

Bouc, C. A., "Microscopic Study of the Mode of Fracture in Filament
    Wound Glass-Resin Composites," T and AM Report No. 234,
    University of Illinois, Nov. 1962.

Braddick, D. M., Jackson, P. W. and Baker, A. A., "Some Aspects
    of the Fracture of Boron-Aluminum Composites," J. of Materials
    Science, 6, 1971, pp. 427-438.

Broutman, L. J., "Measurement of the Fiber-Polymer Matrix Interfacial
    Strength," Interfaces in Composites, ASTM STP-452, American
    Society for Testing and Materials, 1969, pp. 27-41.

Brown, W. F., Jr., and Srawley, J. E., Plane Strain Fracture Toughness
    Testing, ASTM STP-410, American Society for Testing and Materials,
    1966.

Cook, J. and Gordon, J. E., "A Mechanism for the Control of Crack
    Propagation in All-Brittle Systems," Proc. of the Royal Society,
    A, 282, 1964, p. 508.

Cooper, G. A. and Kelly, A., "The Tensile Properties of Fiber
    Reinforced Metals: Fracture Mechanics," J. of the Mechanics
    and Physics of Solids, Vol. 15, 1967, p. 276.

Cooper, G. A. and Kelly, A., "Role of the Interface in the Fracture
    of Fiber-Composite Materials," Interfaces in Composites,
    ASTM STP-452, American Society for Testing and Materials,
    1969, pp. 90-106.

Cooper, G. A. and Sillwood, J. M., "Multiple Fracture in a Steel
    Reinforced Epoxy Resin Composite," J. of Materials Science,
    7, 1972, pp. 325-333.

Corten, H. T., "Micromechanics and Fracture Behavior of Composites,"
    Modern Composite Materials, ed. by Broutman, L. J. and Krock,
    R. H., Addison-Wesley, Reading, Massachusetts, 1967.

Corten, H. T., "Influence of Fracture Toughness and Flaws on the
    Interlaminar Shear Strength of Fibrous Composites,"
    Fundamental Aspects of Fiber Reinforced Plastic Composites,
    ed. by Schwartz, R. T. and Schwartz, H. S., Interscience,
    New York, 1968, pp. 89-107.

Cottrell, A. H., "Strong Solids," Proc. of the Royal Society, A,
    Vol. 282, 1964, p. 2.

Dow, N. F., "Study of Stresses Near a Discontinuity in a Filament
    Reinforced Composite Metal," Report R 63SD61, General Electric
    Co., 1963.

Felbeck, D. K. and Orowan, E., "Experiments on Brittle Fracture of
    Steel Plates," The Welding Journal Supplement, Nov. 1955.

Gilliland, S. M., unpublished work (1967), quoted in Kelly, A.,
    "Interface Effects and the Work of Fracture of a Fibrous
    Composite," Proc. of the Royal Society, A, 319, 1970,
    pp. 95-116.

Goan, J. C. and Prosen, S. P., "Interfacial Bonding in Graphite-
    Fiber-Resin Composites," Interfaces in Composites, ASTM STP-452,
    American Society for Testing and Materials, 1969, pp. 3-26.

Greszczuk, L. B., "Theoretical Studies of the Mechanics of the
    Fiber-Matrix Interface in Composites," Interfaces in Composites,
    ASTM STP-452, American Society for Testing and Materials, 1969,
    pp. 42-58.

Griffith, A. A., "The Phenomena of Rupture and Flow in Solids,"
    Philosophical Transactions, Proc. of the Royal Society, A,
    221, 1920, pp. 163-198.
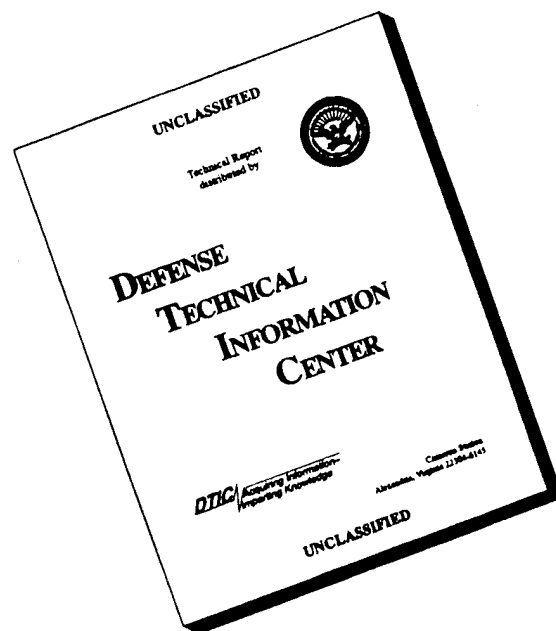
Grinius, V. G., "Micromechanics - Failure Mechanism Studies,"
    AFML-TR-66-177, August, 1966.

Gurney, C. and Hunt, J., "Quasi-Static Crack Propagation,"
    Proc. of the Royal Society, A, 297/8, 1967, p. 508.

Gutfreund, K., Broutman, L. J. and Jaffe, E. H., "Interfacial
    Investigations of Boron Fiber-Reinforced Plastics,"
    Advanced Fibrous Reinforced Composites, SAMPE, Vol. 10, 1966.

Hammond, M. L., Lindquist, P. F. and Brace, R. H., "Structure of
    Vapor-Deposited Boron Filaments," AFML-TR-66-358, November,
    1966.

Harris, B., Beaumont, P. W. R., Moncunill de Ferran, E., "Strength
    and Fracture Toughness of Carbon Fibre Polyester Composites,"
    J. of Materials Science, 6, 1971, pp. 238-251.

Harred, D. L. and Eeglegley, R. T., "Some General Aspects of
    Interfaces in Composites," Advanced Fibrous Reinforced
    Composites, SAMPE, Vol. 10, 1966.

Heintuch, R. A., "On the Tensile Fracture Characteristics of
    Unidirectional Boron-Epoxy Composites with Controlled
    Filament Packing Geometry," Ph.D. dissertation, University of
    Michigan, 1970.

Herring, H. W. and Steele, J. H., "Tensile Fracture of Unidirectional
    B-Al Composite," paper presented at the Fourth Annual Spring
    Meeting of the Metallurgical Society of AIME, Boston, May, 1972.

Herzog, J. A., "Filaments, Fibers and Metal Matrix Composites,"
    AFML-TR-67-244, October, 1967.

Hoover, W. R. and Allred, R. E., "The Toughness of Borsic/Al Composites
    with Weak Fiber/Matrix Bonds," paper presented at the Fourth
    Annual Spring Meeting of the Metallurgical Society of AIME,
    Boston, May, 1972.

Hosford, W. F., personal communication, 1972.

Irwin, G. R. and Kies, J., "Fracturing and Fracture Dynamics,"
    Welding Research Journal, (Research Supplement), 1952.

Irwin, G. R. (1960), quoted in Polakowski, N. H. and Ripling, E. J.,
    Strength and Structure of Engineering Materials, Prentice-Hall,
    Inc., Englewood Cliffs, New Jersey, 1966, p. 424.

Irwin, G. A. and Wells, A. A., "A Continuum-Mechanics View of
    Crack Propagation," Metallurgical Reviews, Vol. 10, No. 38,
    1965, pp. 223-270.

Kelly, A., Strong Solids, Oxford University Press, London, 1966.

Kelly, A., "Interface Effects and the Work of Fracture of a
    Fibrous Composite," Proc. of the Royal Society, A, 319,
    1970, pp. 95-116.

Kelly, A. and Davies, G. J., "The Principles of the Fibre
    Reinforcement of Metals," Metallurgical Reviews, Vol. 10,
    No. 37, 1965, p. 1.

Kelly, A. and Lilholt, H., "Stress-Strain Curve of a Fibre-
    Reinforced Composite," Phil. Mag., Vol. 20, August, 1969,
    pp. 311-328.

Kelly, A. and Tyson, W. R., "Tensile Properties of Fiber-Reinforced
    Metals: Copper/Tungsten and Copper/Molybdenum," J. of the
    Mechanics and Physics of Solids, Vol. 13, 1965, p. 329.

Kreider, K. and Leverant, G., "Boron Aluminum Composites
    Fabricated by Plasma Spraying," Advanced Fibrous Reinforced
    Composites, SAMPE, Vol. 10, 1966, p. F-1-9.

Krock, R. H. and Broutman, L. J., "Principles of Composites and
    Composite Reinforcement," Modern Composite Material, ed. by
    Broutman, L. J. and Krock, R. H., Addison-Wesley, Reading,
    Massachusetts, 1967.

Lee, H. and Neville, K., Handbook of Epoxy Resins, McGraw-Hill,
    New York, 1967.

Long, Robert W., Organic Chemistry of Synthetic High Polymers,
    Interscience Publishers, New York, 1967.

Ludema, K. C., personal communication, 1970.

McGarry, F. J., "Crack Propagation in Fiber Reinforced Plastic
    Composites," Fundamental Aspects of Fiber Reinforced Plastic
    Composites, ed. by Schwartz, R. T. and Schwartz, H. S.,
    Interscience, New York, 1968, pp. 63-87.

Mehan, R. L., "Fabrication and Evaluation of Sapphire Whisker
    Reinforced Alumina Composites," Symposium on Metal Matrix
    Composites, ASTM, June, 1967.

"Plastic Properties Chart," Modern Plastics Encyclopedia, 1972,
    Vol. XLI.

Mullin, J., Berry, J. M. and Gatti, A., "Some Fundamental Fracture
    Mechanisms Applicable to Advanced Filament Reinforced Composites,"
    J. Composite Materials, Vol. 2, No. 1, January, 1968, p. 82.

Mullin, J. V., Gatti, A. and Ferry, J. M., "The Role of Bond
Strength in the Fracture of Advanced Filament Reinforced
Composites," Composite Materials: Testing and Design,
ASTM STP-460, American Society for Testing and Materials,
1969, pp. 573-582.

Murr, L. E., Electron Optical Applications in Materials Science,
McGraw-Hill Book Company, New York, 1970.

Orowan, E., "Fracture and Strength of Solids," Report on Progress
in Physics, Physical Society, London, Vol. 12, 1949, p. 185.

Outwater, J. O. and Murphy, M. C., "On the Fracture Energy of
Unidirectional Laminates," Section 11-c, 24th Annual Technical
Conference, Reinforced Plastics/Composites Division, The
Society of the Plastics Industry, Inc., 1969.

Prosen, S. P., "Composite Materials' Testing," Composite Materials:
Testing and Design, ASTM STP-460, American Society for Testing
and Materials, 1969, pp. 5-12.

Rosen, B. W. and Dow, N. F., "Mechanics of Failure of Fibrous
Composites," Fracture, ed. by Liebowitz, H., Vol. 7, Academic
Press, New York, 1972, pp. 611-674.

Sambell, R. A. J., Briggs, A., Phillips, D. C. and Bowen, D. H.,
"Cabon Fibre Composites with Ceramic and Glass Matrices,"
J. of Materials Science, 7, 1972, pp. 676-681.

Sattar, S. A. and Kellogg, D. H., "The Effect of Geometry on the
Mode of Failure of Composites in the Short Beam Shear Test,"
Composite Materials: Testing and Design, ASTM STP-460,
American Society for Testing and Materials, 1969, pp. 62-71.

Schuster, D. M. and Scala, E., "The Mechanical Interaction of
Sapphire Whiskers with a Birefringed Matrix," Transactions,
American Institute of Mining, Metallurgical, and Petroleum
Engineers, Vol. 230, No. 1635, 1964.

Shell, "Epon Resin Curing Agent Z," Bulletin SP-24-C, Shell Chemical
Company, 1962.

Sih, G. C., Paris, P. C. and Irwin, G. R., "On Cracks in Rectilinearly
Anisotropic Bodies," International Journal of Fracture Mechanics,
1, Sept., 1965, pp. 189-203.

Srawley, J. E. and Brown, W. F., Jr., "Fracture Toughness Testing
Methods," Fracture Toughness Testing and Its Applications,
ASTM STP-381, American Society for Testing and Materials,
1965, pp. 133-198.

Sutton, W. H. and Rauch, H. W., Jr., "Review of Current Developments in New Refractory Fibers and Their Utilization as High Temperature Reinforcements," Advanced Fibrous Reinforced Composites, SAMPE, Vol. 10, 1966.

Talley, C. P., "Mechanical Properties of Glassy Boron," J. of Applied Physics, Vol. 30, 1959, p. 1114.

Tattersall, H. G. and Tappin, G., "The Work of Fracture and Its Measurement in Metals, Ceramics and Other Materials," J. of Materials Science, 1, 1966, 296-301.

Tetelman, A. S. and McEvily, A. S., Jr., Fracture of Structural Materials, John Wiley, New York, 1967.

Tetelman, A. S., "Fracture Processes in Fiber Composite Materials," Composite Materials: Testing and Design, ASTM STP-460, American Society for Testing and Materials, 1969, pp. 473-502.

Toland, R. H., "Failure Modes in Impact Loaded Composite Materials," paper presented at the Fourth Annual Spring Meeting of the Metallurgical Society of AIME, Boston, May, 1972.

Wolock, I. and Neuman, S. B., "Fracture Topography," Fracture Processes in Polymeric Solids, ed. by Rosen, B., Interscience, New York, 1964, pp. 235-290.

DISCLAIMER NOTICE

UNCLASSIFIED

Technical Report
distributed by

**DEFENSE
TECHNICAL
INFORMATION
CENTER**

DTIC Acquiring Information-
Imparting Knowledge

Cameron Station
Alexandria, Virginia 22304-6145

UNCLASSIFIED

**THIS DOCUMENT IS BEST
QUALITY AVAILABLE. THE
COPY FURNISHED TO DTIC
CONTAINED A SIGNIFICANT
NUMBER OF PAGES WHICH DO
NOT REPRODUCE LEGIBLY.**